Harmonic Interaction between weak AC systems and VSC-based HVDC schemes

By

Ernst Krige

Thesis presented in fulfilment of the requirements for the degree
Master of Science in Electrical Engineering at the University of Stellenbosch

Supervisor:

Prof. H.J. Vermeulen

Co-supervisor:

Prof. H. du T. Mouton

Department of Electronic and Electrical Engineering

December 2012

Declaration

By submitting this thesis electronically, I declare that the entirety of the work contained therein is my own, original work, that I am the sole author thereof (save to the extent explicitly otherwise stated), that reproduction and publication thereof by Stellenbosch University will not infringe any third party rights and that I have not previously in its entirety or in part submitted it for obtaining any qualification.

December 2012

Abstract

The implementation of the Caprivi Link Interconnector (CLI) High Voltage Direct Current (HVDC) scheme in 2010 connecting the weak Namibian and Zambian Alternating Current (AC) transmission networks via overhead line is based on Voltage Source Converter (VSC) technology. This world-first combination of attributes presents a unique opportunity to study harmonic interaction between weak AC systems and VSC-based HVDC schemes. Relatively few publications exist that focus on AC and DC harmonic interaction and very few refer to VSC HVDC schemes. Because weak AC systems are much more prone to harmonic distortion than strong AC systems, there is a clear motivation for more detailed work in this field.

In order to understand the context wherein AC and DC harmonic interaction exists, the fields of AC power system harmonic analysis and resonance, VSC switching theory, HVDC scheme configurations, Pulse Width Modulation (PWM) techniques and frequency domain analysis techniques are discussed.

This thesis then presents the concept of Harmonic Amplitude Transfer Ratio (HATR) by a theoretical analysis of AC and DC harmonic interaction due to the fundamental component, as well as harmonic interaction due to scheme characteristic harmonics and is compared to the simulation results obtained from different software solutions. Simulation and modelling techniques for AC and DC harmonic interaction are discussed including AC and DC systems modelling.

The theoretical results and simulation results are compared to the results obtained from a real life case study on the CLI HVDC scheme where a harmonic resonance condition occurred. The correlation of these three sets of results confirms the validity of the theories presented and possible mitigation of the case study resonance problems is explored.

The results and conclusion highlight a variety of interesting points on harmonic sequence components analysis, VSC zero sequence elimination, AC and DC harmonic interaction due to the fundamental component and the HATR for different PWM methods, AC and DC harmonic interaction due to scheme characteristic harmonics, modelling techniques and mitigation for the resonance conditions experienced in the analysed real life case study.

Opsomming

Die implementering van die Caprivi Skakel Tussenverbinder (CLI) hoogspannings-gelykstroom (HSGS) skema in 2010 wat die swak Namibiese and Zambiese Wisselstroom (WS) transmissienetwerke verbind via ‘n oorhoofse lyn is gebasseer op Spanningsgevoerde-omsetter tegnologie. Hierdie wêreld-eerste kombinasie van eienskappe verskaf ‘n unieke geleentheid om harmoniese interaksie tussen swak WS stelsels en Spanningsgevoerde-omsetter Hoogspannings GS stelsels te bestudeer. Relatief min publikasies wat fokus op WS en GS harmoniese interaksie bestaan, en baie min verwys na Spanningsgevoerde-omsetter Hoogspannings GS skemas. Omdat swak WS stelsels baie meer geneig is tot harmoniese verwringing as sterk WS stelsels, is daar ‘n duidelike motivering vir meer gedetaileerde werk in hierdie veld.

Om die konteks te verstaan waarin WS en GS harmoniese interaksie bestaan, word die velde van WS kragstelsel harmoniese analise en resonansie, Spanningsgevoerde-omsetter skakelteorie, Hoogspannings GS skema opstellings, Pulswydte Modulasie (PWM) tegnieke, en frekwensiegebied analiese tegnieke bespreek.

Hierdie tesis stel dan die konsep van Harmoniese Amplitude Oordragsverhouding voor deur ‘n teoretiese analise van WS en GS harmoniese interaksie na aanleiding van die fundamentele komponent, asook harmoniese interaksie a.g.v. harmonieke wat die stelsel kenmerk en word vergelyk met die simulasieresultate verkry uit verskilllende sagteware oplossings. Simulasie- en modelleringstegnieke vir WS en GS harmoniese interaksie word bespreek insluitend WS- en GS stelselmodellering.

Die teoretiese resultate en simulasieresultate word vergelyk met die resultate wat verkry is uit ‘n werklike gevallestudie op die CLI HSGS skema waar ‘n harmoniese resonansie toestand voorgekom het. Die ooreenkomste tussen hierdie drie stelle resultate bevestig die geldigheid van die teorieë soos uiteengeset voor, en die moontlike verbetering van die gevallestudie resonansie probleme word verken.

Die resultate en samevatting beklemtoon ‘n verskeidenheid punte aangaande harmoniese volgorde-komponent analiese, Spanningsgevoerde-omsetter zero-volgorde uitskakeling, WS en GS harmoniese interaksie na aanleiding van die fundamentele komponent en die

Harmoniese Amplitude Oordragsverhouding vir verskillende PWM metodes, WS en GS harmoniese interaksie na aanleiding van skema-kenmerkende harmonieke, modelleringstegnieke, asook verbetering van die resonansie toestande soos ervaar in die analise van die werklike gevallestudie.

Acknowledgements

I would like to express my appreciation to the following persons:

- To my wife Christa, my daughter Clarissa and my son Ian for their unconditional love, continued support and inspiration during difficult circumstances.
- To my colleague and friend Manfred Manchen for his support of this work and assistance with PSCAD modelling and simulations.
- To NamPower for their financial support of this work and consent to publish transmission network specific information.
- To ABB Ludvika, Sweden for consent to publish certain scheme specific information.
- To Prof H.J. Vermeulen and Prof H. Du T. Mouton for their efforts as promoters of this thesis.
- To my Heavenly Father for His enabling grace.

Table of Contents

List of figures

Abbreviations

AC	Alternating Current
AGC	Automatic Generation Control
AIEE	American Institute of Electrical Engineers
ASCI	Auto-Sequentially Commutated Inverter
AVR	Automatic Voltage Regulator
BTB	Back-to-Back
CCC	Capacitor Commutated Converter
CSCC	Controlled Series Capacitor Converter
CLI	Caprivi Link Interconnector
CSI	Current Source Inverter
DC	Direct Current
DCPB	DC Pole Breaker
DF	Distortion Factor
DFT	Discrete Fourier Transform
DLL	Dynamic Link Library
DPF	Displacement Power Factor
DPL	DigSilent Programming Language
DSL	DigSilent Simulation Language
DSM	Demand Side Management
DWT	Discrete Wavelet Transform
EMT	Electromagnetic Transient
ESI	Electricity Supply Industry
ESCR	Effective Short-Circuit Ratio
FACTS	Flexible AC Transmission Systems
FFT	Fast Fourier Transform
GIC	Geomagnetically Induced Currents
GOOSE	Generic Object Orientated Substation Event
HATR	Harmonic Amplitude Transfer Ratio
HP	High-Pass
HVDC	High Voltage Direct Current
IEEE	Institute of Electrical and Electronic Engineers
IGBT	Insulated Gate Bipolar Transistor
LCC	Line Commutated Converter
MSD	Multi-Signal Decomposition

MTDC	Multi-Terminal Direct Current
NPS	Negative Phase Sequence
NRS	National Recommended Standards (South Africa)
OCT	Optical Current Transducer
OPGW	Optical Pilot Ground Wire
OPWM	Optimised Pulse Width Modulation
PCC	Point of Common Coupling
PF	Power Factor
PLC	Power Line Carrier
PLL	Phase-Lock Loop
POD	Power Oscillation Damper
PPS	Positive Phase Sequence
PSS	Power System Stabiliser
PU	Per Unit
PWM	Pulse Width Modulation
QOS	Quality of Supply
RMS	Root Mean Square
RPWM	Random Pulse Width Modulation
RTDS	Real Time Digital Simulator
SAPP	Southern Africa Power Pool
SCADA	Supervisory Control and Data Acquisition
SCO	Synchronous Condenser
SCR	Short-Circuit Ratio
SCR	Silicone Controlled Rectifier
SSR	Sub-Synchronous Resonance
SSSC	Static Synchronous Series Compensator
SSTI	Sub-Synchronous Torsional Instability
STATCOM	Static Compensator
SVC	Static VAR Compensator
SVM	State Vector Modulation
TCP/IP	Transmission Control Protocol/Internet Protocol
TCR	Thyristor Controlled Reactor
TFR	Transient Fault Record
THD	Total Harmonic Distortion
TOV	Transient Overvoltage
UPFC	Unified Power Flow Controller

UPS	Uninterruptable Power Supply
VA	Volt-Ampere
VAR	Volt-Ampere Reactive
VSC	Voltage Source Converter
ZESCO	Zambian Electricity Supply Corporation
ZPS	Zero Phase Sequence

1 Project description and motivation

1.1 Introduction

Since the early 2000's, the eminence of a looming power crisis in the Southern African Power Pool (SAPP) started to crystallise and many power utilities renewed their outlook with regards to their own demand and supply balance by investigating their integrated resource planning, generation capacity increase, inter-connectivity, contingency planning, power supply agreements, power purchase agreements and several aspects of Demand Side Management (DSM).

By 2005, very few of the planned projects that would improve the situation substantially have moved beyond feasibility stage and even fewer were implemented. As a consequence, the power crises started to escalate necessitating load shedding in some of the major SAPP utilities causing frustration and economic pressure in various industries [**1**].

As a result of this regional situation and as part of a drive to decrease its dependency on its only interconnected neighbour (Eskom), the Namibian Power utility during 2007 till 2010 embarked on a project to integrate a High Voltage Direct Current (HVDC) scheme into the Namibian transmission grid to interconnect the Namibian and Zambian networks that were previously only linked via the Eskom and SAPP networks. The idea behind the interconnection is to be able to provide an energy highway between Central and Southern Africa with controllable power and controllable direction of power flow as an energy trading tool between the various SAPP members.

This HVDC link was built for its strategic importance in the region and although initial power flows would be limited to the transfer capabilities of the connecting Alternating Current (AC) grids, its full potential would be realised more and more as the connecting transmission networks are upgraded to fulfil the power transfer requirements posed by local and regional developmental activities and as congestion increases on the other north-south SAPP interconnecting lines. The HVDC scheme would also help to support the weak connecting systems in terms of dynamic stability and voltage support.

This link is the first of its kind where Voltage Source Converter (VSC) technology is used to connect two AC systems via an overhead Direct Current (DC) line and is called the Caprivi Link Interconnector (CLI). The first monopole phase of 300MW connects the two very weak

AC networks via a 952km, -350kV DC overhead line [**2**]. The scheme is designed for a second phase to create a full bipolar scheme rated at 600MW. This first phase implementation of the project won the prize for "Best Fast Track Power Project award" for Africa early in 2011 [**3**].

The addition of this new asset to the NamPower network inevitably introduces a whole range of new aspects with regards to system behaviour and characteristics, uncommon phenomena and new operational scenarios that have to be analysed and understood in order to operate the transmission network as a whole at a world-class standard of reliability, availability, maintainability, efficiency and safety.

These new system behaviours may be such that the way the transmission network was operated in the past might not be valid anymore for certain scenarios and have an effect on operational regimes and operating procedures that have been followed for a few decades.

1.2 Project Motivation

The motivation for this research thesis stems from the technical aspects of the influence that the new HVDC link has on the NamPower and Zambian Electricity Supply Corporation (ZESCO) transmission networks. The two existing networks previously both had their own fault levels and variations, X/R ratios, network protection settings, out-of-step and islanding philosophies, steady state load-flow characteristics, ability to do successful single- or three-phase reclosing, voltage stability, angular stability and network impedance versus frequency responses.

The VSC HVDC scheme now influences all of these aspects in specific parts of the transmission networks and have the effect of bringing many of the design assumptions for existing schemes into question and pose new challenges to existing and trusted operating regimes.

Although this is not the first integration of a HVDC scheme into existing AC networks, this is the first time VSC technology is used with an overhead DC line integrated with two very weak AC systems. Line Commutated Converters (LCC), also known as classical HVDC systems, are well studied and understood with cable or overhead lines. VSC HVDC systems with cable systems are also known as is dealing with weak AC networks. However, the combination of all three of these is a first ever design and implementation attempt and the

first opportunity where theoretical modelling and real life measurements can be compared for this combination to verify system studies and modelling validity [**4**].

Although there are many aspects of influence a new HVDC system has on the existing AC networks as referred to earlier and various interactions between AC and DC systems such as dynamic interaction [**5**], possible Sub-Synchronous Resonance (SSR) with generators or series capacitors and harmonic interaction between AC- and DC-sides, it is this last area of interaction that is of interest for this research thesis.

The effect of AC/DC harmonic interaction could play a significant role in the individual harmonic content or Total Harmonic Distortion (THD) aspect of Quality of Supply (QOS) [**6**], [**7**] that all utilities worldwide have to adhere to as governed by their respective operating licenses, governing bodies or control boards. The increase of harmonic content would also suddenly decrease the available harmonic content budget allowed for customers with non-linear loads to inject allowable harmonic content.

At worst, the effect of AC/DC harmonic interaction under transient conditions could be such that the networks are inoperable and cause transformer saturation or even equipment damage, peak over-voltage trips or over-current trips. This can occur where harmonic series or parallel resonance conditions are created by transmission equipment inductance and capacitive parameter combinations [**8**] and aggravated by a VSC scheme that starts to generate new harmonic orders that under steady state conditions did not exist.

The field of AC/DC harmonic interaction is described in some literature to a certain extent, but is often generalised and not analysed in great detail. This field is very rich in interesting detail and has a lot of depth to be explored. The unique opportunity now exists where simulation models can be tested against converter station theory and real life measurements for an overhead DC line VSC scheme with weak fault level, by using real life case studies that have presented themselves over the first year of commercial operation of the Caprivi Link Interconnector. By this means, AC/DC harmonic interaction can be understood in greater detail and the results and recommendations presented can aid future VSC HVDC project design, implementation, network planning and operations.

1.3 Project Description

The project motivation shows that there is a need for research in the field of VSC AC/DC harmonic interaction and that a unique opportunity exists to obtain results. The key questions that have to be answered by this research thesis are as follows:

- Is VSC AC/DC harmonic interaction a phenomenon to be reckoned with in modern VSC HVDC schemes or could this phenomenon generally be disregarded?
- What is the detailed mechanism by which AC/DC harmonic interaction works?
- Under which conditions do VSC AC/DC harmonic interaction become prominent and how does it influence the connected AC systems?
- When VSC AC/DC harmonic interaction is present and causes problems, how can it be resolved or mitigated?

In order to answer these questions, certain objectives have to be set in order to lay the right theoretical foundations, create valid simulation models and cases and to have the necessary field measurements and records to verify and compare all findings. Once this is done, the key questions can be answered and conclusions and recommendations can be formulated. This gives rise to the following objectives:

- Explore the theory pertaining to the fields that form part of the picture of AC/DC harmonic interaction. These could include:
  - VSC theory
  - Pulse Width Modulation (PWM) switching techniques and harmonic content
  - AC/DC interaction theory
  - Power system harmonics and sequence analysis
  - AC network resonance studies and filter design
- Examine modelling techniques for VSC and AC transmission systems
  - Electromagnetic Transient (EMT) dynamic modelling of transmission equipment and VSCs
  - Harmonic analysis and frequency domain modelling techniques
  - Relevant simulation case studies
- Compare different simulation software packages
  - PSCAD/EMTDC studies

  - Real Time Digital Simulator (RTDS) studies
  - DigSilent PowerFactory studies
  - Matlab simulations
  - Excel mathematical models
  - Lingo64 non-linear solving models
- Investigate and obtain case study data to compare with theory and simulations
  - NamPower National Control Centre event records
  - HVDC transient fault recordings
- Select tools to analyse fault records with to be able to compare with simulation results
  - Transient Fault Recorder software (TFRPlot from ABB)
  - Matlab
  - Excel
- Compare all results and relevant cases to formulate general and specific conditions and derive conclusions.
- If recommendations can be made, test recommended solutions where applicable and practical
- Identify unanswered or new questions and recommend future work

1.4 Document Overview

1.4.1 Chapter 2 – Literature study

This chapter examines the different fields that have relevance to the thesis topic as set out in the objectives and combines relevant inputs from published journals, books, conference proceedings, international standards and other references. These inputs are used as guidance on the specific topic with regards to previous research, but are also evaluated against one another and against the findings of this research thesis for validity and applicability.

First, background information is given on the networks and utilities for which the research is performed in order to understand the parameters within which the analysed scheme operates. Next, an overview is given of HVDC schemes with some focus on VSC HVDC schemes and the typical composition of VSC HVDC schemes. The unique features of the analysed scheme are discussed here in detail.

Subsequently, the foundation of power system harmonics, sequence components, resonance and sensitivity is laid before continuing into VSC theory and valve switching techniques. This is followed by AC/DC harmonic interaction theory, after which modelling and simulation techniques to implement these theories are discussed.

1.4.2 Chapter 3 – Alternating Current and Direct Current harmonic interaction

This chapter builds on the foundations laid in the previous chapter on the combination of relevant sources and further explores the different fields of power system harmonic sequence components, VSC switching operation, harmonics generation and AC/DC harmonic interaction. The purpose of this is to go into more detail and give new perspectives, relationships and understanding of existing theories, illustrate some theories by using practical examples and to set the scene for the next chapter.

1.4.3 Chapter 4 – Harmonic interaction simulation and modelling techniques

This is a more practical chapter on how the relevant power system components and harmonic interaction phenomena can be modelled using different software packages and what tools can be used to analyse the data generated. The creation of specific electromagnetic transient harmonic sources is demonstrated and the harmonic interaction results from different software packages are compared to the theories presented in Chapters 2 and 3.

1.4.4 Chapter 5 – Case study

The purpose of the case study is to use a real life example to prove that the theories presented and the simulation models and results and agree with the real power system harmonic interaction results. The case background and methodology are presented, after which the network configuration and frequency response are explained. Thereafter, the case study line and reactor energisation is simulated (without VSC present) and compared to records from the real life harmonic resonance occurrence. The VSC harmonic interaction effect is then verified by using another simulation package and certain case specific results and conclusions drawn.

1.4.5 Chapter 6 – Results and conclusions

The most important results and findings throughout the thesis are summarised and a short discussion of each is presented to put it in context and show why these results are significant or valuable to the industry.

1.4.6 Appendices

- Appendix A – Harmonic sequence analyser code
- Appendix B – Case study event list
- Appendix C – Complex vector, Clarke's ($\alpha\beta$) components and d-q components

2 Literature Study

2.1 Background information on interconnected AC systems

2.1.1 Namibian transmission system

The Namibian power system is characterised by long, high voltage transmission lines that have traditionally been lightly loaded with a few rings and many radial systems in order to cover the approximately 824,292km^2 [**9**] of sparsely populated area. The main transmission voltages are 400kV, 330kV, 220kV and 132kV with the peak demand in the order of 550MW. The three generation stations are situated at Ruacana (330MW hydro), Windhoek (Van Eck 120MW coal power station) and Walvisbay (24 MW Paratus diesel plus 22.5MW Anixas "clean" diesel).

The NamPower grid is connected to the South African power grid (operated by Eskom) via a 400kV and double 220kV lines to the Eskom Aries and Aggeneis substations respectively. The NamPower network is also connected to the Zambian network from the Zambezi substation via a 220kV line to the Sesheke substation. The fault levels on transmission level of the NamPower system varies from 1600MVA to as low as 150MVA. Fig 2.1 shows the geographical orientation and voltage levels of the major interconnecting lines.

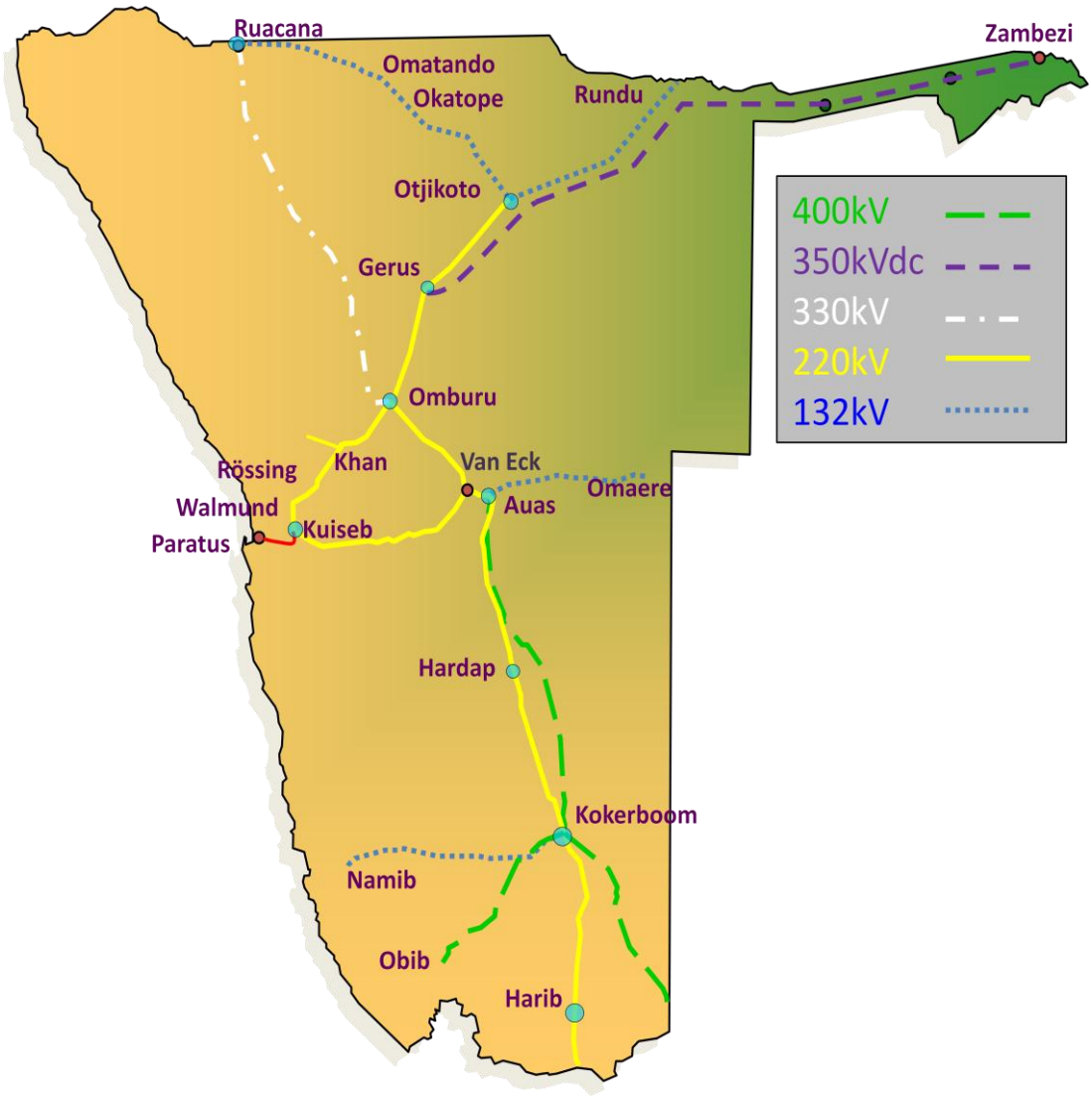

Fig. 2.1 NamPower transmission network (Courtesy NamPower)

2.1.2 Southern African Power Pool interconnected grids

The Southern African Power Pool (SAPP) consists of a few role players of which Eskom is a major player in terms of comparative generation capacity (rotating masses and spinning reserve) and interconnected tie lines. Previously the connection between Gerus and Zambezi was seen as a weak AC connection via South Africa, Zimbabwe and Zambia. Eskom provides a swing bus for the Namibian grid in terms of load/frequency support and NamPower currently still falls under the control area of Eskom. An overview of the SAPP system is shown in Fig. 2.2.

With the commissioning of the Caprivi Link Interconnector, an alternative path was created between Zambia and Namibia. Although this provides a direct exchange of energy between the two utilities, under steady state conditions there is no inadvertent flow of energy as the

power flow on the HVDC link is controlled. During disturbances, Eskom still acts as a swing bus to the NamPower system and any the change in power flow on the CLI HVDC link is seen as a change of load to the Zambian (ZESCO) system and has not been included in the ZESCO Automatic Generation Control (AGC) system.

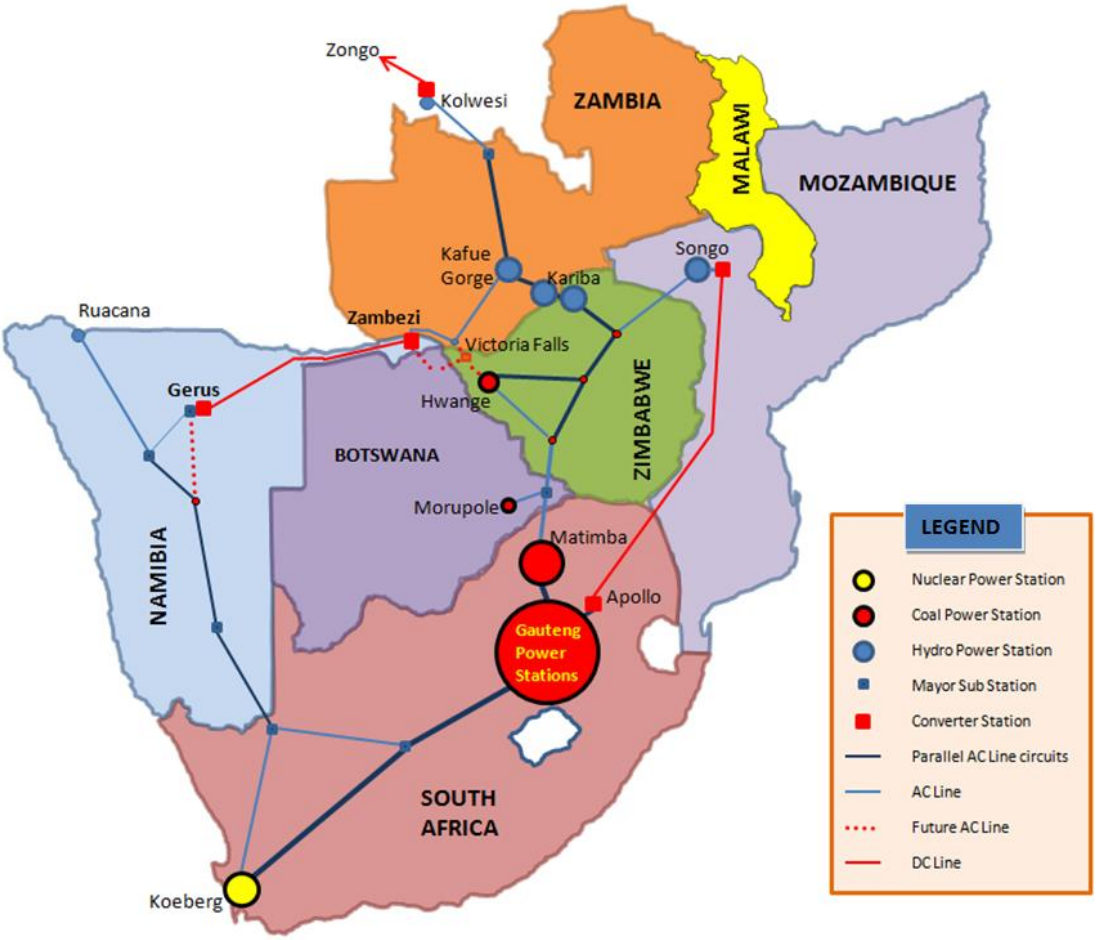

Fig. 2.2 SAPP network (Courtesy NamPower)

The Zambian system has generation sources, amongst others, in the vicinity of the CLI HVDC link at Victoria Falls and Kafue Gorge. Due to the long 220kV connection between Kafue Town and Sesheke, the fault level at Sesheke and Zambezi is very low and varies around 180MVA to 250MVA. This pose some challenges to a LCC or classical HVDC scheme, but is handled better by the VSC HVDC technology [**10**] - [**11**]. As will be shown later, the fault level (and relative change in fault level) has a definite influence on the movement of harmonic resonant points [**8**], [**12**].

Dynamically, the NamPower network frequency is determined by the Eskom network and inter-area oscillations occur between the Ruacana generators and groups of generators in the

Eskom system. During faults close to the NamPower backbone that are not cleared within 400ms to 600ms, the Ruacana generators have accelerated due to loss of load and started to move out of step with the Eskom system. The main cause of instability during transient conditions is the impedance of the long 521km 330kV line connecting the Ruacana and Omburu substations. Various out-of-step and power swing tripping schemes have been implemented [**13**].

During normal network conditions in the Zambian and Namibian systems, the CLI HVDC scheme is set to allow energy flow in either direction, but with the norm being to import from Zambia to Namibia. The frequency is determined by the connected AC systems and the Phase-Lock Loop (PLL) elements of the VSC controllers follow the frequency within a certain band.

A likely occurrence is a split in the Zambian network, where the southern part of Zambia islands with the CLI HVDC scheme. In this event, the CLI HVDC scheme would go into frequency control mode and would attempt to stabilise the Zambian network frequency by either injecting power into or extracting power from the Zambian network according to a preset power/frequency droop. It has been observed that a fixed droop setting has definite risks to both networks and an adaptive frequency droop controller has been developed and implemented to avoid excessive power shifts for the sake of frequency stabilisation.

Each of the converter stations can be run in a normal mode meaning it is synchronised to the AC network be it in power control mode or DC voltage control mode. Alternatively, one of the converters can function in frequency control mode feeding a passive network or forming part of an islanded network with other generation present where the VSC scheme gives the 50Hz heartbeat for the connected AC system. The CLI HVDC scheme also acts as a powerful Static Compensator (STATCOM) to do reactive power compensation in either voltage (VAC) or reactive power (Q) control mode with a +-200MVAR capability [**2**], [**13**].

2.2 Overview of High Voltage Direct Current technology

2.2.1 History of classical- and Voltage Source Converter High Voltage Direct Current

Although the first theoretical examination and implementation of HVDC power transmission was done by Marcel Deprez during 1881 and 1882, the classical HVDC scheme as we know

it today has been around since 1939, following the successful development of the mercury-arc valve for high voltage applications by Dr Uno Lamm of ASEA (Sweden). His invention of using a system of grading electrodes with a single phase valve construction provided the basis for larger peak-inverse withstand voltages [**14**]. The first commercial HVDC scheme was commissioned in 1954 between the Swedish mainland at Västervik and the island of Gotland using these mercury-arc valves with a rating of 20MW transported over 98km at 100kV [**15**], [**16**], [**17**].

The advent of the development of transistor technology and consequentially power electronics devices like the thyristor or Silicon Controlled Rectifier (SCR) during the late 1950's had an immense effect on static-converter technology, especially as power ratings, control speeds and strategies improved [**10**], [**14**]. The first thyristor-based HVDC scheme, known as the Eel River scheme, was built in 1972 in Canada and was used as a 320MW back-to-back HVDC scheme between two provincial power systems [**16**]. The first thyristor-based HVDC scheme in Africa built in 1977 is the Cabora Bassa HVDC scheme which is a bipolar scheme operated at +-533kV with a capability of 1920MW. It connects the Cabora Bassa hydro-electric generation scheme in Mozambique to the Eskom network at the Apollo transmission station [**15**].

During the 1990's, the fast development in high power semiconductors with current turn-off capabilities, such as Gate Turn-off Thyristors (GTO's) and Insulated Gate Bipolar Transistors (IGBT's), allowed for the development of forced-commutated Voltage Source Converters (VSC) for power transmission applications [**14**], [**18**], [**19**]. The combination of DC-side energy storage in DC capacitors with forced commutated VSCs gives the ability to generate a synchronous voltage at any phase angle and amplitude as limited by the converter and DC capacitor energy storage [**20**], [**21**]. These characteristics have the following advantages for VSC-based schemes over classical HVDC schemes [**10**]:

- Active and reactive power can be controlled almost independently.
- As a voltage source with storage capability, it can supply fault level which makes it more suitable for weak AC systems. Thus there is no requirement for Synchronous Condensers (SCO's) to increase the fault level and thus no mechanical inertia that could contribute to angular instability.
- Absorption of reactive power is realised by solid-state means instead of passive components and a reduction in size of the total installation is possible.

- Low frequency resonance due to shunt passive components as well as SSR due to series compensation can be mitigated.
- Fast control and high switching frequencies allow for active filtering of harmonics and different switching schemes to optimise efficiency and transient stability.
- Because of forced commutation, problems associated with classical HVDC schemes such as misfire, fire-through, commutation failure and backfire can be avoided [**14**], [**16**].
- Features such as islanded operation (frequency control) and "black start" capability are now easier to implement.

The main disadvantage of a VSC compared to a classical HVDC is that the switching losses are typically higher due to the fact that higher switching frequencies are generally utilised and that more complex circuit configurations might be required to limit total harmonic content [**10**], [**22**].

2.2.2 High Voltage Direct Current scheme configurations

2.2.2.1 Overview of High Voltage Direct Current scheme configurations

In general, High Voltage Direct Current (HVDC) schemes can be classified into a number of categories with regards to basic configurations regardless of being classified as LCC schemes (also referred to as classical schemes) or VSC HVDC schemes. These are discussed in the remainder of this section.

2.2.2.2 Back-to-back High Voltage Direct Current interconnection schemes

Back-to-back High Voltage Direct Current (BTB HVDC) interconnection schemes consist of two converters connected back-to-back without any DC line as shown in Fig 2.3. These back-to-back schemes are often used to interconnect between different AC grids where the power flow needs to be controlled, to couple between AC grids with different frequencies or to de-couple two AC networks dynamically from each other where existing dynamics problems necessitate this [**10**], [**11**], [**14**], [**23**].

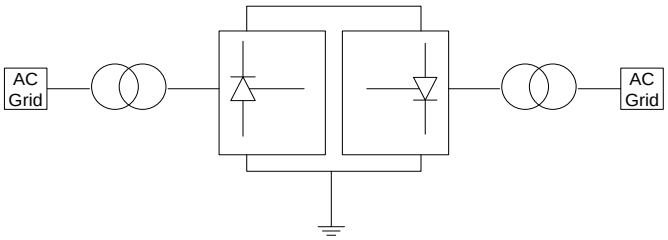

Fig. 2.3 BTB HVDC scheme [10], [14]

2.2.2.3 Monopolar schemes with earth return and/or metallic return

In monopolar HVDC schemes, two converters are connected via a DC line or cable [**16**] and often have either an earth return or a metallic return as shown in Fig 2.4. It can be shown that using an earth return may have almost four times less line losses than a metallic return, but in case of electrode line- or station outages, a metallic return could prove a viable contingency arrangement [**14**]. During metallic return operation, both converter stations will be earthed via the station earth of one converter [**13**] .

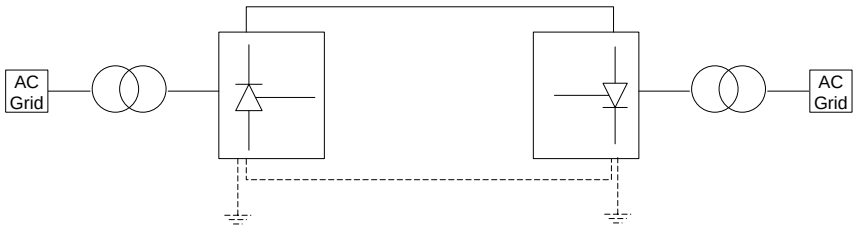

Fig. 2.4 Monopolar HVDC scheme [14], [16]

2.2.2.4 Bipolar schemes

The bipolar scheme is one of the most common schemes and is effectively a combination of two monopolar schemes. One pole would be positive and the other negative with reference to ground potential. The two monopolar schemes share the same earth return and can be operated one at a time with earth return during at outage on the other monopolar scheme. During balanced bipole operation, virtually zero current will flow in the earth return [**14**], [**16**]. Fig. 2.5 shows the typical layout of a bipolar HVDC scheme.

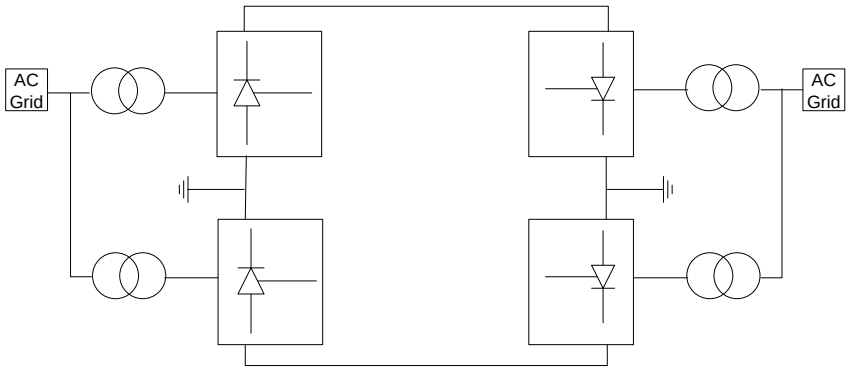

Fig. 2.5 Bipolar HVDC scheme [14], [16]

2.2.2.5 Multi-terminal Direct Current schemes

Multi-terminal Direct Current (MTDC) schemes can be described as a group of converters connected to a common DC bus from where power can be imported or exported [**14**]. Coordination in terms of stable DC voltages, stable power and DC-side harmonics between schemes is becoming more important with complex multi-terminal schemes [**24**]. One possible MTDC layout is shown in Fig. 2.6.

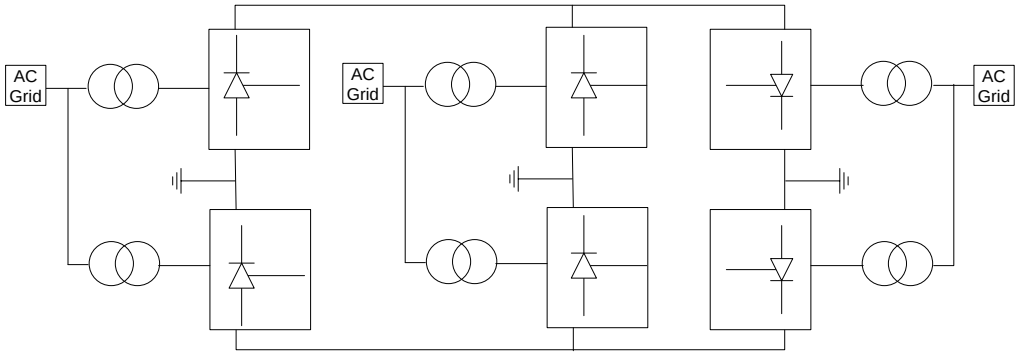

Fig. 2.6 MTDC scheme [14]

2.2.3 Other Voltage Source Converter technology and applications

Apart from VSC HVDC transmission schemes, other VSC Flexible AC Transmission System (FACTS) devices also exist. These include the Static Synchronous Compensator (STATCOM), Unified Power Flow Controller (UPFC) and the Static Synchronous Series Compensator (SSSC) [**11**].

Although a VSC HVDC scheme is also effectively a STATCOM, the STACOM alone is used in applications requiring rapid response to transient conditions, smooth voltage control over a

wide range of operating conditions and active harmonic filtering. Two such examples in the United States are the VELCO Essex STATCOM rated at +133/-41 MVA at 115 kV and the SDG&E Talega STATCOM iBTB rated at l00MVA with voltage level at 138 kV [**11**].

The UPFC consists of one series- and one parallel connected VSC with a common DC link and energy storage using DC capacitors as shown in Fig. 2.7. This device can control both the transmitted active- and reactive power, as well as the busbar voltage where the parallel connected VSC is situated. The series element is effectively a SSSC and the parallel element is effectively a STATCOM. Combined, these two elements give independent active and reactive power flow over the connected line. The UPFC is functionally used for voltage regulation, series compensation and phase shifting. The combinations of these functions provide a very useful and versatile device for situations where high operating flexibility is required [**10**], [**11**].

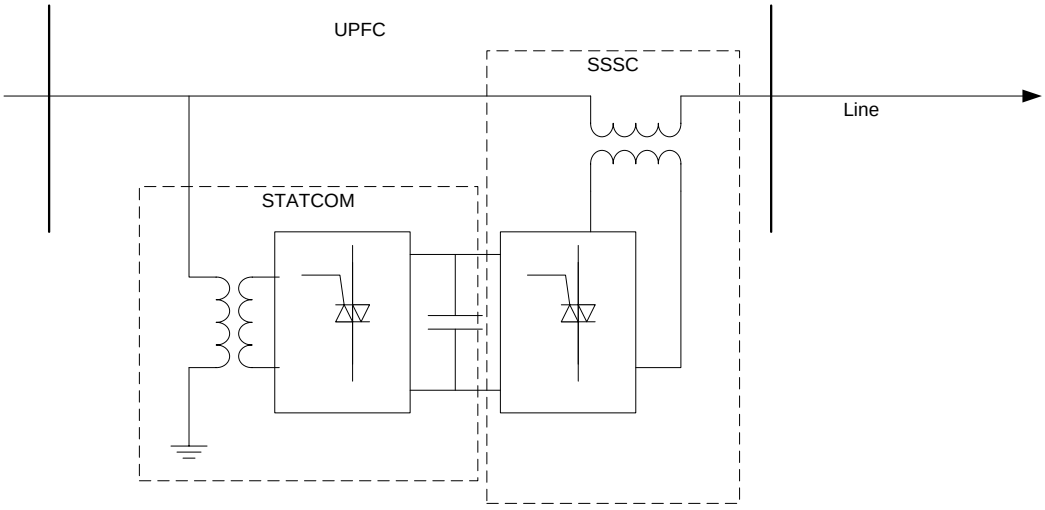

Fig. 2.7 UPFC overview [10]

2.2.4 Current Source Converter technology and applications

Just as a VSC is a stiff DC voltage source provided by a DC capacitance, a Current Source Converter (CSC), also known as a Current Source Inverter (CSI), is a stiff DC current source provided by a DC inductance. A series-connected transistor and diode arrangement is used to provide a bidirectional voltage blocking, unidirectional current conducting switch.

A common implementation of a current source converter is an Auto-Sequentially Commutated Inverter (ASCI) device. Although the same fixed frequency modulation strategies used in VSC applications can be used in CSCs and although CSC circuit

configurations have a lot of potential in high power drive systems, these advantages have not been widely exploited to date [**22**].

2.2.5 Capacitor Commutated Converter HVDC configurations

Non-conventional HVDC circuit configurations such as the Capacitor Commutated Converter (CCC) and Controlled Series Capacitor Converter (CSCC) have been proposed [**25**] with the aim to provide improved immunity to commutation failure, lower load rejection over-voltages and increased stability margins in power control mode. Although ferro-resonance is a danger associated with CSCC configurations, this can be mitigated by controlling the amount of series compensation.

2.3 Voltage Source Converter High Voltage Direct Current scheme composition and main components

2.3.1 Overview of Voltage Source Converter High Voltage Direct Current scheme composition

According to the CIGRE Protocol for reporting the operational performance of HVDC links [**26**], the Institute for Electrical and Electronic Engineers (IEEE) Guide for the Evaluation of the Reliability of HVDC Converter Stations [**27**] and partially by other sources [**14**], [**16**], [**28**], [**29**], a complete interconnected HVDC scheme is generally divided into the following main categories and sub-categories:

- AC and auxiliary equipment:
  - AC filters and shunt banks
  - AC control and protection
  - Converter transformer
  - Synchronous compensator (not applicable to VSC schemes)
  - Auxiliary equipment and auxiliary power
  - Other AC switchyard equipment
- Valves:
  - Valve electrical
  - Valve cooling
  - Valve capacitor

  - Phase reactor (added recently for VSC schemes)

- DC Control and Protection:
  - Local control and protection
  - Master control and protection
  - Control and protection telecommunications

- Primary DC equipment:
  - DC smoothing reactor
  - DC switching equipment
  - DC ground electrode
  - DC ground electrode line
  - DC filters
  - DC switchyard and valve hall equipment

- DC Line
- External AC network

For VSC-based HVDC schemes the converter reactor, also known as the phase reactor, have been added recently by CIGRE as per requirement by manufacturers and utilities and has not been published yet at the date of completion of this thesis. The VSC HVDC scheme that this investigation targets as a case study example as referred to in Section 1.1 consists of the main components as shown in the simplified single line representation in Fig. 2.8 [**13**]:

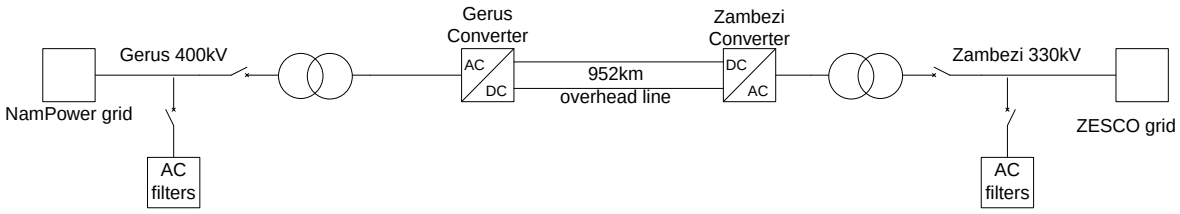

Fig. 2.8 CLI VSC overview (Courtesy NamPower)

The first phase of the project as implemented is a 300MW monopole scheme [**2**] comprising of the two converter stations, i.e. Gerus- and Zambezi Converter stations. The main components of the scheme are shown by the simplified single line diagrams in Fig. 2.9 and Fig. 2.10 respectively.

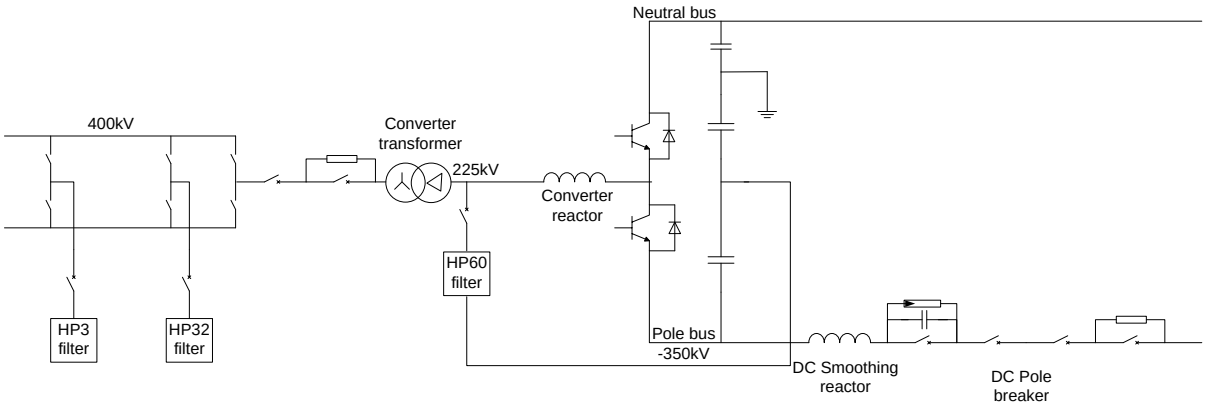

Fig. 2.9 Gerus Converter station simplified single line diagram (Courtesy NamPower)

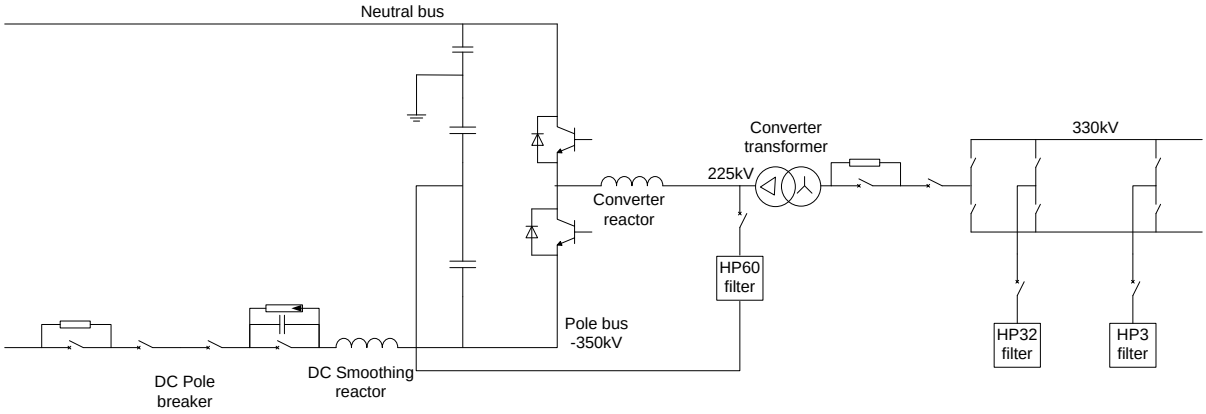

Fig. 2.10 Zambezi Converter station simplified single line diagram (Courtesy NamPower)

The CLI scheme that will be used for the case studies has the main circuit equipment and functions detailed below. Some detail have been omitted to comply with confidentiality clauses between the Utility and the Contractor.

2.3.2 Direct Current Pole Breaker and other primary Direct Current equipment

On the DC side of the converter station, there are various types of equipment like links/disconnectors, high frequency filters, optical current transformers (OCTs) and surge arrestors (detail not shown). The links/disconnectors allow for different operating configurations such as metallic return and earth return, with parallel or single DC line configurations in earth return configuration. The high frequency filters filter out switching-frequency noise as well as accommodating the Power-Line Carrier (PLC) system. Surge

arrestors provide protection against switching and lightning impulses. The OCTs, Rogovski coils and voltage dividers provide inputs to the protection and control system.

The Direct Current Pole Breaker (DCPB), consisting out of four separate units, is used during DC line faults in conjunction with a auto-restart switching scheme in order to clear DC faults. The word "breaker" is slightly misleading as a breaker cannot really break current. It is only subsequent to a zero-crossing of a current waveform that opening mechanisms and arc extinguishing methods can stop the current driven by strong inductive components in the system from flowing. The same applies for a DC breaker. In order to break the current, a zero crossing is created by commutating the DC current to a capacitor that resonates with the series line inductance. This resonance gives opportunity for a zero crossing for the second breaker to open. The third breaker opens a few milliseconds later in case the first zero crossing is missed. The fourth breaker is used to bypass or switch in a damping resistor during energising from the DC line side to limit converter transformer inrush currents [**13**].

2.3.3 Direct Current smoothing reactor

The DC smoothing reactor is used to limit transient over-currents during DC line faults and also plays an important role in the DC side filtering design. The total harmonic content found on the DC side of a 2-level VSC can be divided into DC and AC harmonics, or pole and ground mode harmonics. DC harmonics modulated over from the AC side depend on the relative fundamental current magnitude, modulation index and power factor.

AC-side zero sequence harmonics can be transferred via the mid-point connection and High-Pass (HP60) filter to the DC side and are not cross-modulated. An ideal symmetrical system will cause the DC-side harmonic content to contain both pole mode and ground mode harmonics.

The smoothing reactor value is chosen such that it does not resonate with the DC line and interconnected systems [**13**].

2.3.4 Insulated Gate Bipolar Transistor Valves

Each of the three phases from the AC system is connected to the midpoint of two IGBT stacks (175kV DC). Each of the stacks contains a certain number of positions, of which a certain percentage plus one position relates to the number of redundant positions and extra margin to avoid tripping the converter. Each IGBT has a resistive and capacitive voltage divider circuit that allows for even voltage distribution across all the IGBT's.

The IGBT positions for each valve are fired simultaneously either in Optimised Pulse Width Modulation (OPWM) mode (under steady state conditions with cancellation techniques) at 23rd harmonic, or normal PWM with third harmonic injection (under transient conditions with high zero sequence content) mode at 33rd harmonic [**13**].

2.3.5 Direct Current capacitors

The DC capacitors located between the pole- and midpoint buses and neutral bus to ground have the purpose to store energy to help maintain a stable DC voltage, as well as to provide fault level during AC faults [**13**].

2.3.6 Converter reactor

The converter reactor is a crucial piece of equipment in the AC/DC conversion process of the converter stations. On the valve side of the converter reactor, the voltage waveform is that of the PWM-switched DC voltage while on the AC side of the reactor the voltage waveform is much closer to a fundamental component AC waveform at 225kV, but with a DC offset of -175kV and several harmonic components. The converter reactor inductance with the converter transformer gives the impedance required to control active and reactive power flow [**13**].

2.3.7 Converter Transformer

The 300MVA 400/225kV or 330kV/225kV converter transformers connects the HVDC scheme to the AC power system at the desired voltage level (in this case 330kV or 400kV) and has a wide tap changer range in order to cater for different operating modes like reduced DC voltage operation (in case of bush fires), black start conditions, etc. The transformer, although built as three single phase transformers, has a star connection on the High Voltage side and a delta connection on the converter (225kV) side. The delta connection does not allow zero-sequence currents to flow into it [**8**] and simplifies external filter requirements. The relatively high transformer impedance aids the converter reactor to obtain a bigger phase angle change for active and reactive power control [**13**].

2.3.8 Converter Alternating Current breaker

The converter AC breaker connects the HVDC scheme to the AC grid and has the ability to do several opening and closing operations in a short time in order to complete DC line fault clearing sequences. The AC breaker also has a resistor with bypass breaker that is switched during energising sequences in order to limit inrush currents into converter transformer, or to

limit inrush currents into the adjacent 315MVA coupling transformer during black start operation [**13**].

2.3.9 Alternating Current filters

The scheme has three main AC filter banks, named according to their tuned frequencies, namely HP60, HP32 and HP3. The HP60 filter connected between the converter reactor and converter transformer has fairly flat impedance versus frequency response between the 55^{th} and 70^{th} harmonic order to filter our higher order harmonic distortion.

The HP32 filters are connected to the 330kV and 400kV AC busbars. This filter also has a flat and damped response and caters for the 28^{th} to 35^{th} harmonic orders during OPWM operation. It also targets the 33^{rd} harmonic order during PWM transient operation that would normally occur only as a zero phase sequence harmonic, but would under unbalanced conditions occur as positive- and negative phase sequence components on the HV side of the converter transformer.

The HP3 filters are also connected to the 330kV or 400kV AC busbars. The HP3 filter at Gerus converter station is tuned to 150Hz and caters for AC network 3^{rd} harmonic sensitivity in that area. The HP3 filter at Zambezi is tuned to around 115Hz (closer to an HP2) and gives a better response in terms of impedance magnification for the Zambian network. It will, however, be shown that this tuning is not perfectly suited for transient and/or unbalanced conditions [**13**].

2.3.10 Cooling and auxiliary equipment

The IGBT switching losses in the VSC scheme is significant and a pressurised water-cooled system is used to transport heat away from the IGBT valves to be dissipated through cooling fans outside the building. The AC and DC auxiliary systems include redundant medium voltage (22kV) and low voltage (0.4kV) switchgear, diesel generator, battery banks (110VDC and -50VDC), Uninterruptable Power Supply (UPS) systems and fire protection systems [**13**].

2.3.11 Protection and Control equipment

The protection and control equipment consists out of various cubicles where plant signals terminate and are converted to protocol communications. Three individually redundant control and protection systems monitor different areas of the scheme and communicate via Ethernet communications networks with redundant network switches and interfaces. The

valve control and firing are controlled from one of these systems, but the lower level firing pulses are done by individual and redundant valve control units.

Other equipment, such as line fault locators, power quality meters, tariff meters, fibre optic terminal equipment (primary inter-station communications via Optical Pilot Ground Wire (OPGW)) and PLC equipment (secondary inter-station communications), also form part of the scheme. The OPGW line has 6 repeater stations and the PLC system has one repeater station along the almost 1000 kilometres of line. Supervisory Control and Data Acquisition (SCADA) data and engineering data is carried back to the control centre in Windhoek via OPGW or digital PLC systems via Transmission Control Protocol / Internet Protocol (TCP/IP) based protocols (IEC60870-5-104) with redundant routing options. The HVDC scheme also interfaces with the AC substation automation systems that use the IEC61850 standard for publisher/subscriber information interchange. Aspects such as the practical implementation of substation interlocking and bus zone protection via generic object orientated substation event (GOOSE) messages will not be discussed as part of this thesis [**13**].

2.4 Power system harmonic analysis overview

2.4.1 Fundamentals of power system harmonics

The generation of electricity by a utility is ideally required to be at a constant frequency, e.g. 50Hz or 60Hz, and to be purely sinusoidal. Even if this was the case, the sinusoidal voltage that is applied to non-linear loads cause non-sinusoidal currents to flow through these devices or loads. System impedances such as lines, transformers, etc between generation points and loads can cause non-sinusoidal voltage drops, especially when non-sinusoidal load currents are drawn. As a result, the voltage presented to load terminals also contains components that contribute to the supply voltage not to be purely sinusoidal. Even linear loads presented with non-sinusoidal voltages will then draw non-sinusoidal currents. These non-sinusoidal components are considered QOS pollution and is referred to as power system harmonics occurring as harmonic voltage- and harmonic current components [**8**], [**12**], [**16**], [**22**], [**30**], [**31**], [**32**], [**33**], [**34**]. The term “harmonics” is a very broad term and is often misused. Proper reference should be made using more descriptive and contextual terms such as “harmonic component”, “harmonic distortion”, “harmonic order”, etc.

Power system harmonic components are theoretical constructs and are normally represented as independently rotating phasors with rotational speeds of integer multiples of the fundamental frequency rotational speed with a specific phase offset in relation to the fundamental phasor. In a three-phase system harmonic components have certain phase-rotation or sequence component characteristics. Harmonic components that do not rotate at integer multiples of the fundamental frequency, called inter-harmonics, also exist in certain cases and are often observed under transient conditions. Although this concept brings forth some conflicting theoretical implications, it will not be discussed here [**8**], [**12**]**,** [**35**]**,** [**36**].

According to the work of Jean Baptiste Joseph Fourier (1768–1830) as first published in 1878 [**37**], any periodic waveform $f(\mathrm{t})$ can be expanded in the form of a Fourier series as follows [**8**], [**12**], [**16**], [**22**], [**34**], [**38**]:

$$f(\mathrm{t}) = a_0 + \sum_{n=1}^{\infty} \left(a_n \cos \frac{2\pi nt}{T_0} + b_n \sin \frac{2\pi nt}{T_0} \right) \tag{2.1}$$

where a_0 is the mean value of the periodic signal $f(\mathrm{t})$ over one period given by the relationship

$$a_0 = \frac{1}{T_0} \int_{-T_0/2}^{T_0/2} f(t)\, dt. \tag{2.2}$$

The coefficients a_n and b_n are given by the relationships

$$a_n = \frac{2}{T_0} \int_{-\frac{T_0}{2}}^{\frac{T_0}{2}} f(t)\, \cos \frac{2\pi nt}{T_0}\, dt, \qquad n = 1,2, \ldots \tag{2.3}$$

and

$$b_n = \frac{2}{T_0} \int_{-\frac{T_0}{2}}^{\frac{T_0}{2}} f(t)\, \sin \frac{2\pi nt}{T_0}\, dt, \qquad n = 1,2, \ldots \tag{2.4}$$

where T_0 denotes the period of the waveform.

A simpler and more elegant form of the Fourier series is the complex exponential Fourier series using the relationships

$$\cos\left(\frac{2\pi nt}{T_0}\right) = \frac{1}{2}\left(e^{\frac{j2\pi nt}{T_0}} + e^{-\frac{j2\pi nt}{T_0}} \right) \tag{2.5}$$

and

$$\sin\left(\frac{2\pi nt}{T_0}\right) = \frac{1}{2}\left(e^{\frac{j2\pi nt}{T_0}} - e^{-\frac{j2\pi nt}{T_0}}\right). \tag{2.6}$$

This gives

$$f(\mathrm{t}) = a_0 + \sum_{n=1}^{\infty}\left((a_n - \mathrm{j}\,b_n)\,e^{\frac{j2\pi nt}{T_0}} + (a_n + \mathrm{j}\,b_n)\,e^{\frac{-j2\pi nt}{T_0}}\right). \tag{2.7}$$

Let c_n denote a complex coefficient related to a_n and b_n by the relationships

$$c_n = \begin{cases} a_n - \mathrm{j}b_n, & \mathrm{n} > 0 \\ a_0, & \mathrm{n} = 0 \\ a_n + \mathrm{j}b_n, & \mathrm{n} < 0. \end{cases} \tag{2.8}$$

It follows that

$$f(\mathrm{t}) = \sum_{n=-\infty}^{\infty} c_n\, e^{\frac{j2\pi nt}{T_0}} \tag{2.9}$$

where

$$c_n = \frac{1}{T_0}\int_{-\frac{T_0}{2}}^{\frac{T_0}{2}} f(t)\, e^{\frac{-j2\pi nt}{T_0}}\, dt, \qquad n = 0, \pm 1, \pm 2, \ldots. \tag{2.10}$$

The reason for using the complex exponential Fourier series and negative frequency components are not only to provide a compact and more elegant mathematical description of a periodic signal [**38**], but will later also help to give insight into the frequency domain representation of the phase rotation of harmonic sequence components.

For discrete valued functions for numerical/computational purposes, the Discrete Fourier Transform (DFT) or Fast Fourier Transform (FFT) is used. The discrete valued time domain function $\mathrm{x}(\mathrm{t_n})$ is transformed into the frequency domain function $X(\mathrm{f_k})$ of discrete components given by the relationship [**12**]

$$X(\mathrm{f_k}) = \frac{1}{N}\sum_{n=0}^{N-1} \mathrm{x}(\mathrm{t_n})\mathrm{e}^{-\mathrm{j}2\pi\mathrm{kn/N}} \quad k = 0 \ldots N-1, N = 2^m \tag{2.11}$$

where N is the number of samples per period.

The FFT is has a much more efficient computational algorithm and for large numbers of N a significant computation time saving is achieved. The FFT takes advantage of the similarity of many of the elements of the matrix formed by $e^{-j2\pi kn/N}$ and by factorising this matrix of into $log_2 N$ individual or factor matrices such that there are only two non-zero elements in each row of these matrices, one of which is always unity [**12**], [**38**], [**39**].

2.4.2 Characteristic harmonic orders of power systems

Due to the symmetries found in power system wave shapes, the harmonics that normally occur are referred to as characteristic harmonics. In general, the symmetry properties of the wave shapes give rise to the following effects [**8**], [**12**], [**16**], [**28**], [**38**]:

- Odd symmetry: $f(-t) = -f(t)$
  This results in al the $a_n$terms cancelling out and the Fourier series containing only sine terms.
- Even symmetry: $f(-t) = f(t)$
  This results in al the $b_n$terms cancelling out and the Fourier series containing only cosine terms.
- Half-wave symmetry: $-f(t) = f(t \pm \frac{T}{2})$
  This results in a cancellation of all even order harmonics and a zero DC component.

In power systems, except where non-linearities cause half-wave symmetry to be compromised, only odd harmonics are generated. Phenomena such as transformer saturation by heavy loading or inrush currents can remove half-wave symmetry that introduces lower order even harmonics [**8**], [**12**], [**16**], [**28**], [**34**], [**40**], [**41**].

2.4.3 Power system harmonic sequence components

In order to explain the harmonic interaction phenomena introduced by VSC schemes, it is important to establish the concept of harmonic sequence components.

On a basis of inspection, [**8**] describes the individual harmonic components of balanced three phase power systems to be entirely of positive-, negative-, or zero sequence by using the Fourier representation of phase voltages:

$$\boldsymbol{V_a}(t) = V_1\cos(\omega_0 t) + V_2\cos(2\omega_0 t) + V_3\cos(3\omega_0 t) + \cdots \quad (2.12)$$

$$\begin{aligned}\boldsymbol{V_b}(t) &= V_1\cos\left(\omega_0 t - 120^\circ\right) + V_2\cos\left(2\omega_0 t - 240^\circ\right) + V_3\cos\left(\omega_0 t - 360^\circ\right) + \cdots \\ &= V_1\cos\left(\omega_0 t - 120^\circ\right) + V_2\cos\left(2\omega_0 t + 120^\circ\right) + V_3\cos(\omega_0 t) + \cdots \quad (2.13)\end{aligned}$$

$$\begin{aligned}\boldsymbol{V_c}(t) &= V_1\cos\left(\omega_0 t + 120^\circ\right) + V_2\cos\left(2\omega_0 t + 240^\circ\right) + V_3\cos\left(\omega_0 t + 360^\circ\right) + \cdots \\ &= V_1\cos\left(\omega_0 t + 120^\circ\right) + V_2\cos\left(2\omega_0 t - 120^\circ\right) + V_3\cos(\omega_0 t) + \cdots \quad (2.14)\end{aligned}$$

It can be seen from the pure phase rotation of these quantities that the 1st, 4th, 7th, etc. harmonic orders are positive phase sequence, the 2nd, 5th, 8th, etc. harmonic orders are negative phase sequence and the 3rd, 6th, 9th, etc. harmonic orders are zero phase sequence harmonic orders [**12**]. It is also accepted that zero sequence harmonics disappear in line voltages and that triplen harmonics cannot flow into a delta or in the absence of a ground connection [**8**]. This will be further analysed and discussed in Section 3.1.1.

A more solid theoretical approach to reach the same result was presented 1918 by Charles Legeyt Fortescue [**34**], [**42**] to show that "*any set of N unbalanced phasors (that is, any such polyphase signal) could be expressed as the sum of N symmetrical sets of balanced phasors, for values of N that are prime. Only a single frequency component is represented by the phasors.*"

$$\begin{bmatrix}E_a\\E_b\\E_c\end{bmatrix} = \begin{bmatrix}\mathbf{1} & \mathbf{1} & \mathbf{1}\\ \mathbf{1} & \boldsymbol{a^2} & \boldsymbol{a}\\ \mathbf{1} & \boldsymbol{a} & \boldsymbol{a^2}\end{bmatrix}\begin{bmatrix}E_0\\E_1\\E_2\end{bmatrix} \text{ where } \boldsymbol{a} = e^{j\frac{2\pi}{3}}. \quad (2.15)$$

The harmonic sequence components from three-phase waveforms using complex quantities can be determined using the Fortescue Transform as described in [**6**], [**31**]- [**33**], [**42**].

A discrepancy exists, however, in the definition of the complex operator **a,** whereby **a** can be defined to be a harmonic dependant operator, i.e. [**6**]

$\boldsymbol{a}(h) = e^{j\frac{2\pi h}{3}}$ where h is the harmonic order.

Although the concept looks plausible at first glance, it is easy to show that for h=3n, the Fortescue transform, or inverse Fortescue transform, with this harmonic dependant definition of **a** gives the incorrect amplitude result for "triplen" harmonics that are known to be of zero

sequence nature. For any harmonic component, it should be possible to express this harmonic component in its positive phase sequence (PPS), negative phase sequence (NPS) and zero phase sequence (ZPS) components, irrespective of its angular velocity. Relative phase angles are harmonic order dependant, but are taken care of in the harmonic component expression (3.1).

The non-harmonic dependant definition of $\boldsymbol{a} = e^{j\frac{2\pi}{3}}$ for a three-phase system is in fact valid for determining the sequence components of waveforms containing harmonics [**31**]- [**34**] as also acknowledged by Fortescue [**42**]. This is also confirmed by the complex number theoretical expansion given in Section 3.1.1.

Harmonic sequence components can also be determined by using space vector components represented by the Clarke's components [**10**], [**41**].

Another way to determine harmonic sequence components where real time calculation is required, but without introducing the calculation delay typically experienced with discrete time implementations [**12**], has been illustrated by connecting together a group of phase locked loops in a special way in order to simultaneously separate out the sequence- and harmonic components of waveforms typical in power systems [**30**]. A STATCOM was used as a practical example to illustrate the robustness of this technique.

2.5 Principles of resonance and sensitivity

2.5.1 Conditions for resonance

For a true resonance condition to occur, two conditions need to be fulfilled, namely the generation of a certain harmonic order and a sensitivity to that specific harmonic order due to a series or parallel resonance point. The damping of the system will determine if the resonance condition will remain damped or grow out of control while excited. The damping is normally determined by the resistive components in the resonant circuit.

The movement of resonance points due to contingencies, system configurations, operating regimes and the operating points of dynamic devices also plays an important role in the harmonic analysis of a power system [**6**], [**8**], [**12**], [**16**], [**34**], [**35**].

2.5.2 Series resonance

A series resonance condition occurs in a series RLC circuit when the circuit impedance is at a minimum when inductive and capacitive reactance cancels out each other. A small excitation voltage then results in large currents [**8**], [**12**]. For a series RLC circuit, the total circuit impedance is given by

$$Z = R + j(X_L - X_C) \tag{2.16}$$

where R is the resistance, X_L the inductive reactance and X_C the capacitive reactance of the circuit.

It can be shown that $|Z|$ is at a minimum when $X_L = X_C$.

Using the relationship

$$X_L = 2\pi f L \tag{2.17}$$

where L is the inductance, f the circuit frequency and using the relationship

$$X_C = \frac{1}{2\pi f C} \tag{2.18}$$

where C is the capacitance, yields that $|Z|$ is at a minimum when

$$2\pi f_r L = \frac{1}{2\pi f_r C}\ .$$

The resonant frequency f_r of the RLC circuit is thus given by

$$f_r = \frac{1}{2\pi\sqrt{LC}}. \tag{2.19}$$

It can also be shown that the resonant harmonic h_r is given by

$$h_r = \sqrt{\frac{X_C}{X_L}}\ . \tag{2.20}$$

2.5.3 Parallel resonance

A parallel resonance condition occurs in a parallel RLC circuit when the oscillating LC part of the circuit is such that the inductive and capacitive reactances summate to zero and the total parallel circuit impedance is at a maximum. A small excitation current thus results in large voltage [**8**], [**12**]. For a parallel RLC circuit and using the relationships (2.17) and (2.18), the total circuit impedance is given by

$$Z = \left(\frac{1}{R} + j\left(\frac{1}{X_L} - \frac{1}{X_C}\right)\right)^{-1} \tag{2.21}$$

$$= \left(\frac{1}{R} + j\left(\frac{1}{2\pi f L} - 2\pi f C\right)\right)^{-1}. \tag{2.22}$$

It can be shown that $|Z|$ is at a maximum when $X_L = X_C$.

Using the relationships from (2.17) and (2.18), it yields that $|Z|$ is at a maximum when

$$2\pi f_r L = \frac{1}{2\pi f_r C}.$$

The resonant frequency f_r of the RLC circuit is thus given by

$$f_r = \frac{1}{2\pi\sqrt{LC}}. \tag{2.23}$$

It can also be shown that the resonant harmonic h_r is given by

$$h_r = \sqrt{\frac{X_C}{X_L}}. \tag{2.24}$$

2.5.4 System impedance versus frequency plots

In general for transmission systems, the positive phase sequence (PPS) impedance and negative phase sequence (NPS) impedance is assumed to be very similar. However, in the vicinity of large generation plant, the negative phase sequence can be slightly less due to the fact that generator negative phase sequence impedance is less than positive phase sequence impedance. The reason for this is that in the presence of NPS, the generator rotor sees a 2nd harmonic rotating in an opposite direction to that of the fundamental PPS. This causes rotor flux to saturate and lessens the flux penetration from the stator and thus yields a smaller impedance value [**16**], [**17**].

Although system impedance versus frequency could be plotted for both the positive and negative frequency domain due to different PPS and NPS system impedance, this is generally not done for harmonic studies due to the small differences encountered [**8**], [**17**].

One representation of the frequency response of a transmission network is the system impedance magnitude plotted against frequency to show parallel and series resonant points as shown in Fig. 2.11. Accompanying this diagram should be another one showing the real and

imaginary values of the impedance to indicate at what frequencies the system is inductive or capacitive as shown in Fig. 2.12 [**8**], [**12**].

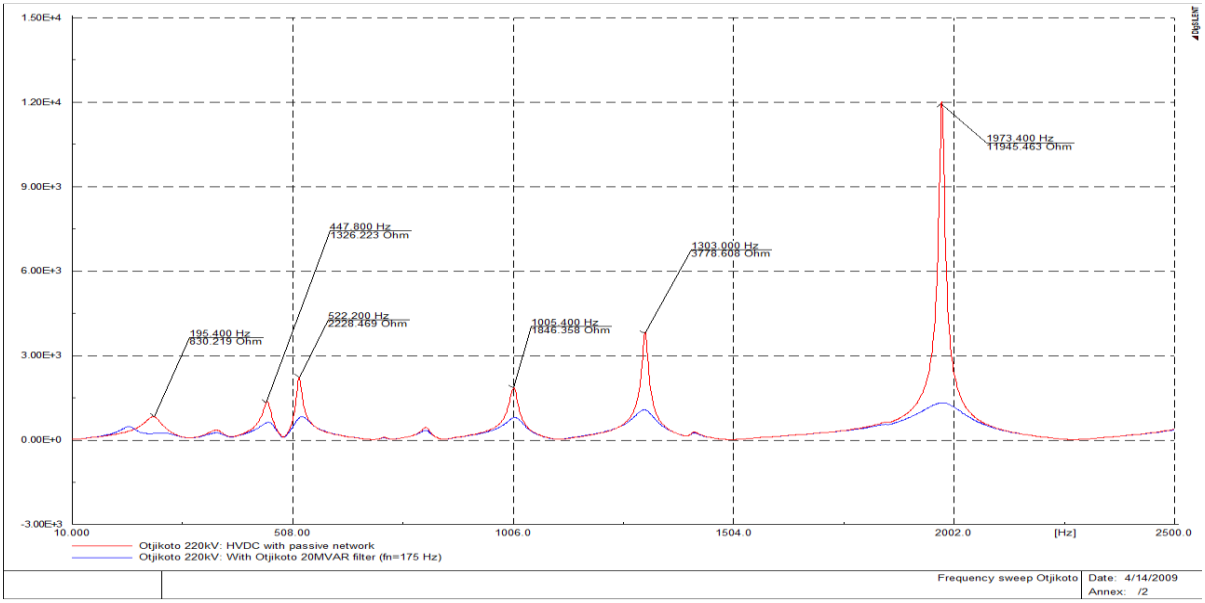

Fig. 2.11 Impedance magnitude versus frequency plot (Courtesy NamPower)

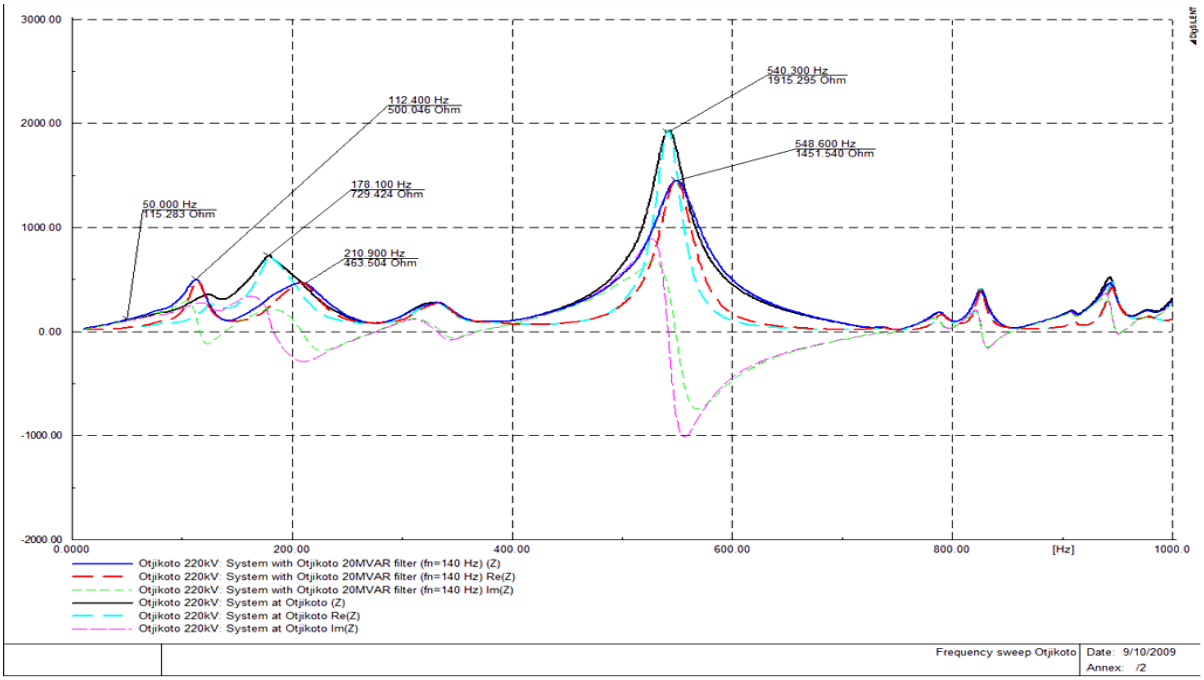

Fig. 2.12 Impedance, real and imaginary versus frequency plot (Courtesy NamPower)

Another representation used in filter design is an impedance XY plot as shown in Fig. 2.13, but here the resonant point frequency locations are not so clearly visible at first [**8**].

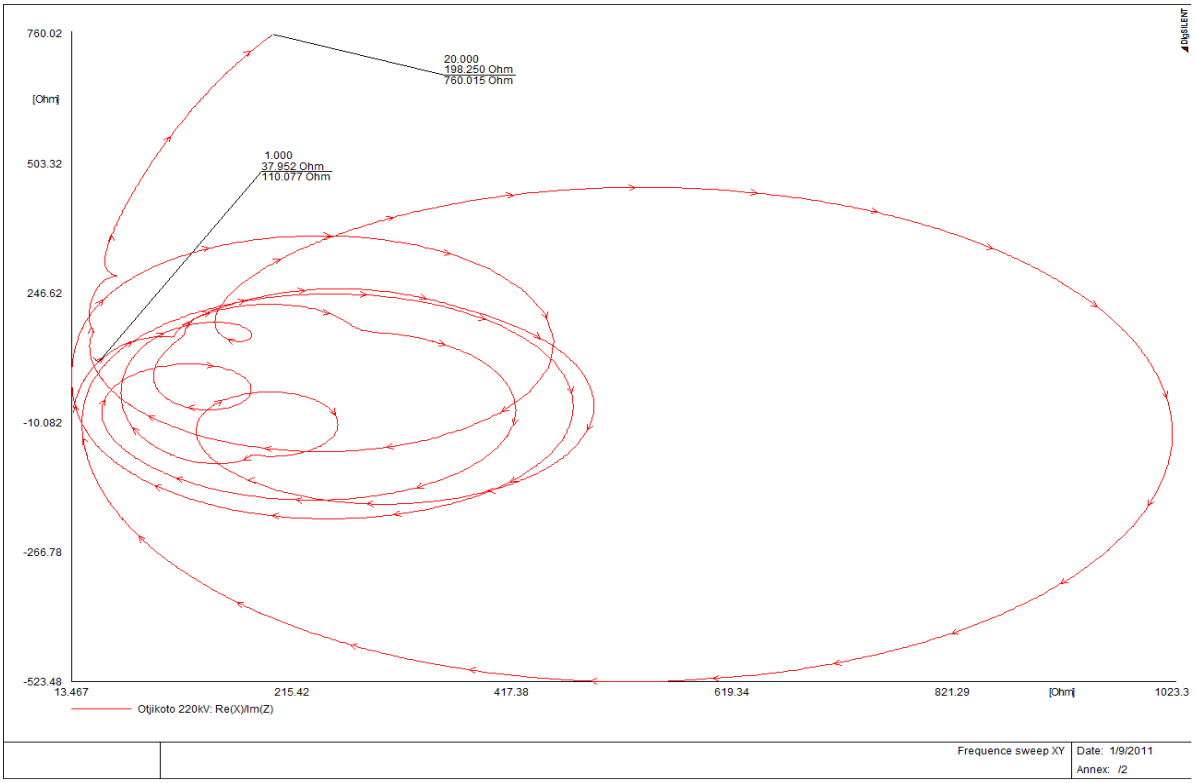

Fig. 2.13 Impedance XY plot (Courtesy NamPower)

All series and parallel resonance points seen in an impedance plot are not necessarily problematic. A rule of thumb for transmission systems to avoid dangerous resonance points is to consider a window as shown in Fig. 2.14. This window includes the following area where f is the frequency, $f_0 = 50Hz$ and Z_{f_0} is the system impedance at the nominal frequency of 50Hz. The window is defined by the relationship:

$$0.5\left|Z_{f_0}\right|\frac{f}{f_0} < |Z(f)| < 2\left|Z_{f_0}\right|\frac{f}{f_0} \tag{2.25}$$

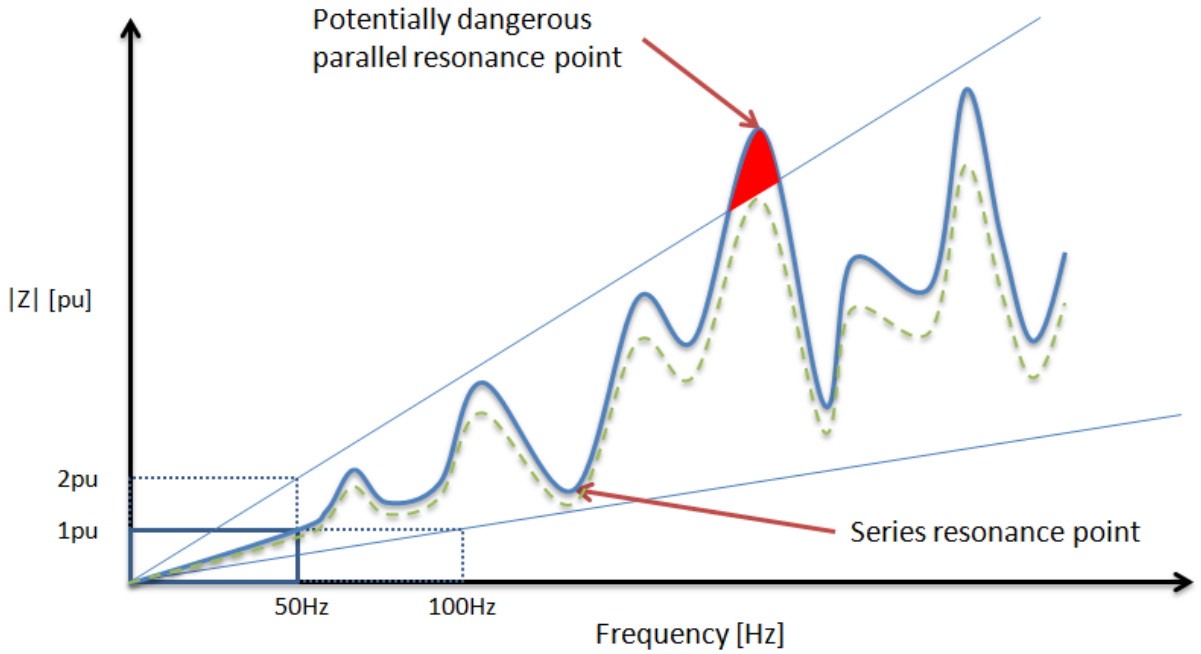

Fig. 2.14 Parallel and series resonant points [13]

For the harmonic integration of new equipment such as filter banks in the transmission system, resonant points that move outside this area defined by the thumb rule combined with the measured background harmonics normally give a good indication of probable resonance problems [**13**]. (*No clear published references for this rule of thumb could be found, except for experiences from trusted filter bank designers*.)

The reason for the typical system impedance increase of roughly $h = \frac{f}{f_0}$ over the frequency sweep is the dominance of inductive components in the transmission system, where $X(h) = hX_L$ with h being the harmonic order [**8**].

2.5.5 Simplified system modelling and capacitor banks

Due to the characteristics of transmission system equipment i.e. a generator with series line inductance and parallel capacitance, the system is considered to be predominantly inductive at the nominal operating frequency. At frequencies above the first parallel resonance point but below the next series resonant point, the system impedance could move to the capacitive region. In this region, the system behaviour would change completely. Where a reactor switched onto the system would normally lower the voltage, it would now raise the voltage. Where a capacitor bank switched onto the system would normally raise the voltage, it would now lower the voltage. For systems with very long transmission lines, low fault levels and at

high transmission voltages, the first parallel resonance point can move down very close to the operating frequency. The danger of a 50Hz resonance condition becomes eminent and must be properly managed [**13**].

When investigating the probable resonance point of a capacitor bank added to a system, an approximate model can be used where the system is modelled only as a series resistance and inductance. Adding a pure capacitor bank to the system then yield the following results [**8**]:

Using the relationships from (2.17) and (2.18), it yields that

$$L = \frac{X_L}{2\pi f} \tag{2.26}$$

and

$$C = \frac{1}{2\pi f X_C}. \tag{2.27}$$

The nominal frequency f_0 in Hz is related to the nominal angular velocity ω_0 in radians per second by

$$f_0 = \frac{\omega_0}{2\pi}. \tag{2.28}$$

Using (2.26) and (2.27), let

$$LC = \left(\frac{X_L}{X_C}\right)\left(\frac{1}{2\pi f_0}\right)^2 = \left(\frac{X_L}{X_C}\right)\left(\frac{1}{\omega_0}\right)^2. \tag{2.29}$$

For resonance to occur, $X_L = X_C$. By substituting (2.28) and (2.29) into (2.23), the resonant frequency f_r is given by the relationship

$$f_r = \frac{1}{2\pi\sqrt{LC}} = \frac{\omega_0}{2\pi\sqrt{\frac{X_L}{X_C}}}. \tag{2.30}$$

Let the circuit inductive reactance X_L be equal to the modelled system series reactance X_S, and let the system short circuit power S_{sc} , be given by the relationship

$$S_{sc} = \frac{V^2}{X_S} \tag{2.31}$$

where V is the busbar voltage where the capacitor bank is connected.

The reactive power Q_C delivered by the capacitor bank is given by the relationship

$$Q_C = \frac{V^2}{X_C}. \tag{2.32}$$

Using (2.31) - (2.32) and substituting into (2.30) yields that

$$f_r = f_0\sqrt{\frac{X_C}{X_S}}$$
$$= f_0\sqrt{\frac{S_{sc}}{Q_C}}. \quad (2.33)$$

The resonant harmonic h_r is therefore given by the relationship

$$h_r = \frac{f_r}{f_0} = \sqrt{\frac{S_{sc}}{Q_C}}. \quad (2.34)$$

As an example, according to the rule of thumb, a 40MVAR plain capacitor added to a system with a fault level of 800MVA at any voltage level will resonate with the system at the $\sqrt{\frac{800}{40}} = 4.47$th harmonic. Should the fault level increase in future, the resonant point will move towards the 5th harmonic and could pose problems should there be 5th harmonic generation in the area.

To provide for system contingencies and future fault level and where only a reactive power requirement is put forward and not to filter a specific harmonic order from the system, damped C-type filters tuned to about 10Hz below the resonant harmonic are often used. These filters are tuned such so as not participate directly in harmonic interactions and also to cater for system frequency variations, but still to provide the required reactive power at 50Hz [**13**].

Passive filter design for industrial applications using genetic algorithms to achieve the correct Power Factor (PF) consisting of the Displacement Power Factor (DPF) and Distortion Factor (DF) is an interesting recent development [**43**].

In cases where the placement of passive filters would cause too many complications with either the creation of new resonance points or the movement of resonant points due to system contingencies and fault level variations, either wide-band series/parallel filter solutions or active filtering systems could be considered [**44**].

2.6 Voltage Source Converter theory overview

2.6.1 Forced commutated voltage source converters

The principle behind voltage source converters is the fact that a stiff DC voltage source behind converted AC outputs gives voltage outputs instead of current outputs. Because the commutation instants between valves are controllable and independent of the AC voltage, it gives full control over the output of the converter. This is the principle of forced commutated or self-commutated valve switching [**10**].

A common configuration for a three phase forced commutated converter VSC is the two level bridge using IGBT valves with anti-parallel diodes as depicted in Fig. 2.15. Each bridge arm can conduct current in both directions because of the uni-directionality offered by the diodes and voltage polarity across each IGBT and diode switch combination. A change in power flow direction can now be realised by changing the DC current direction. This is done by changing the DC voltage of opposing converter stations allowing DC current to flow in the desired direction. The stiff DC source is provided by the DC capacitors that can store a significant amount of energy. Design considerations include active and reactive power capability, harmonic injection limits, valve switching losses and cost implications [**10**], [**22**].

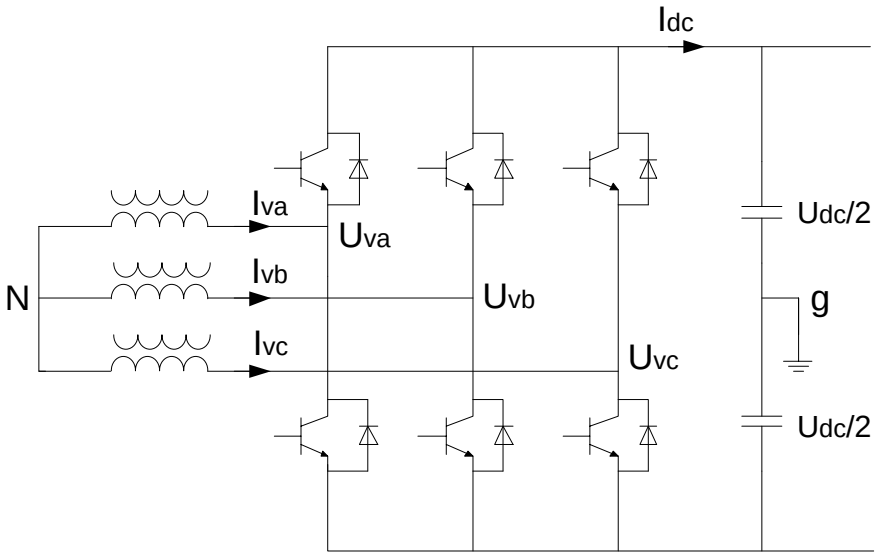

***Fig. 2.15 Basic VSC circuit layout** [10]*

2.6.2 Active and reactive power flow control

For any two interconnected AC power systems, the active and reactive power flow is determined by the connecting impedance as well as the magnitude and angle between the two

voltage vectors [**10**], [**16**], [**45**]. In this case, the VSC scheme represents one voltage source connected to an AC system via the combined converter reactor- and converter transformer impedances as shown in Fig. 2.16 (also see Section 2.3.6 and Section 2.3.7):

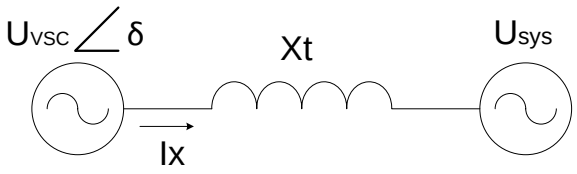

Fig. 2.16 Relative voltage angles and impedance (adopted from [10], [16])

The real power P that flows from the converter to the system is given by the relationship [**10**]

$$P = \frac{U_{sys}U_{VSC}}{X_t} sin(\delta), \tag{2.35}$$

where U_{sys} is the system voltage, U_{VSC} is the VSC terminal voltage, X_t is the reactance connecting the VSC to the system and δ denotes the voltage angle between the VSC and the system. Similarly, the reactive power that will be exchanged between the VSC and the system is given by the following relationship [**10**]:

$$Q = \frac{U_{VSC}(U_{VSC} - U_{sys}cos\ (\delta))}{X_t} \tag{2.36}$$

From these equations it can be seen that for no voltage angle difference, the real power equals zero and the reactive power is determined by the difference in voltage magnitudes. If $U_{sys} > U_{VSC}$, Q is smaller than zero and implies inductive operation (VSC absorbs reactive power). If $U_{VSC} > U_{sys}$, Q is larger than zero and implies capacitive operation (VSC delivers reactive power to the system).

For equal voltage magnitudes, the reactive power equals zero and the real power is determined by the voltage angle between the two vectors. If $\delta > 0$, power flows from the VSC to the system (inverter operation) and if $\delta < 0$, power flows from the system to the VSC (rectifier operation).

From the active and reactive power flow equations (2.35)-(2.36) it has been shown that four quadrant power control is possible and although active and reactive power can be controlled almost independently, there is a certain measure of coupling introduced by the VSC scheme

itself, as well as the connected AC systems. For reactive power control, the modulation index controls the AC voltage magnitude and the reactive power flow and the firing instant of the valves in relation to the AC side voltage determines the voltage phase angle and active power flow. The power capability graph is limited by the AC current capability of the converter (thermal limit) and the AC and DC voltage limits of the converter [**10**], [**16**].

For the voltages and currents shown in Fig. 2.17, the converter equations can be defined.

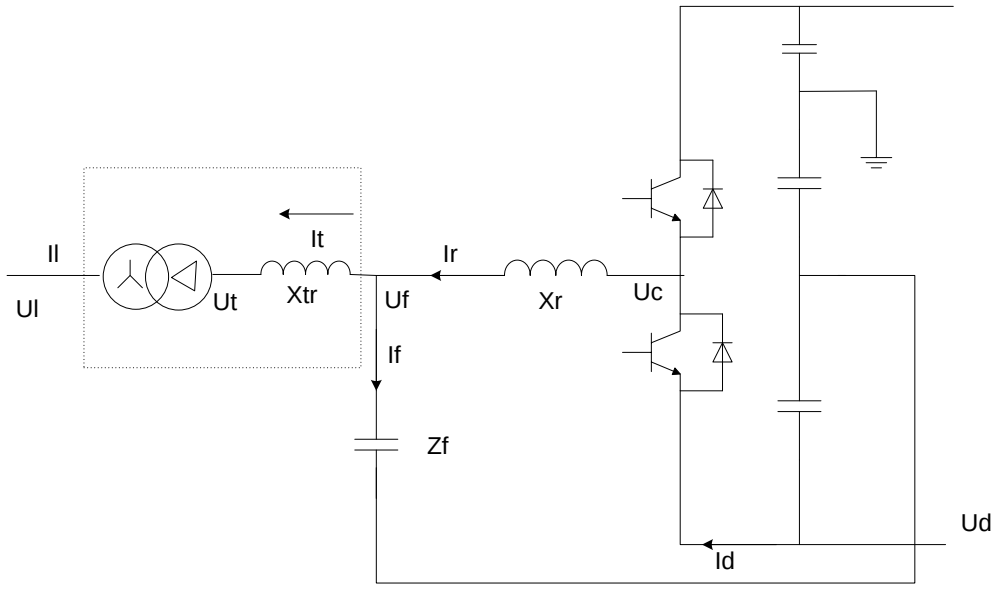

Fig. 2.17 VSC circuit quantities and flows (Courtesy ABB Sweden)

The converter voltage U_c is given by the relationship

$$U_c = U_f + X_r I_r \tag{2.37}$$

where U_f is the AC filter bus voltage, X_r is the converter reactor reactance and I_r is the current through the converter reactor.

The current I_r is given by the relationship

$$I_r = I_t + I_f \tag{2.38}$$

where I_t is the total current through the converter transformer and I_f is the current through the filter impedance Z_f.

The AC filter bus voltage U_f is given by the relationship

$$U_f = U_t + X_{tr} I_t \tag{2.39}$$

where U_t is the voltage on the primary side of the converter transformer connected to the system and X_{tr} is the converter transformer reactance.

The filter current I_f is given by the following relationship:

$$I_f = \frac{U_f}{Z_f} . \tag{2.40}$$

The converter equations as defined in (2.37) – (2.40) are shown as a vector diagram in Fig. 2.18.

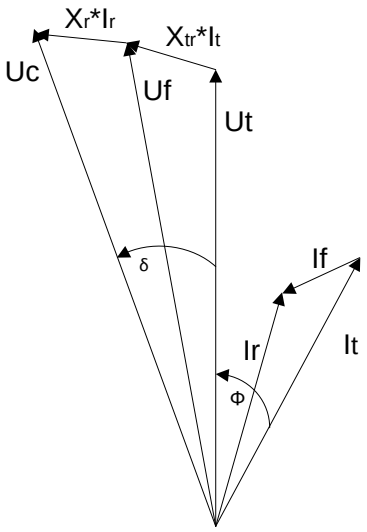

Fig. 2.18 VSC circuit vector representation (Courtesy ABB Sweden)

In Fig. 2.18 Uc can be equated to the converter voltage (U_{VSC}) and Ut to the system voltage (U_{sys}) without the transformer ratio and tap changer. Angle δ is the voltage angle across the converter reactor and transformer impedances and angle Φ is the angle between output voltage and current.

The illustration of a generator and infinite bus system with graph (generated by an Excel model and equations) in Fig. 2.19 and Fig. 2.20 shows the change in active power flowing between two systems as the voltage vector between them gradually increases due to a difference running frequencies. During a power swing condition (see relevance to Section 2.1.2) the same applies [**13**].

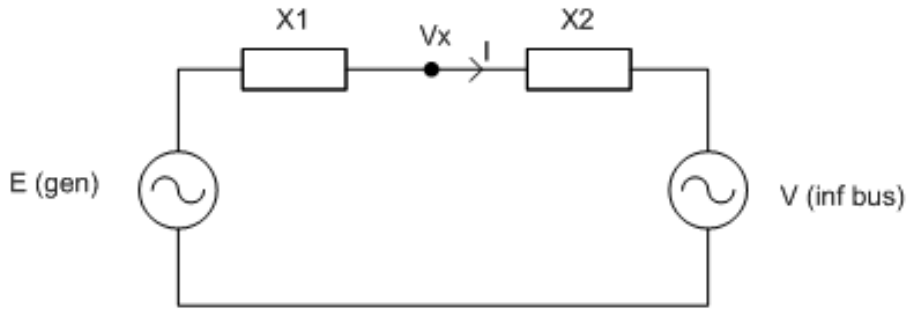

Fig. 2.19 Generator connected to infinite bus (adopted from [16])

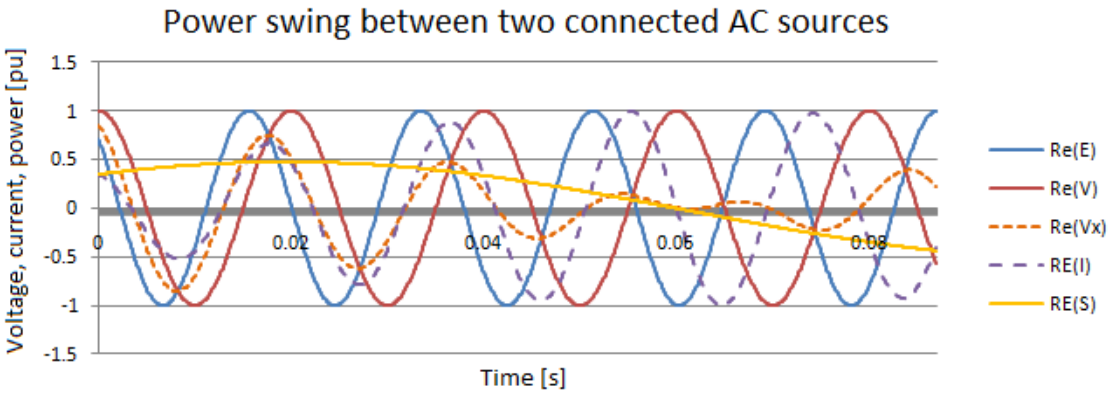

Fig. 2.20 Power swing of generator against infinite bus [13]

2.6.3 Insulated Gate Bipolar Transistor valve switching and operation principle

The operation principle of different VSC bridge configurations are generally the same and commutation takes place between valves connected to the same phase. For a three phase AC system, three sets of output voltages can be created at the desired frequency by switching the correct IGBTs sequentially at the correct times. The direction of current through each bridge arm is determined by which element, i.e. diode or IGBT, is conducting.

The basic relationships between AC and DC side quantities can be determined using the equivalent circuit shown in Fig. 2.21 [**10**], [**22**].

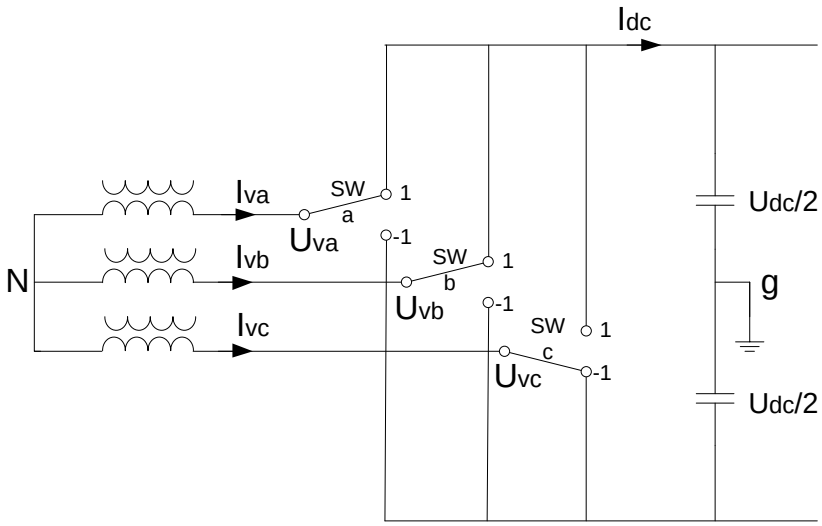

Fig. 2.21 VSC switching circuit [10], [22]

For this description, the switches commutate at fundamental frequency as shown in Fig. 2.22. The value of each switch (sw_x) is either 1 or -1 depending on whether the switch is connected to the positive or negative terminal of the DC voltage. Let the phase quantities U_{va}, U_{vb}, or U_{vc} with reference to ground be given by:

$$U_{xg} = sw_x * \frac{U_{dc}}{2} \quad where\ x = a, b, or\ c \tag{2.41}$$

The floating point neutral voltage to ground U_{Ng} is then given by the relationship

$$U_{Ng} = \frac{1}{3}(U_{ag} + U_{bg} + U_{cg}). \tag{2.42}$$

The output phase voltages will then be given by the relationship

$$U_x = U_{xg} - U_{Ng} = \left(sw_x * \frac{U_{dc}}{2}\right) - \frac{1}{3}(U_{ag} + U_{bg} + U_{cg}) \tag{2.43}$$

$$= \left(sw_x * \frac{U_{dc}}{2}\right) - \frac{1}{3}\left(sw_a * \frac{U_{dc}}{2} + sw_b * \frac{U_{dc}}{2} + sw_c * \frac{U_{dc}}{2}\right)$$

$$= \left(3sw_x * \frac{U_{dc}}{6}\right) - \frac{U_{dc}}{6}(sw_a + sw_b + sw_c)$$

$$= \frac{U_{dc}}{6} * (3sw_x - (sw_a + sw_b + sw_c)). \tag{2.44}$$

Let:

$$k_a = \frac{1}{6} * (2sw_a - sw_b - sw_c) \tag{2.45}$$

$$k_b = \frac{1}{6} * (2sw_b - sw_a - sw_c) \tag{2.46}$$

and

$$k_c = \frac{1}{6} * (2sw_c - sw_a - sw_b). \tag{2.47}$$

This gives the phase quantities for the VSC in terms of the DC voltage and basic switching functions [**10**], [**22**]:

$$\begin{bmatrix} U_a(t) \\ U_b(t) \\ U_c(t) \end{bmatrix} = \begin{bmatrix} k_a(t) \\ k_b(t) \\ k_c(t) \end{bmatrix} * U_{dc}(t) \tag{2.48}$$

The relationship between the switching positions and functions are shown in Fig. 2.22:

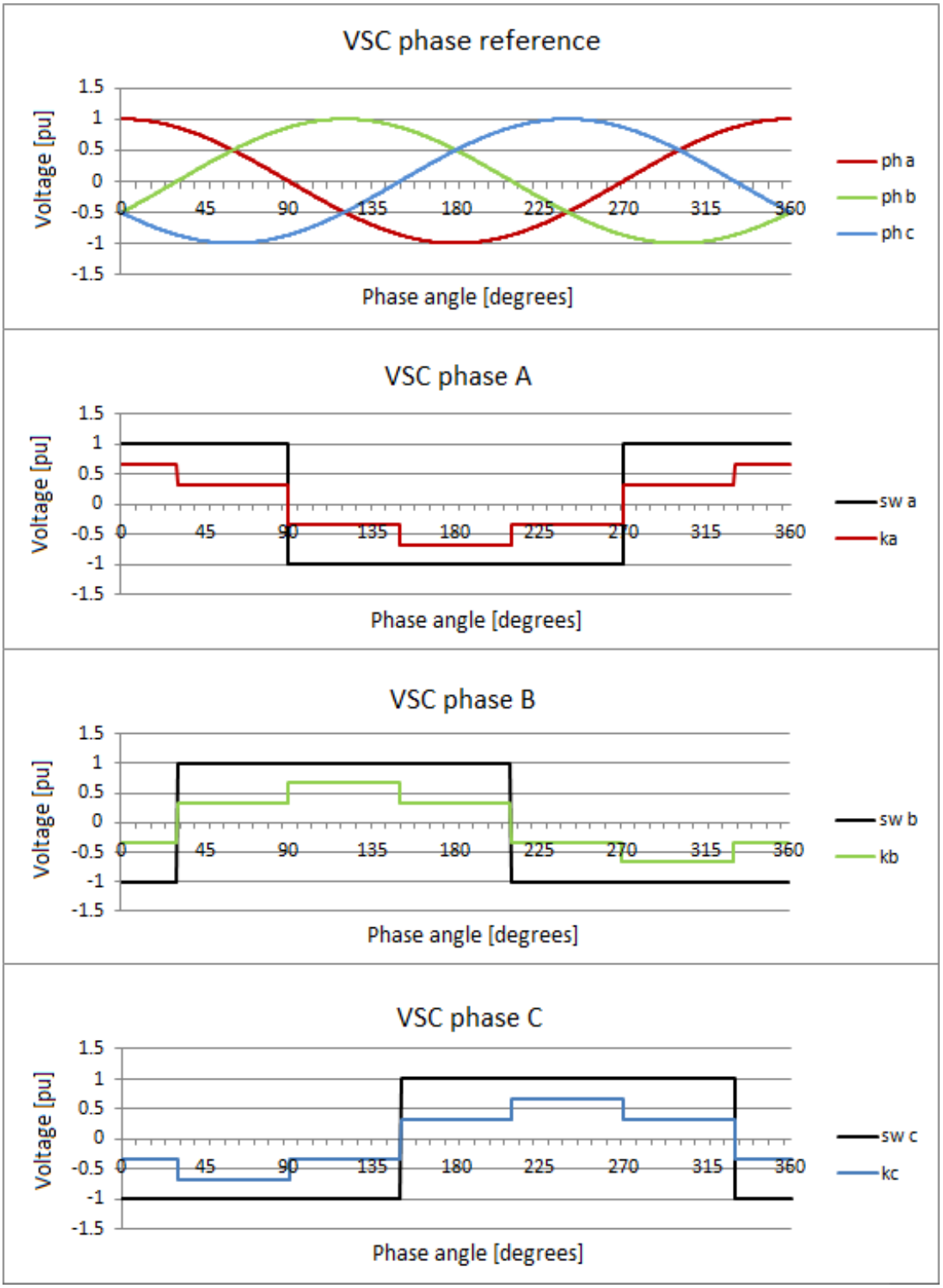

Fig. 2.22 VSC switching functions [10], [22]

The active power relationship between the AC and DC sides of the VSC is given by the relationship

$$p(t) = U_{dc}(t) * I_{dc}(t) = [i_a(t) \quad i_b(t) \quad i_c(t)] \begin{bmatrix} U_a(t) \\ U_b(t) \\ U_c(t) \end{bmatrix}. \tag{2.49}$$

It follows from (2.48) and (2.49) that

$$I_{dc}(t) = [i_a(t) \quad i_b(t) \quad i_c(t)] \begin{bmatrix} k_a(t) \\ k_b(t) \\ k_c(t) \end{bmatrix}. \tag{2.50}$$

The basic VSC relationships presented above are valid for any VSC circuit configuration, while the switching functions themselves depend on the converter switching frequency, modulation strategies, converter circuit configuration and transformer connections.

2.6.4 Insulated Gate Bipolar Transistor valve switching techniques and application

2.6.4.1 Overview of switching techniques

Section 2.6.3 explained the basic VSC switching principles and Fig. 2.22 effectively shows a square wave switching scheme switching at fundamental frequency. As will be shown Section 3.2.1, the harmonic content and thus fundamental component amplitude of the square wave switched waveform cannot be manipulated. Therefore specific valve switching techniques must be applied in order to have control over harmonic content and AC voltage magnitude [**28**], [**22**], [**46**].

Each of the different techniques and variations of techniques can be described in detail, providing interesting mathematical results when applying Fourier analysis to investigate the harmonic content. This section will only investigate the basic functionality and outcomes of a few switching techniques as this is not the main focus of the thesis. In Section 3.2, the switching techniques commonly used in VSC schemes will be investigated further as these influence harmonic cross-modulation. This section will consider the single phase application of these techniques in order to illustrate the fundamental concepts, while the next chapter will apply this to three phase systems.

2.6.4.2 Pulse Width Modulation

Switching techniques like PWM are used to control the AC output voltage independent of the DC voltage and to have some control over the harmonic content generated. To achieve this, the duty cycles of the converter switches are varied at a higher carrier frequency in order to control the average fundamental quantities [**22**], [**46**].

A (normally) sinusoidal output reference is compared to a triangular or saw-tooth wave shape. Depending on the comparison result, the output is switched between the two DC polarities. If the amplitude of the sinusoidal reference is controlled with respect to the triangular wave, the output voltage is varied. This ratio of the reference to the triangular carrier wave is called the modulation index [**28**]:

$$m_a = \frac{V_{control}}{V_{tri}} \tag{2.51}$$

The number of times the triangular wave is duplicated within one sinusoidal fundamental frequency f_1, is called the switching- or carrier frequency f_s. This gives the frequency modulation ratio [**28**]

$$m_f = \frac{f_s}{f_1}. \tag{2.52}$$

The fundamental component for modulation in the linear range is given by the relationship [**28**]

$$V_{a1} = \frac{m_a V_{dc}}{2}. \tag{2.53}$$

The PWM strategies described over the years can effectively be subdivided into three categories [**22**]:

- **Naturally sampled PWM**: The high frequency carrier signal is compared to the reference or target waveform and switching occurs at every intersection. The reference wave is assumed to have an infinite resolution and effectively refers to an analogue control system implementation [**22**].
- **Regularly sampled PWM:** The high frequency signal is compared to the reference or target waveform which itself has discrete values, i.e. has been quantified and regularly sampled. Switching occurs at every intersection. This implementation is suitable for digital systems implementation. If a sawtooth carrier it not used, but a triangular carrier wave,

sampling can be symmetrical or asymmetrical. Each of these choices has a slight effect on the fundamental component as well as individual harmonic amplitudes [**22**].

- **Direct PWM:** Also known as current-regulated modulation, switching occurs such that the integrated output of the converter is equal to, or within a certain band of the integrated target reference waveform. Two methods apply here, namely tolerance band control and fixed frequency control [**28**].

A PWM technique to increase the maximum available modulation index and thus the fundamental component magnitude applicable to three-phase inverters is called third-harmonic reference injection. By using this technique, the modulation index can be increased up to 1.15 by including a third harmonic injection of one-sixth without moving into the over-modulation region. The third harmonic injection is a common mode injection and has no effect on the phase to phase fundamental output voltage [**22**].

2.6.4.3 Square wave switching

Square wave switching is a special case of sinusoidal PWM where the modulation index $m_a$is so large that intersections between the carrier and reference waveform occur only when the reference waveform reaches a zero-crossing (see Fig. 2.22). The fundamental component is given by [**22**], [**28**]:

$$V_{a1} = \frac{4}{\pi}\left(\frac{V_{dc}}{2}\right) = 0.637V_{dc} \tag{2.54}$$

The frequency analysis of this switching scheme is continued in Section 3.2.1. The advantage of this scheme is the low number of switching instants and thus lower losses for high power applications. The drawback as stated in the introduction of this section is that the harmonic content and fundamental component amplitude cannot be controlled.

2.6.4.4 Optimised/programmed Pulse Width Modulation

The principle behind OPWM or programmed harmonic elimination is that an output waveform is constructed by switching at specific angles during the fundamental cycle. This waveform is effectively a square-wave switching scheme that is combined with PWM in order to typically control the fundamental component while minimising desired harmonic components [**22**], [**28**].

The switching angles are determined by pre-determining for each desired modulation index what the switching angles need to be to cancel out certain harmonics. If the modulation ratio $m_f = n$, then the number of angles available to switch at are $\frac{n-1}{2}$. These angles are normally numbered $\alpha_1,\ \alpha_2, \ldots\ \alpha_{\frac{n-1}{2}}$. The equations that these angles have to fulfil simultaneously are the formulas for the Fourier coefficients for the harmonic orders that are to be minimised, as well as the fundamental component or modulation index determination [**22**], [**28**].

Solving these equations can be done my using an n-dimensional form of Newton's method, or by using other non-linear solving algorithms provided by software packages such as Matlab, Lingo64 and even Excel. Other methods have also been described by [**47**]. These equations can be solved to control the fundamental- and harmonic components specifically, to obtain certain performance characteristics according to a specification (eg. certain allowable individual harmonic content or THD) or to minimise losses [**22**], [**47**], [**48**].

The maximum fundamental frequency component for this scheme is the same as for the square-wave switching scheme and is given by [**22**], [**28**]:

$$V_{a1} = \frac{4}{\pi}\left(\frac{V_{dc}}{2}\right) = 0.637V_{dc} \tag{2.55}$$

2.6.4.5 Random Pulse Width Modulation

Where applications of PWM is required where spectral energy cannot be concentrated at specific discrete frequencies, e.g. due to unwanted mechanical vibration in electrical machines as a result of pulsating flux from current harmonics, one approach is to spread to spectral energy over the frequency band and is referred to as Random Pulse Width Modulation (RPWM). This must be achieved without substantially increasing harmonic losses, considering band-limited noise generation and at the same time maintaining a linear transfer function between the fundamental input and output of the scheme [**22**], [**49**].

To implement this, the period of the carrier frequency is randomly varied, while remaining triangular within each half carrier period in order to maintain linearity of the modulation process. In this way, the PWM duty cycle remains proportional over any single period of the carrier signal to the value of the reference signal [**22**], [**49**].

2.6.4.6 Space Vector Modulation

Space Vector Modulation (SVM) is not a different modulation technique as such, but is a method to view phase quantities in a different space/domain in order to make use of a stationary plane as opposed to a rotating plane when doing online control [**10**]. (Also see Appendix C). Using the Clarke and Park transforms, but with zero sequence components included, the d-q-0 space vectors are used to represent the three phase quantities. For a three-phase inverter, only eight possible switch positions are possible, of which two are short circuit positions of the output. The remaining six positions represent active voltages as shown in Fig. 2.22 and forms a rotating hexagon on the d-q plane for each switching instant [**22**].

Using the d-q-0 transformation gives the advantage that complex number calculations need not to be done online by the control system and simplifies control strategy implementation [**10**], [**13**].

2.7 Alternating Current / Direct Current systems interaction overview

2.7.1 Dynamic interactions

2.7.1.1 Overview of dynamic interactions

With regards to dynamic interaction between AC and DC systems, a complete study can be dedicated to this topic. However, only a few concepts are highlighted here that have to be taken into account in the designing, commissioning and operating HVDC schemes [**4**], [**14**], [**16**]. Although similar, there are some subtle differences between the interactions observed when considering classical HVDC schemes as opposed to modern VSC schemes:

2.7.1.2 Short-circuit ratio

Most AC/DC interactions (dynamic and harmonic) are strongly influenced by the AC system strength compared to the HVDC scheme strength. This is often referred to as the system fault level or system short-circuit ratio (SCR).

$$SCR = \frac{AC\ system\ short\ circuit\ MVA}{DC\ converter\ MVA\ rating} \tag{2.56}$$

Although most sources refer to the classical HVDC converter MW rating, for VSC schemes the MVA rating can also be used. A definition that includes the effects of AC-side equipment such as filters, synchronous condenser, etc., is the Effective Short-Circuit Ratio (ESCR). The

ESCR classification is used traditionally to identify schemes in terms of potential interaction problems [**14**], [**16**]. With reference to the ESCR, the risk for problems can be summarised as follows:

- ESCR > 3: High
- 2< ESCR<3: Low
- ESCR<2: Very low

The ESCR of the Zambezi converter station is less than 0.7 under some network conditions [**13**]. This indicates the significance of the references to the achievement of operating a VSC scheme with overhead line on very weak AC systems [**4**].

The SCR or ESCR concepts have to be handled with caution as these definitions assume only a fundamental component fault current contribution, as well a constant contribution over the sub-transient and transient time windows. In reality, the fault current contribution changes significantly during the first fundamental cycle in accordance with the network time constant and DC capacitance discharge. Saturation effects and harmonic current contributions also effects AC protection systems. As a result, protection coordination and discrimination based on relay capabilities and reaction times become more complex. Modern relays that react during the first quarter cycle may need to be set differently to relays that rely on a half or full cycle buffered digital information [**13**], [**16**], [**17**].

2.7.1.3 Dynamic voltage interaction

During AC or DC system disturbances, the temporary blocking of the HVDC scheme could cause significant overvoltages due to the AC filter equipment still connected to the possibly weak AC systems. Depending on the fault clearing sequence, certain Transient Overvoltage (TOV) equipment capabilities have to be observed, as well as regulatory QOS requirements. Filter selection under weak network conditions can also be set differently to stronger network conditions to alleviate extreme TOV conditions to some extent. The reactive power requirements will also change during the blocked state due to the sudden change in active power flow. For VSC schemes, active voltage regulation can only resume after de-blocking again.

Another dynamic voltage problem can occur during high resistance DC line faults where the AC systems supply the fault, but at a fault level less than the converter rated power capability. During these conditions, the weak AC networks can suffer from severe voltage

depressions or even voltage collapse if networks are incorrectly configured until the high resistance fault is cleared by the HVDC protection [**13**]- [**16**].

2.7.1.4 Active and reactive power

For classical HVDC schemes, the amount of reactive power consumed in per unit (pu) is normally between 0.5pu and 0.6pu of the real power and typically has to be provided externally by filter banks close to the scheme. This is due to the fact that the connected AC system may already be approaching surge impedance loading and thus is unable to supply reactive power whilst maintaining voltage stability [**10**], [**14**], [**16**].

For VSC schemes, reactive power can be absorbed or generated according to the AC voltage set-point within the capability curve and MVA rating of the scheme. The VSC scheme is thus more suitable for weak network conditions. Reactive power absorption or generation, however, normally comes at a price in terms of increased converter switching losses [**10**], [**13**].

2.7.1.5 Sub-synchronous resonance

A resonance condition can occur between the mechanical generator turbine torsional oscillation modes and AC network electrical characteristics if negative damping components such as series capacitance are present. This resonance occurs below the synchronous frequency of 50Hz, normally 10-20Hz and is thus called Sub-Synchronous Resonance (SSR) [**14**], [**16**].

A HVDC scheme can also form a negative damping element in the AC transmission grid if the bandwidth of the current or power controllers is within the modes of oscillation of a turbine generator that is not de-coupled effectively enough by the connecting AC transmission system. Sub-synchronous Torsional Instability (SSTI) studies have to be done to investigate control system bandwidth, gains and phase relationships [**5**], [**10**], [**14**], [**16**].

2.7.1.6 Interaction with other system dynamic devices

As in the case of sub-synchronous resonance, HVDC control systems and the incorporation of power oscillation dampers (POD) have to be designed taking into account the existing transmission and generation dynamic devices control systems such as Static VAR Compensators (SVCs), generator Automatic Voltage Regulators (AVR's) and Power System Stabilisers (PSS's). If HVDC frequency controllers are present for islanded operation with other smaller generation, the frequency/power droop settings of the HVDC scheme and

generators also have to be correctly matched in conjunction with under-frequency load-shedding schemes present in the system [**10**], [**13**], [**16**].

2.7.2 Harmonic interaction

2.7.2.1 Overview of harmonic interaction

Although harmonic interaction has been described by some literature, most of these sources describe interaction for LCC or classical HVDC schemes. As an example, [**14**] refers to a 12-pulse classical HVDC scheme in terms of the cross-modulation of characteristic and non-characteristic harmonic orders.

The following sections will look at harmonic interaction for VSC schemes by the transfer of a DC-side harmonic to the AC-side as two sidebands and how an AC-side driving harmonic is translated to the DC-side. Lastly a summary of harmonic transfer rules are given.

2.7.2.2 Voltage Source Converter harmonic order transferred from Direct Current side to Alternating Current side

From Fourier analysis of VSC switching waveforms in Figure 2.22, Section 2.6.3 for a two level converter commutating at fundamental frequency [**10**], [**22**]:

$$\boldsymbol{k_{va}(t)} = \frac{2}{\pi}\sum_{n=1}^{\infty}(-1)^{\frac{n+3}{2}}.\frac{\cos\left(n(\omega t - \delta)\right)}{n} \tag{2.57}$$

$$\boldsymbol{k_{vb}(t)} = \frac{2}{\pi}\sum_{n=1}^{\infty}(-1)^{\frac{n+3}{2}}.\frac{\cos\left(n\left(\omega t - \delta - \frac{2\pi}{3}\right)\right)}{n} \tag{2.58}$$

$$\boldsymbol{k_{vc}(t)} = \frac{2}{\pi}\sum_{n=1}^{\infty}(-1)^{\frac{n+3}{2}}.\frac{\cos\left(n\left(\omega t - \delta + \frac{2\pi}{3}\right)\right)}{n} \tag{2.59}$$

For (2.57) to (2.59), δ denotes the phase angle between the AC voltage at the point of common coupling (PCC) and the VSC output voltage. Also, $n = 6m \pm 1, m = 0,1,2,\ldots$

Using Space Vector Notation from Section 2.6.4.6 and Appendix C, the complex vector that represents the three switching functions is given by [**10**]:

$$\boldsymbol{k_v(t)} = \frac{2}{\pi}\sum_{n=1}^{\infty}(-1)^{\frac{n+3}{2}}.\frac{e^{\pm jn(\omega_1 t-\delta)}}{n} \tag{2.60}$$

The complex vector $\boldsymbol{k_v(t)}$ is the sum of independently rotating vectors each rotating at a different nω clockwise or anti-clockwise depending on the exponent's sign. A positive sign implies positive phase rotation in the three-phase domain and a negative sign implies negative phase rotation in the three-phase domain.

Considering only the dominating fundamental component for now, the following approximation can be made for high power VSC converters:

$$\boldsymbol{k_v(t)} \cong \frac{2}{\pi}e^{j(\omega_1 t-\delta)} \tag{2.61}$$

Using the basic VSC relationships (2.48) and (2.50) presented in Section 2.6.3 and using the space vector transformation from Appendix C:

$$\boldsymbol{u_v(t)} = \boldsymbol{k_v(t)}.U_{dc}(t) \tag{2.62}$$

$$\mathbf{I_{dc}(t)} = \frac{3}{2}Re\left(\boldsymbol{i_v(t)}\,.\,\boldsymbol{k_v^*(t)}\right) \tag{2.63}$$

If a DC-side voltage harmonic is introduced at $\omega = 2\pi f$, the total DC voltage by superposition is given by [**10**]:

$$\mathbf{U_{dc}(t)} = U_{dc0} + U_{dch}\,.\cos(\omega t) \;=\; U_{dc0} + \left(\frac{U_{dch}}{2}.e^{+j\omega t} + \frac{U_{dch}}{2}.e^{-j\omega t}\right) \tag{2.64}$$

Substitute (2.61) and (2.64) into (2.62):

$$\boldsymbol{u_v(t)} = \frac{2U_{dc0}}{\pi}e^{j(\omega_1 t-\delta)} + \frac{U_{dch}}{\pi}.e^{j((\omega_1+\omega)t-\delta)} + \frac{U_{dch}}{\pi}.e^{j((\omega_1-\omega)t-\delta)} \tag{2.65}$$

- Thus a harmonic on the DC side will be transferred to the AC side as two side-bands given that: ($\omega > \omega_1$)
- For ($\omega_1 - \omega$) < 0 implicates a negative phase sequence component.
- For ($\omega_1 + \omega$) > 0 implicates a positive phase sequence component.

2.7.2.3 Voltage Source Converter harmonic transferred from Alternating Current side to Direct Current side

From [**10**] and Appendix C:

$$\boldsymbol{i_{(n)}(t)} = \mathrm{I_{m(n)}}\, e^{\pm j(\omega_n t+\varphi_n)} \tag{2.66}$$

Substitute (2.61) and (2.66) into (2.63):

$$\mathbf{I_{dc}(t)} = \frac{3}{2} Re\left(\frac{2}{\pi}.\mathrm{I_{m(n)}}\, e^{j(\pm\omega_n - \omega_1)t+(\delta_1 \pm \varphi_n)}\right) \tag{2.67}$$

- A positive sequence harmonic on the AC side transferred to the DC side gives only one of the side-bands at (ω_n- ω_1).
- A negative sequence harmonic on the AC side transferred to the DC side gives only one of the side-bands at (ω_n+ ω_1).
- An unbalanced harmonic on the AC side (with positive and negative phase sequence components) will give two side-bands on the DC side [**10**]:

$$\boldsymbol{i_{(n)}(t)} = \mathrm{I_{mp(n)}}\, e^{+j(\omega_n t+\varphi_{p(n)})} + \mathrm{I_{mn(n)}}\, e^{-j(\omega_n t+\varphi_{n(n)})} \tag{2.68}$$

$$\mathbf{I_{dc}(t)} = \frac{3}{\pi} Re\left(\mathrm{I_{mp(n)}}\, e^{+j(\omega_n - \omega_1)t+\delta+\varphi_{p(n)}} + \mathrm{I_{mn(n)}}\, e^{-j(\omega_n + \omega_1)t-\delta+\varphi_{n(n)}}\right) \tag{2.69}$$

2.7.2.4 Alternating Current / Direct Current Harmonic transfer summary

The representation in Fig. 2.23 shows the summary of the AC/DC harmonic transfer rules as derived above where the symbol (+) denotes PPS and (-) denotes NPS in the Space Vector Domain:

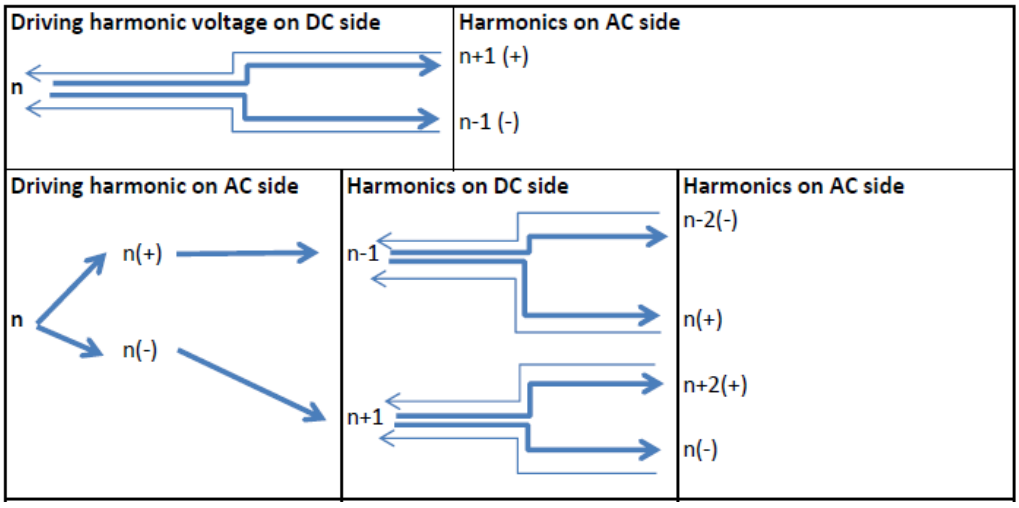

Fig. 2.23 Harmonic transfer rules (adopted from [10])

Note that a single balanced three phase harmonic on the AC side only generates a single side band on the DC and not both sides. Else, the wrong conclusion could be made that VSC schemes do not only transfer harmonics between the AC to DC sides, but also proliferate the number of harmonics infinitely [**10**].

2.8 Simulation techniques for electromagnetic transient- and harmonic studies

2.8.1 Transmission lines

The different mathematical models that exist to model transmission lines vary from the simple T model and nominal or equivalent PI models with simple L and C parameters to more complex and optionally distributed models where every physical attribute determining the L and C components are taken into account. These range from the conductor bundling, material conductivity, conductor spacing, tower geometry, ground resistivity, phase transpositions, mutual couplings, etc. In general, the main parameters reduce to a series resistance, series inductance, shunt capacitance and shunt conductance [**8**], [**40**].

Where multiple circuits on the same structure need to be taken into account, this geometry must be indicated, as well as the parameters of line length and voltage level. Earth wire spacing and conductor parameters are also important aspects [**12**], [**40**].

Typically a lumped or distributed model can be selected in software packages depending on the intended simulation purpose. The increase in resistance and decrease in internal inductance due to skin effect is proportional to $\sqrt{\omega}$. For frequency sweeps above 1kHz and for EMT- and harmonic distortion studies where long lines are present, a distributed model with frequency dependant parameters, where both the surge impedance Z_c and the propagation factor γ are a function of the frequency, should be utilised for accurate results [**8**], [**12**], [**13**], [**50**].

2.8.2 Power transformers

Transformer models in software packages are generally defined to include MVA rating, positive- and zero sequence winding impedance in percentage and normally referred to the HV MVA rating, copper losses, magnetizing impedance, zero-sequence magnetizing impedance, tertiary winding parameters if a three winding transformer, vector group and phase shift, neutral earthing parameters and tap changer parameters [**40**], [**50**], [**51**].

These parameters relate to the equivalent transformer circuit with an ideal voltage transformation ratio, effective primary and secondary series resistances, primary and secondary leakage reactances, shunt conductance that resembles iron losses and shunt inductive susceptance that is equivalent to the quadrature magnetising current at no load [**40**], [**16**], [**50**].

The transformer vector group, zero sequence circuit modelling and stray capacitances are important to model correctly for EMT and harmonic studies. For studies of specific effects such as transformer inrush currents and ferro-resonance [**52**], inter-winding stray capacitances, winding to ground stray capacitances and core saturation should be included in the transformer model. Saturation characteristics can normally be entered as a two-slope, polynomial, or piece-wise linear approximation. Here the knee-point flux, linear (unsaturated) reactance, saturated reactance and saturation exponent are common parameters. Residual flux or remanence that plays a role in transformer energisation and inrush currents and Ferro-resonance can also be modelled by specifying the d, q, 0 residual flux components. Geomagnetically Induced Currents (GIC) can also be modelled by using the transformer saturation parameters in conjunction with a DC voltage source in the transformer neutral connection [**50**], [**51**].

2.8.3 Synchronous generators

Generators and motors are probably the most complex equipment to accurately model, with many parameters applicable to different types of transient phenomena. These range from synchronous, transient, to sub-transient and are important for protection- and EMT studies.

Important parameters are the direct axis synchronous reactance (Xd), direct axis transient reactance (Xd'), direct axis sub-transient reactance (Xd"), armature time constant (Td), direct axis transient time constant (Td'), direct axis sub-transient time constant (Td"), open circuit voltage (E) and machine inertia constant (H) [**40**], [**50**].

Other machine stability parameters are the rotor saliency represented by the quadrature axis parameters Xq, Xq' and Xq" and the associated time constants T'_{qo} and T''_{qo}. The excitation system modelling and governor system modelling depending on the prime mover type is also important to model correctly for dynamic studies especially when considering machine stability and the designing of power system stabilisers [**16**], [**40**].

With regards to harmonic studies, the machine sub-transient reactances and flux saturation values are of importance. Harmonic content can cause increased copper and iron losses and

thus increased heat is a resultant effect. Pulsating torques is another effect that results due to the interaction of harmonic-generated magnetic fields and fundamental frequency magnetic fields. The rotor harmonics are also generated as a result of stator harmonics at one order less than the stator harmonic order (h_f-1) where the stator harmonic order is of positive or negative phase rotation in the space vector domain. Harmonic orders of PPS and NPS pairs can give rise to pulsating torques. For example, a combination of PPS harmonics (harmonic orders of 4,7,10,...) and NPS harmonics (harmonic orders of 2,5,8,11) can give rise to pulsating torques due to rotor harmonic orders of 3,6,9,12,... . Should the natural frequency of the machine be close to one of these harmonic orders, super-synchronous resonance and torsional oscillation leading to serious mechanical damage can occur [**8**].

2.8.4 Reactors, capacitors and filter banks

Reactors and capacitors are generally modelled simply as inductive (L) or capacitive (C) components and in combination to form filter banks. The reactor series resistance (R) is also modelled although normally relatively small. Filter bank configurations can range from a simple series L and C combination, to a C-type filter with C1, C2, L and parallel R value, to a double-tuned filter with series-parallel L and C combinations. In some packages, the filter MVAR rating, tuning frequency and quality factor can be entered and the relevant L and C values are automatically calculated. The three phase filter connection in star (where neutral earthing details come into play) or delta with stray capacitances is also important for zero-sequence circuit modelling [**8**], [**40**], [**50**].

2.8.5 Voltage Source Converter High Voltage Direct Current

For HVDC Voltage Source Converters, PWM switching elements and a PLL is normally used in conjunction with DC capacitors, series reactor and or transformer, AC-side filters, DC-side filters, DC line, etc. The complexity of the PWM element can vary from a steady-state voltage source for loadflow simulations, to detailed firing control to simulate exact valve firing in EMT studies. In order to protect the intellectual property of valve control techniques, dynamic link library (DLL) files with valve control code are often compiled from code to serve as a “black box” where manufacturer models are to be distributed to clients. Several controllers are normally present to model the HVDC control system at each converter station, namely DC voltage control, AC voltage or reactive power controllers, phase locked loop to synchronise fire instants with AC system voltage and power control. Phase angle measurement between the AC system and the valves across the converter reactor and

transformer is also required as an input to the active and reactive power controllers [**14**], [**22**], [**50**], [**51**].

2.8.6 Harmonic loads

Normal loads can be modelled to be frequency dependent as either a series or parallel combination of resistance and inductance whereby which these will draw different harmonic currents due to harmonic voltages. This would be valid for harmonic load flows as well as for EMT studies [**8**], [**50**].

For harmonic loads [**53**], the common practice is to specify harmonic currents as a percentage of fundamental current in either balanced or unbalanced fashion. This can be used to model for example a specific variable speed drive according to manufacturer data. A 6-pulse VSD would for instance draw 5^{th}, 7^{th}, 11^{th}, 13^{th}, 17^{th}, 19^{th} ... harmonics, while a 12-pulse VSD would draw 11^{th}, 13^{th}, 23^{rd}, 25^{th}, etc. This method is normally only applicable to harmonic loadflow studies. For EMT studies, harmonic EMT loads have to be modelled specifically for certain software applications [**8**], [**12**], [**50**].

The hybrid time/frequency domain modelling of non-linear components proposed by B.C. Smith et al [**54**] could also be used.

2.8.7 Dynamic models and simulation

Dynamic simulations are normally classified either as time domain root mean square (RMS) or EMT simulations. The purpose of RMS studies are to observe the RMS values of waveforms rather than instantaneous values and generally slower transient conditions where slower control system phenomena such as generator AVR and governor behaviours, power system stabilisers, sub-synchronous resonance due to series capacitors or control system interactions, etc. need to be studied. Inter-machine and inter-area oscillation modes can be better observed without the 50Hz component cluttering the waveform. The purpose of EMT studies are to do small time step simulations in the microsecond range to observe instantaneous values of waveforms to study electromagnetic transient effects during events like equipment energisation, breaker pre-strike, fault conditions, harmonic- and resonance phenomena, saturation, transferred saturation, ferro-resonance, travelling wave effects, TOV and surge arrester studies [**8**], [**13**], [**40**], [**16**], [**50**], [**51**].

For dynamic studies, i.e. RMS or EMT, every dynamic device in the system would normally have its control system modelled either as a piece of programmed code, a compilation of

logic functions, or a combination. These devices would include SVC's, HVDC schemes, generator governor and AVR systems and automated reactor switching schemes.

The simulation time step size has a definite influence of the accuracy in some applications like HVDC VSC schemes, but impacts negatively simulation execution time and requires more processing power. This is where RTDS systems play an important role in factory testing of systems as real-time simulations connected the actual plant protection and control system hardware has a definite advantage. Yet, the quality of the output data is no better than a normal computer using the same time step size and model to calculate the same output results, although taking much longer to complete [**13**], [**40**], [**50**], [**51**].

2.8.8 Harmonic modelling and simulations

All equipment in the power system that has frequency dependant parameters must be properly modelled in order to get accurate results when performing harmonic simulations. The simplest harmonic simulation is a harmonic loadflow where essentially a normal loadflow is performed at different frequencies and harmonic loads modelled to generate harmonic voltages or currents with specified amplitudes and phase angles at specific frequencies. In this way, pre-existing background harmonics that have been measured in the field can also be modelled to get an accurate picture should new harmonic loads be added to the system [**55**], [**53**].

For certain devices such as VSCs, an EMT model may be required to do time domain simulations of the valve switching [**56**]. The EMT time domain waveforms from these simulations then need to be analysed to determine the harmonic content in order to model an accurate equivalent harmonic load. In most cases, the dynamics of the control system behind the VSC element may perform such that a single harmonic load or PWM harmonic content cannot be modelled and a harmonic loadflow study may prove insufficient. In this case, frequency domain analyses of EMT waveforms are required to do a harmonic analysis [**8**], [**23**], [**35**], [**50**], [**51**]. As referenced in Section 2.8.6, the hybrid time/frequency domain modelling of non-linear components proposed by W. Wiechowski et al [**54**] could also be used.

2.8.9 Frequency domain analysis

2.8.9.1 Simulation frequency sweep

The impedance versus frequency sweep simulation is done to ascertain the network frequency response and to identify series and parallel resonance points. Although the impedance magnitude is normally sufficient, the imaginary part of the impedance sometimes gives useful information if the system will behave predominantly inductive or capacitive at a certain frequency.

These frequency sweeps are useful in filter bank designs when adding a filter to an existing network with known background harmonics. The network frequency response with and without the filter under different contingencies can be compared to generate a harmonic amplification curve to see what existing harmonics will be amplified and by how much. The filter tuning frequency and quality factor can then be varied to obtain the best magnification curve depending on the purpose of the filter. The magnification curves are to be compiled for all different system contingencies and fault levels to ensure robust designs [**8**], [**12**], [**40**], [**50**].

2.8.9.2 Fast Fourier Transformation – effects, limitations and alternatives

In practice, time domain waveforms that are generated by real life Transient Fault Records (TFRs) or by time domain EMT simulations often have to be analysed to determine the frequency domain information contained in it. For this, the most common transformation used by modern computing systems is the Fast Fourier Transformation (FFT). However, this sensitivity of the FFT to both the time resolution of the simulation and the periodicity of the overall waveform has been highlighted. Where the small magnitude sideband or baseband harmonics are of interest in harmonic analysis of PWM techniques using time simulation studies, the FFT is only effective for exact integer carrier harmonic orders [**22**], [**39**].

According to the sampling theorem, the sampling frequency must at least be twice the highest frequency contained in the original waveform to correctly transfer information to the sampled system. The frequency component at half the sampling frequency is called the Nyquist frequency. Misinterpretation of frequencies above the Nyquist frequency as lower frequencies is called aliasing, but can be avoided by passing the original time domain signal through a band-limited low pass filter with cut-off frequency set appropriately below the Nyquist frequency [**12**], [**38**].

The windowing effect is inevitable as time domain functions can practically only be observed for a limited time period with implied infinite periodicity. This effect can introduce errors in the frequency spectrum as this effective multiplication by a rectangular window in the time domain results in convolution in the frequency domain with a sinc pulse function. If the window function is not synchronised to multiples of the fundamental frequency, non-periodic noise will contribute to spectral leakage. This convolution in the frequency domain also gives rise to the picket fence effect whereby the time domain function is effectively filtered by a series of filters at integer multiples of 1/T where T is the sampling period. If the analysed signal contains non-discrete, non-orthogonal frequencies, the non-ideal effect of the DFT filter will cause such frequencies to be seen by more than one such time domain filter at a time, but at reduced amplitude. This effect can be reduced by zero-padding. Adding a number of zero values to the time domain waveform normally equal to the original record length effectively increases the sampling period T by introducing extra DFT filters between the original filters. Yet, the bandwidth of the original filters still depends on the original sampling period and is not affected by zero-padding [**12**], [**38**], [**57**].

Alternatives to the FFT also exist, namely the Walsh transform, Hartley transform and the Wavelet transform. If phase information is not required, the Hartley transform is an efficient alternative to the FFT. The discrete implementation of the Wavelet Transform (DWT) is normally implemented using Multi-Signal Decomposition (MSD) on different scales starting at the Nyquist frequency downwards depending on the resolution required. High and low pass filters are used to split each signal to the next scale level [**12**], [**58**]. The “fast non-similarity wavelet transform” method has also been developed and describes techniques to decrease computation time and to reduce storage space [**59**].

2.9 Simulation tools

2.9.1 General discussion on software simulation tools

In the power systems- and power electronics environment, there are many simulation packages and tools available to assist the engineer in the modelling, simulation and analysis of power systems including high-voltage devices that contain power electronics and control systems. These tools also assist with the representation of data and interpretation of results.

The danger with any computerised simulation is that no mathematical model is a 100% identical copy of reality and that any incorrect input parameter may give the wrong output

results. The principle of garbage in, garbage out applies. Certain modelling assumptions or simplifications could also yield different results than measured in reality.

The other danger of computerised simulations is that of simply pressing a button and getting results without doing some hand calculations to at least get an idea of what the results should look like and just blindly accepting the simulation outputs. Results should make intuitive sense and unexpected phenomena should be investigated and plausible reasons investigated and tested.

Each simulation tool or package has certain strong points and certain weaknesses depending on their intended purpose, developmental history, software platforms, operating systems, etc. Each tool should be known and understood in order to select the right tool for the task required. If two similar tools can do the same job, it could be worthwhile to compare results and to try to identify and understand differences in results in order to make better choices for future studies. License costs versus benefits also play a definite role, as well as after-sales technical support, online support, etc. [**8**], [**12**], [**13**].

2.9.2 PSCAD/EMTDC

PSCAD/EMTDC is a power systems simulation tool that has been developed over many years and started off in the 1970's as EMTDC (Electromagnetic transients and DC) as inspired by Dr. Hermann Dommel's paper on Digital Computer Solution of Electromagnetic Transients in Single- and Multiphase Networks [**60**]. The first version were utilised at Manitoba Hydro on mainframe computers using punched cards and were used to analyse the Nelson River HVDC power system in Manitoba, Canada. The first lines of code were written Dennis Woodford at Manitoba Hydro who extended Dr Dommel's equations to HVDC systems.

PSCAD is the graphical visual interface to EMTDC in which circuits are constructed, simulations run and results plotted. Typical PSCAD studies include [**51**]:

- Contingency studies of AC networks consisting of rotating machines, exciters,
- governors, turbines, transformers, transmission lines, cables and loads
- Relay coordination
- Transformer saturation effects

- Insulation coordination of transformers, breakers and arrestors
- Impulse testing of transformers
- Sub-synchronous resonance (SSR) studies of networks with machines, transmission lines and HVDC systems
- Evaluation of filter design and harmonic analysis
- Control system design and coordination of FACTS and HVDC; including STATCOM, VSC and cycloconverters
- Optimal design of controller parameters
- Investigation of new circuit and control concepts
- Lightning strikes, faults or breaker operations
- Steep front and fast front studies
- Investigate the pulsing effects of diesel engines and wind turbines on electric networks

PSCAD/EMTDC is a very suitable tool and often the preferred tool for any EMT-related study and therefore also for the analysis of HVDC schemes and harmonic interaction as pertaining to the topic of this thesis, although the setting up of models and cases can take some time and a certain amount of experience helps to correctly set up all the components.

With newer corporately endorsed 64-bit operating systems like Windows7, it may take some time to correctly set up all the components and FORTRAN compiler. Initialisation of PSCAD models and control systems has to be done in the correct manner to reach steady state values. Then taking and storing snapshots with steady-state values to start the next simulation can be done in order to save some time [**13**], [**51**].

2.9.3 DigSilent PowerFactory

Although DigSilent PowerFactory is perhaps a younger simulation tool, it caters for a wide variety of studies, options and functions for different types of studies with an all-in-one program, compiler, good models and a visual graphical user interface. Among the license options that are selectable are:

- Loadflow (Balanced or three-phase unbalanced)
- Optimal power flow

- Short circuit (complete, according to ANSI or according to IEC)
- Stability functions (RMS, long term, EMT)
- Flicker analysis
- Contingency analysis
- Reliability analysis
- Generator adequacy analysis
- Optimal Capacitor placement
- Modal analysis
- Network reduction (Loadflow, short circuit)
- Harmonic calculation
- Frequency sweep
- Filter analysis
- Distance Protection (Relay models)
- Over-current protection (Relay models)
- Other tools (DGS import and export)
- State estimation

The building of networks, models and organisation of model parameters and data in the "Data Manager" is simple and fairly intuitive. The setting up of cases, network variations, initialisation of models, etc is also fairly simple to do. The 64-bit versions of PowerFactory with multi-threading enabled runs a fair amount quicker than on a 32-bit system with single processor.

The state estimation and RMS function have been used by NamPower as a real-time simulator connected with the National Control Centre SCADA system to aid system controllers in decision-making by providing a real time updated simulation environment from system snapshots from where a certain operation can then be performed and the results ascertained before performing the operation on the live system.

For protection-related studies, almost all modern protection relay models are available for PowerFactory from the various relay manufacturers and can easily be used for protection studies, settings calculations and other verification studies such as exporting a simulated EMT file to a Comtrade format, importing into a waveform generator such as the Omicron

test set and injecting the voltages and currents into the real relay. Hereby true relay operation can be compared with the relay model in PowerFactory [**13**], [**50**].

For the purpose of this thesis, the frequency sweep function and EMT stability functions could be utilised. Loadflow simulations are almost always done as given and a quick check to see that steady-state results make sense and that the model iterative methods with tolerances solve without problems.

2.9.4 Real Time Digital Simulator systems

The purpose of Real time digital simulator (RTDS) systems is to incorporate specialised software on a specialised hardware platform where small time step simulations need to be executed in real time. As first developed at the Manitoba HVDC Research centre in the 1980's, RTDS Technologies (Inc) produced the world's first real time digital simulator. RTDS systems have a wide area of application and are commonly use for the testing and development of:

- Protection and control schemes
- Control systems of HVDC, SVC, synchronous machines and FACTS devices
- AC and DC system operations and behaviour
- Interaction of AC and DC systems
- Demonstration and training purposes

The visual RTDS environment called RSCAD can run the same compiled code as generated in PSCAD/EMTDC and is often used to switch between desktop studies and RTDS studies. The hardware is based on a modular set up that includes parallel processing features, input/output cards for interfacing to protection and control systems and different modes of inter-card communication to avoid communications bottlenecks [**13**], [**61**].

RTDS systems have also been used in the NamPower network during the testing and commissioning of the Auas SVC and Caprivi Link VSC HVDC schemes [**13**].

2.9.5 Matlab

The Matlab language of technical computing by Mathworks has been around since 1984 and with its multi-domain simulation environment (Simulink) provides a powerful mathematical tool to model anything from complex mathematical functions and algorithms to control

systems, signal processing, power systems, mechanical systems, financial modelling and aeronautical systems, to automotive systems.

Although the application of Matlab is a lot wider than just power systems, many models do exist for power systems components such as lines, transformers, synchronous machines, voltage sources converters, etc.

Other useful functions that can be utilised in this thesis are its efficient FFT function and the .m file programming function to execute sets of Matlab code. Interfacing between Matlab and other simulation tools such as PSCAD, DigSilent PowerFactory, Excel, etc is also possible. Matlab also supports OPC (Open Process Control) data links [**13**], [**62**].

2.9.6 MathCad

MathCad as owned by Parametric Technology Corporation was founded 1985 and is known as an advanced engineering software package that allows the user to analyse/solve mathematical or engineering problems while documenting it in a desired format [**63**].

MathCad has been widely used by power systems engineers in Southern Africa in the calculating and documenting of relay protection settings, generator AVR and PSS design and settings, reactor automation logic, etc. [**13**].

2.9.7 Excel

Although the use of the popular MS Office program Excel for engineering purposes is often frowned upon by some engineers, it is a useful tool for the quick assessment of certain electrical phenomena and to demonstrate certain principles although not simulating all electrical parameters in detail [**64**].

Because of its complex number capability, Excel has been successfully used in filter bank frequency responses, VSC AC/DC harmonic interaction, SVC external devices automated switching schemes, generator governor response tests, SVC operating point harmonics generation, harmonic sequence component analysis, high resolution FFT, transmission line voltage sag, pole slip and power swing simulations, etc. [**13**].

In this thesis Excel has been used in AC/DC harmonic interaction, FFTs and solving of OPWM simultaneous non-linear formulas.

2.9.8 Lingo64

Lingo64 by LINDO Systems Inc is an optimisation software package for linear, non-linear and stochastic programming. Although the user interface is close to a text-based interface, it is very efficient and very flexible [**65**].

In this thesis, Lingo64 has also been used in the solving of OPWM simultaneous non-linear formulas to compare with Excel results.

3 Alternating Current and Direct Current harmonic interaction

3.1 Power system harmonic analysis

3.1.1 Harmonic sequence components

From Section 2.4.3 it was shown that the Fortescue transformation can be applied to non-sinusoidal waveforms in a three phase system to calculate harmonic sequence components and can thus be expanded as follows:

Let $\boldsymbol{V_{kh}}$ denote the harmonic voltage of phase k and of harmonic order h where h = 0,1,2,...:

$$\boldsymbol{V_{kh}} = U_{kh}e^{jh(\omega t+\delta_h)} \tag{3.1}$$

According to (2.9), the total harmonic voltage will be given by the sum of the individual harmonic components. The relative phase angles $(\delta_2, \delta_3, \ldots)$ of the individual harmonic phasors in relation to the fundamental component have been assumed to be zero for this calculation in order to simplify:

$$\boldsymbol{V_a} = U_{a1}e^{j\omega t} + U_{a2}e^{j2\omega t} + U_{a3}e^{j3\omega t} + \ldots \tag{3.2}$$

$$\boldsymbol{V_b} = U_{b1}e^{j(\omega t-\frac{2\pi}{3})} + U_{b2}e^{j(2\omega t-\frac{4\pi}{3})} + U_{b3}e^{j(3\omega t-2\pi)} + \ldots \tag{3.3}$$

$$\boldsymbol{V_c} = U_{c1}e^{j\left(\omega t+\frac{2\pi}{3}\right)} + U_{c2}e^{j\left(2\omega t+\frac{4\pi}{3}\right)} + U_{c3}e^{j(3\omega t+2\pi)} + \ldots \tag{3.4}$$

A representation of the three phase voltages for each harmonic component for h=1, 2, 3 rotating at angular velocity $h\omega$ is shown in Fig. 3.1:

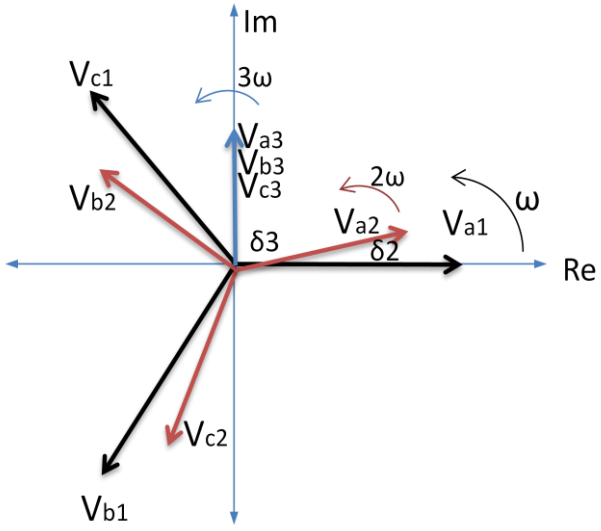

Fig. 3.1 Harmonic component phase rotations

Manipulating (2.15), the sequence components of a three phase system are determined by:

$$\begin{bmatrix} \boldsymbol{V_0} \\ \boldsymbol{V_1} \\ \boldsymbol{V_2} \end{bmatrix} = \frac{1}{3} * \begin{bmatrix} \boldsymbol{1} & \boldsymbol{1} & \boldsymbol{1} \\ \boldsymbol{1} & \boldsymbol{a} & \boldsymbol{a^2} \\ \boldsymbol{1} & \boldsymbol{a^2} & \boldsymbol{a} \end{bmatrix} \begin{bmatrix} \boldsymbol{V_a} \\ \boldsymbol{V_b} \\ \boldsymbol{V_c} \end{bmatrix} \tag{3.5}$$

$$= \frac{1}{3} * \begin{bmatrix} \boldsymbol{1} & \boldsymbol{1} & \boldsymbol{1} \\ \boldsymbol{1} & \boldsymbol{a} & \boldsymbol{a^2} \\ \boldsymbol{1} & \boldsymbol{a^2} & \boldsymbol{a} \end{bmatrix} \begin{bmatrix} U_{a1}e^{j\omega t} + U_{a2}e^{j2\omega t} + U_{a3}e^{j3\omega t} + \dots \\ U_{b1}e^{j(\omega t - \frac{2\pi}{3})} + U_{b2}e^{j(2\omega t - \frac{4\pi}{3})} + U_{b3}e^{j(3\omega t - 2\pi)} + \dots \\ U_{c1}e^{j(\omega t + \frac{2\pi}{3})} + U_{c2}e^{j(2\omega t + \frac{4\pi}{3})} + U_{c3}e^{j(3\omega t + 2\pi)} + \dots \end{bmatrix} \tag{3.6}$$

$\boldsymbol{a_k} = e^{j\frac{k2\pi}{n}}$, where n is the number of phases and k denotes the specific phase (k=0,1,2,...,n-1).

It follows that:

$\boldsymbol{a_0} = e^0 = 1$ for a three phase system to denote the reference phase (a) in this case.

$\boldsymbol{a_1} = e^{j\frac{2\pi}{3}}$ for a three phase system to translate the b phase onto the reference (a) phase.

$\boldsymbol{a_2} = e^{j\frac{4\pi}{3}}$ for a three phase system to translate the c phase onto the reference (a) phase.

Also see [**32**], [**42**].

Assume a balanced system where $U_{ah} = U_{bh} = U_{ch}$.

The total ZPS voltage $\boldsymbol{V_0}$ is then given by the following relationship and shows that ZPS harmonic orders occur where h = 3n:

$$\begin{aligned} \boldsymbol{V_0} &= \frac{1}{3} * (U_{a1}e^{j\omega t} + U_{a2}e^{j2\omega t} + U_{a3}e^{j3\omega t} + \dots + U_{b1}e^{j(\omega t - \frac{2\pi}{3})} + U_{b2}e^{j(2\omega t - \frac{4\pi}{3})} + \\ &\quad U_{b3}e^{j(3\omega t - 2\pi)} + \dots + U_{c1}e^{j(\omega t + \frac{2\pi}{3})} + U_{c2}e^{j(2\omega t + \frac{4\pi}{3})} + U_{c3}e^{j(3\omega t + 2\pi)} + \dots) \\ &= \frac{1}{3} * (3U_{a3}e^{j3\omega t} + 3U_{a6}e^{j6\omega t} + 3U_{a9}e^{j9\omega t} + \cdots) \\ &= U_{a3}e^{j3\omega t} + U_{a6}e^{j6\omega t} + U_{a9}e^{j9\omega t} + \dots \end{aligned} \tag{3.7}$$

The total PPS voltage $\boldsymbol{V_1}$ is given by the following relationship and shows that PPS harmonic orders occur where h = 3n+1:

$$\boldsymbol{V_1} = \frac{1}{3} * (U_{a1}e^{j\omega t} + U_{a2}e^{j2\omega t} + U_{a3}e^{j3\omega t} + \ldots + U_{b1}e^{j(\omega t - \frac{2\pi}{3})}.e^{j\frac{2\pi}{3}} +$$
$$U_{b2}e^{j(2\omega t - \frac{4\pi}{3})}.e^{j\frac{2\pi}{3}} + U_{b3}e^{j(3\omega t - 2\pi)}.e^{j\frac{2\pi}{3}} + \ldots + U_{c1}e^{j(\omega t + \frac{2\pi}{3})}.e^{j\frac{4\pi}{3}} +$$
$$U_{c2}e^{j(2\omega t + \frac{4\pi}{3})}.e^{j\frac{4\pi}{3}} + U_{c3}e^{j(3\omega t + 2\pi)}.e^{j\frac{4\pi}{3}} + \ldots)$$
$$= \frac{1}{3} * (U_{a1}e^{j\omega t} + U_{a2}e^{j2\omega t} + U_{a3}e^{j3\omega t} + \ldots + U_{b1}e^{j\omega t} + U_{b2}e^{j\left(2\omega t - \frac{2\pi}{3}\right)} +$$
$$U_{b3}e^{j\left(3\omega t + \frac{2\pi}{3}\right)} + \ldots + U_{c1}e^{j\omega t} + U_{c2}e^{j\left(2\omega t + \frac{2\pi}{3}\right)} + U_{c3}e^{j\left(3\omega t + \frac{4\pi}{3}\right)} + \ldots)$$
$$= \frac{1}{3} * (3U_{a1}e^{j\omega t} + 3U_{a4}e^{j4\omega t} + 3U_{a7}e^{j7\omega t} + \cdots)$$
$$= U_{a1}e^{j\omega t} + U_{a4}e^{j4\omega t} + U_{a7}e^{j7\omega t} + \ldots \quad (3.8)$$

Lastly follows that the total NPS voltage $\boldsymbol{V_2}$ is given by the following relationship and shows that NPS harmonic orders occur where h = 3n+2:

$$\boldsymbol{V_2} = \frac{1}{3} * (U_{a1}e^{j\omega t} + U_{a2}e^{j2\omega t} + U_{a3}e^{j3\omega t} + \ldots + U_{b1}e^{j(\omega t - \frac{2\pi}{3})}.e^{j\frac{4\pi}{3}} +$$
$$U_{b2}e^{j(2\omega t - \frac{4\pi}{3})}.e^{j\frac{4\pi}{3}} + U_{b3}e^{j(3\omega t - 2\pi)}.e^{j\frac{4\pi}{3}} + \ldots + U_{c1}e^{j(\omega t + \frac{2\pi}{3})}.e^{j\frac{2\pi}{3}} +$$
$$U_{c2}e^{j(2\omega t + \frac{4\pi}{3})}.e^{j\frac{2\pi}{3}} + U_{c3}e^{j(3\omega t + 2\pi)}.e^{j\frac{2\pi}{3}} + \cdots$$
$$= \frac{1}{3} * (U_{a1}e^{j\omega t} + U_{a2}e^{j2\omega t} + U_{a3}e^{j3\omega t} + \ldots + U_{b1}e^{j\left(\omega t + \frac{2\pi}{3}\right)} + U_{b2}e^{j(2\omega t)} +$$
$$U_{b3}e^{j\left(3\omega t + \frac{4\pi}{3}\right)} + \ldots + U_{c1}e^{j\left(\omega t + \frac{4\pi}{3}\right)} + U_{c2}e^{j(2\omega t)} + U_{c3}e^{j\left(3\omega t + \frac{2\pi}{3}\right)} + \cdots)$$
$$= \frac{1}{3} * (3U_{a2}e^{j2\omega t} + 3U_{a5}e^{j5\omega t} + 3U_{a8}e^{j8\omega t} + \ldots)$$
$$= U_{a2}e^{j2\omega t} + U_{a5}e^{j5\omega t} + U_{a8}e^{j8\omega t} + \ldots \quad (3.9)$$

This gives the information for Table 3.1 for the characteristic phase rotation of power system harmonics *under balanced conditions* and is also confirmed by [**8**], [**34**]:

Table 3.1: Harmonic order phase rotations

ZPS	PPS	NPS	ZPS	PPS	NPS
DC	1	2	33	34	35
3	4	5	36	37	38
6	7	8	39	40	41
9	10	11	42	43	44
12	13	14	45	46	47

15	16	17	48	49	50
18	19	20	51	52	53
21	22	23	54	55	56
24	25	26	57	58	59
27	28	29	60	61	62
30	31	32	63	64	65

It can also be shown that for phase-phase quantities, eg. $\boldsymbol{V_{ab}}$, zero sequence components disappear as given by the following relationship:

(Assume a balanced star-connected system where $U_{ah} = U_{bh} = U_{ch}$)

$$\boldsymbol{V_{ab} = V_b - V_a}$$

$$= (U_{b1}e^{j(\omega t-\frac{2\pi}{3})} + U_{b2}e^{j(2\omega t-\frac{4\pi}{3})} + U_{b3}e^{j(3\omega t-2\pi)} + \dots) - (U_{a1}e^{j\omega t} + U_{a2}e^{j2\omega t} + U_{a3}e^{j3\omega t} + \dots)$$

$$= U_{b1}(e^{j\left(\omega t-\frac{2\pi}{3}\right)} - e^{j\omega t}) + U_{b2}(e^{j\left(2\omega t-\frac{4\pi}{3}\right)} - e^{j2\omega t})$$

$$= U_{b1}(e^{j\omega t}(e^{-\frac{j2\pi}{3}} - 1)) + U_{b2}(e^{j2\omega t}(e^{-\frac{j4\pi}{3}} - 1)$$

$$= \sqrt{3}U_{b1}e^{j\left(\omega t-\frac{5\pi}{6}\right)} + \sqrt{3}U_{b2}e^{j\left(2\omega t+\frac{5\pi}{6}\right)}$$

$$= \sqrt{3}(U_{b1}e^{j(\omega t-\frac{5\pi}{6})} + U_{b2}e^{j\left(2\omega t+\frac{5\pi}{6}\right)}) \quad (3.10)$$

With a perfectly balanced system but with the presence of harmonics it can be seen that positive, negative and zero sequence components can occur.

However, in a practical power system, there is always a measure of unbalance causing harmonic orders that would characteristically occur for example as a ZPS harmonic, also to contain PPS and NPS components.

For example, the zero sequence (3^{rd}, 9^{th}, ...) harmonic orders generated by Thyristor-Switched Reactors (TCR's) in SVC's that are dependent on firing angle, normally circulate in the strategically chosen TCR delta connections or delta winding of the SVC transformers [**8**]. Under unbalanced conditions, such as during single phase faults and reclosing cycles in the system, TCR firing mismatch, inductor tolerances and unbalance in the system due to long un-transposed lines or load imbalance, these harmonic orders would not circulate but escape

from the delta connection. These "triplen" harmonic orders that do not normally occur outside delta connections, but that occur only during transient unbalanced conditions, could cause undesired resonant conditions either locally, e.g. SVC low voltage busbar, or in the system given that the system is sensitive to that specific harmonic order.

In Table 3.1, the DC component is shown as a zero sequence component, which is true under perfectly balanced conditions like with all other characteristic ZPS harmonic orders. It can however be seen in Fig. 5.5 and Fig. 5.9 in Chapter 5 that where a VSC contributes DC components during transient conditions and given that a VSC cannot produce ZPS, these DC components occur as equal PPS and NPS components in the sequence domain, relating in the phase domain to two positive DC phase quantities and one negative DC phase quantity of double the amplitude of the other two phases. Although in practice the concept of DC phase rotation could be considered meaningless given that the vectors do not rotate, the "stationary" vectors' translation to the phase domain gives some interesting theoretical and practical implications that are not discussed further as part of this thesis.

The graphs in Figs. 3.2 - 3.4 show the harmonic content generated by a SVC TCR at a given firing angle. The harmonic content and sequence components of the phase harmonics have been calculated in Excel:

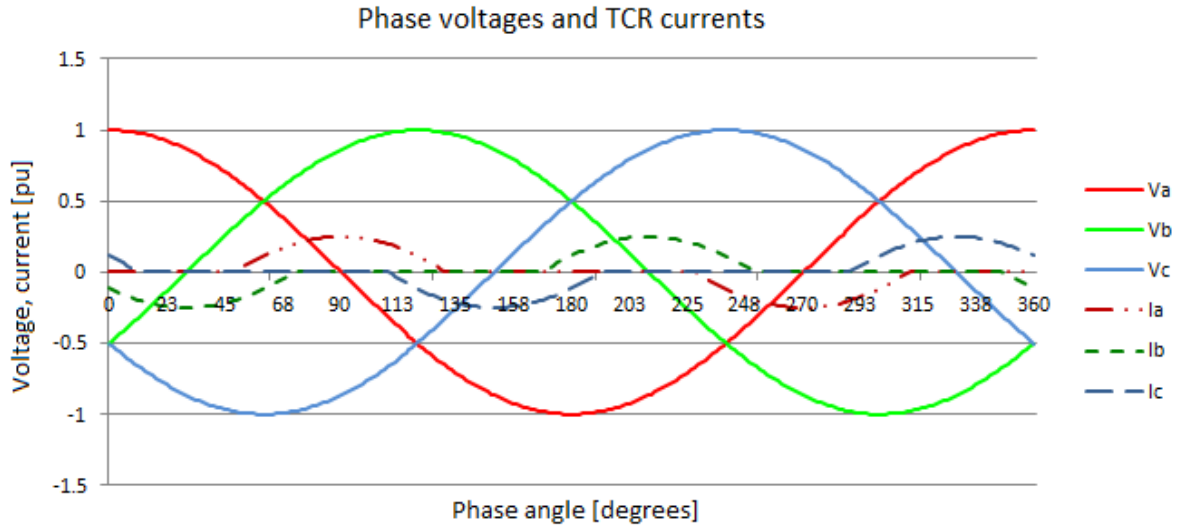

Fig. 3.2 SVC TCR phase voltages and currents

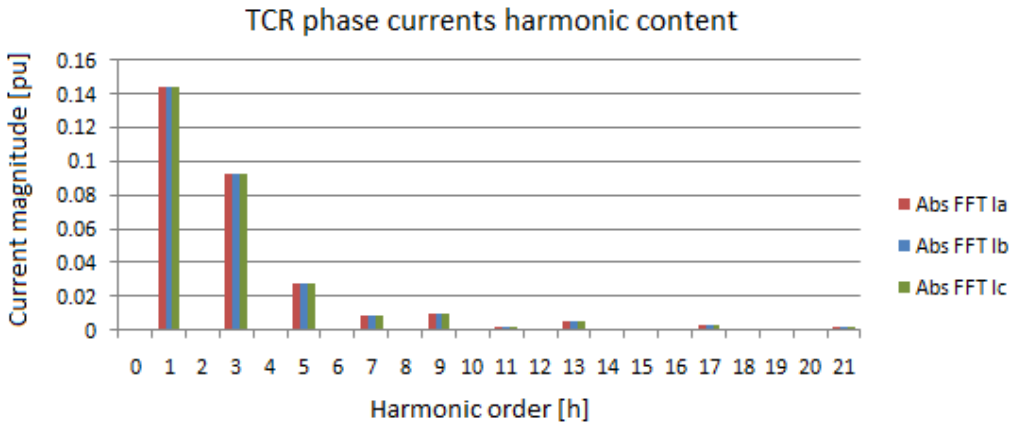

Fig. 3.3 SVC TCR phase currents harmonic content

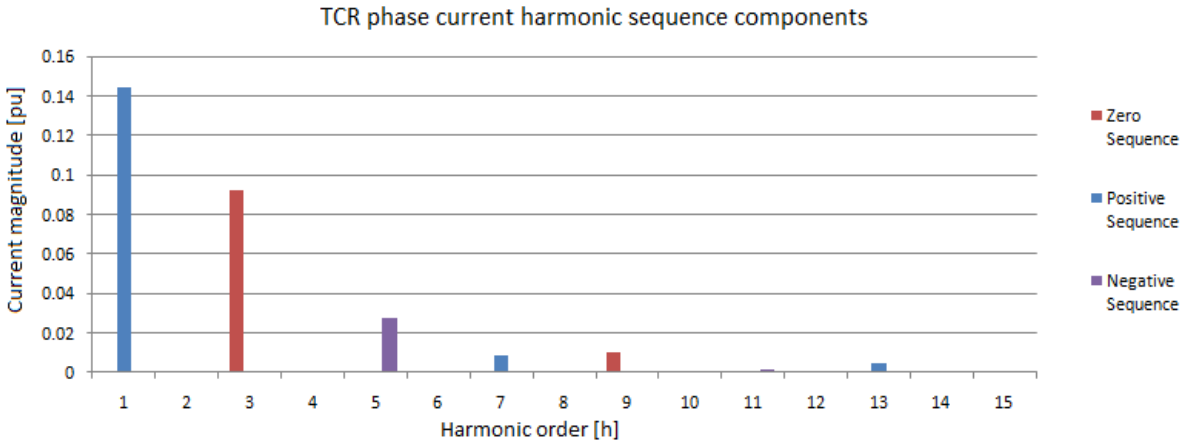

Fig. 3.4 SVC TCR phase current harmonic sequence components

It can be seen that the TCR current harmonic sequence components calculated by using the FFT and Fortescue transform follows the results in Table 3.1 as presented above, as well as the characteristic odd harmonics described by Section 2.4.2.

The current harmonic content versus firing angle for a TCR generated in Excel is shown in Fig 3.5. This illustrates why some resonant problems can be TCR operating point dependant as mentioned in Section 2.5.1.

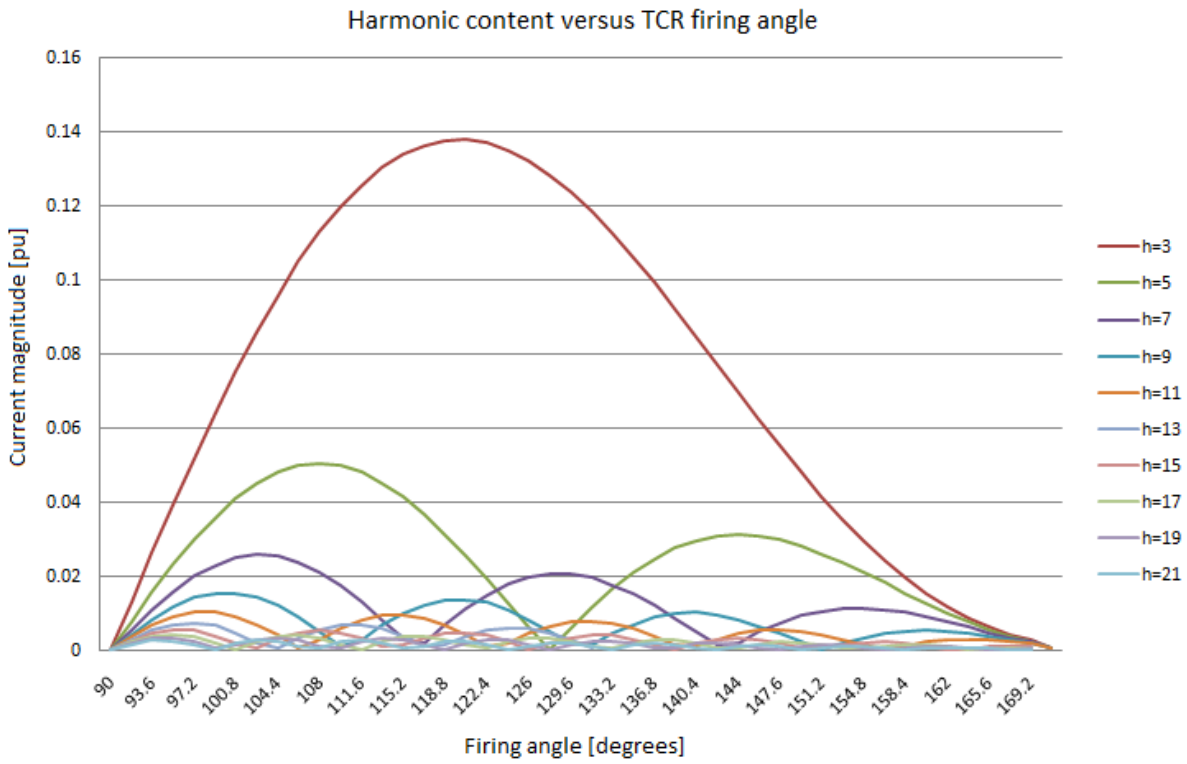

Fig. 3.5 SVC harmonic generation versus firing angle

3.1.2 Phase rotation in the frequency domain

When analysing a three phase system with or without the presence of harmonic components, positive or negative phase rotation in the sequence domain can be observed and confirmed in the frequency domain by doing a Fourier transform on the phase domain waveforms.

In the sequence domain, a phasor with positive phase rotation is given by:

$$\boldsymbol{V_1} = U_1 e^{j\omega t} \tag{3.11}$$

In the sequence domain, a phasor with negative phase rotation is given by:

$$\boldsymbol{V_2} = U_2 e^{-j\omega t} \tag{3.12}$$

Using (2.15) in the phase domain and ignoring V_0 for this purpose, the reference phase "a" would be given by the relationship

$$\boldsymbol{V_a} = \boldsymbol{V_1} + \boldsymbol{V_2} = U_1 e^{j\omega t} + U_2 e^{-j\omega t}. \tag{3.13}$$

According to the complex exponential Fourier series in (2.9), the total harmonic voltage signal, where h denotes the harmonic order, is given by the relationship

$$\boldsymbol{V_h} = \sum_{h=-\infty}^{\infty} U_h e^{h(j\omega t+\delta)} \quad .$$

This gives rise to the following result

$$\boldsymbol{V_{ah}} = U_1 e^{j\omega t} + U_{-1} e^{-j\omega t} \,, \tag{3.14}$$

where U_{-1} in the phase domain is equal to the previously denoted U_2 in the sequence domain.

Thus a negative phase sequence component at any multiple of the fundamental frequency can be regarded as a phasor with a negative frequency. This makes sense when considering the result of Section 2.7.2.4.

This is also confirmed by the following example in Figs. 3.6 – 3.8 where an FFT is performed on a waveform containing both positive and negative phase sequence components. The resultant FFT in Fig.3.8 also shows the NPS component in the negative frequency domain where $U_1 = 1$, $U_2 = 0.2$ and U_t is the resultant voltage phasors shown in Fig. 3.6:

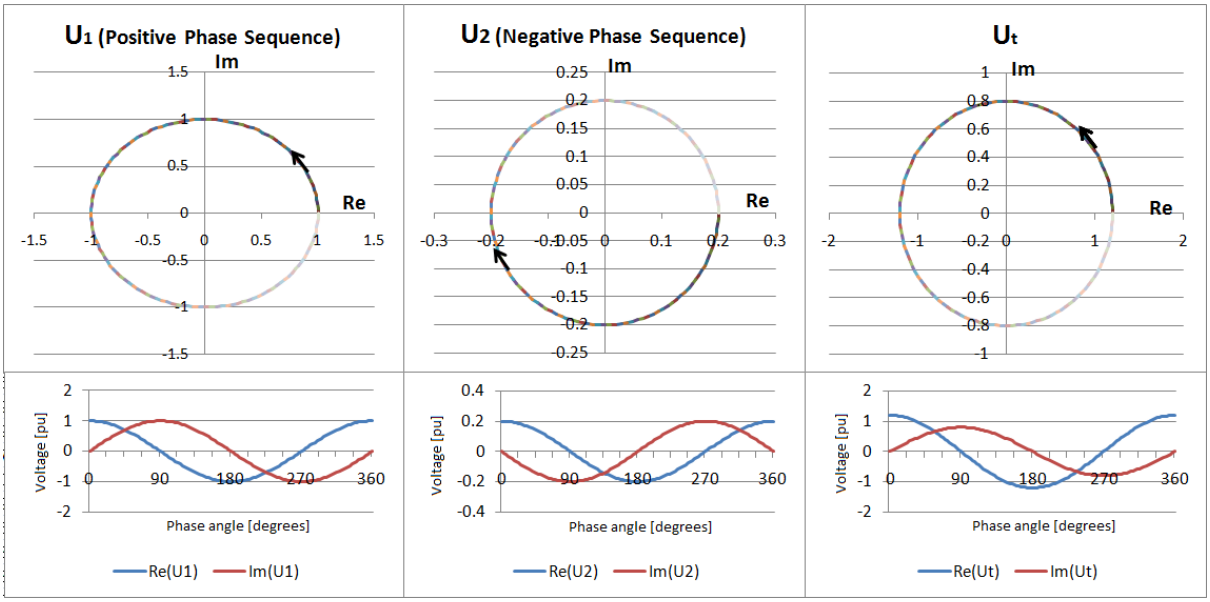

Fig. 3.6 Positive and negative phase rotation in time domain

First the FFT of the real part of U_t is calculated and then the FFT of the imaginary part of U_t is calculated resulting only in real valued frequency components. Recording the positive and negative frequency domain quantities gives the results shown in Fig. 3.7 where the FFT of the real part of U_t contains PPS and NPS components of 0.6 each. The FFT of the imaginary part of U_t contains a PPS component of 0.4 and a NPS component of -0.4. Summating the

PPS and NPS components gives a total PPS component again of 1 and a NPS component of 0.2 .

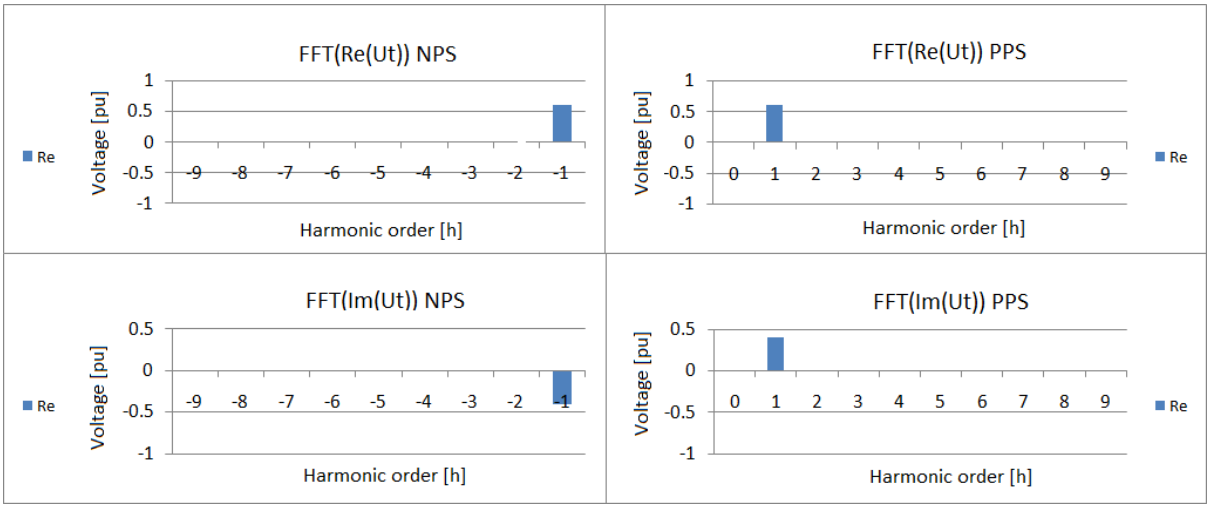

Fig. 3.7 Frequency domain components of separate time domain components

To confirm the results, an FFT is done on the time domain total voltage U_t as shown in Fig. 3.8:

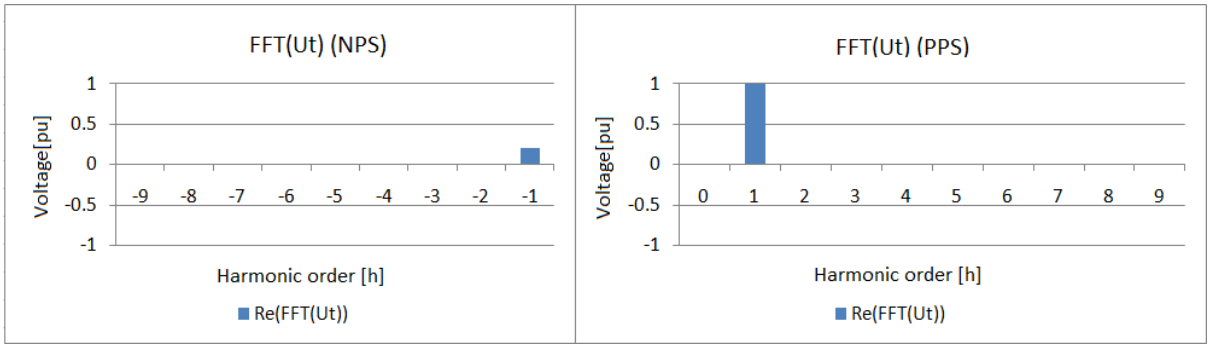

Fig. 3.8 Frequency components of summated time domain components

It can be seen that for $U_1 = U_{-1}$, U_t will contain no imaginary component and equal PPS and NPS components. The example above also confirms the well known identities of:

$$\cos(\omega t + \delta) = \frac{1}{2}\left(e^{j\omega t+\sigma} + e^{-(j\omega t+\sigma)}\right) \tag{3.15}$$

$$\sin(\omega t + \delta) = \frac{1}{2j}\left(e^{j\omega t+\sigma} - e^{-(j\omega t+\sigma)}\right) \tag{3.16}$$

3.2 Voltage Source Converter switching operation and harmonic generation

3.2.1 Voltage Source Converter switching at fundamental frequency

In Section 2.6.3, the basic VSC switching operation was discussed and the relationship between AC and DC quantities has been derived. This basic VSC switching operation at fundamental frequency equates to the square wave switching scheme discussed in Section 2.6.4.3. This square wave switching scheme was discussed and the fundamental component was given by (2.54) as:

$$V_{a1} = \frac{4}{\pi}\left(\frac{V_{dc}}{2}\right) = 0.637V_{dc}$$

A frequency domain analysis of the waveforms in Fig. 2.22 confirms the fundamental component magnitude as shown in Fig. 3.9:

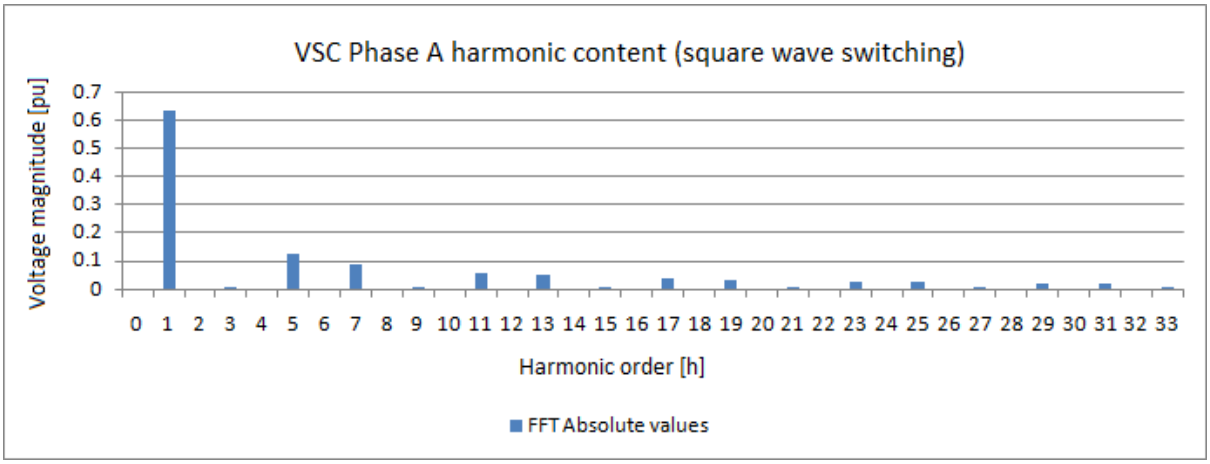

Fig. 3.9 Square wave switching scheme harmonic components

The figure above also shows the harmonic content for the three-phase square wave switching scheme. All odd harmonic orders occur except for the "triplen" zero sequence harmonics that are suppressed. Thus, the harmonics generated are given by $h = 6n \pm 1, (n = 1,2,3, \dots)$.

This implies a characteristic zero sequence harmonic elimination and can also be shown by using the VSC switching formula (2.43) in Section 2.6.3 and adding a common mode or Zero Phase Sequence component to phase components:

Let $U'_{ag} = U_{ag} + U_0$, $U'_{bg} = U_{bg} + U_0$ and $U'_{cg} = U_{cg} + U_0$.

It follows that

$$U'_x = U'_{xg} - U'_{Ng} = \left(sw_x * \frac{U_{dc}}{2} - U_0\right) - \frac{1}{3}\left(U'_{ag} + U'_{bg} + U'_{cg}\right)$$

$$= \left(sw_x * \frac{U_{dc}}{2} - U_0\right) - \frac{1}{3}\left(sw_a * \frac{U_{dc}}{2} + sw_b * \frac{U_{dc}}{2} + sw_c * \frac{U_{dc}}{2} - 3U_0\right)$$

$$= \left(3sw_x * \frac{U_{dc}}{6}\right) - U_0 - \frac{U_{dc}}{6}(sw_a + sw_b + sw_c) + U_0$$

$$= \frac{U_{dc}}{6} * \left(3sw_x - (sw_a + sw_b + sw_c)\right) = U_x\,. \tag{3.17}$$

The result above confirms that zero sequence components are not transferred or produced by a VSC scheme. The only exception exists with configurations where zero sequence components are transferred to the DC side via a midpoint filter coupling.

3.2.2 Pulse Width Modulation

As described in Section 2.6.4.2, switching techniques like PWM is used to be able to control the AC output voltage independent of the DC voltage and to have some control over the harmonic content generated. A sinusoidal output reference is compared to a triangular (or saw-tooth) wave shape. Depending on the comparison result, the output is switched between the two DC polarities. If the amplitude of the sinusoidal reference is controlled with respect to the triangular wave, the output voltage is varied. This ratio of the reference to the triangular wave is called the modulation index as given by (2.51): $m_a = \frac{V_{control}}{V_{tri}}$

The number of times the triangular wave is duplicated within one sinusoidal fundamental frequency f_1, is called the switching- or carrier frequency, f_s. This gives the frequency modulation ratio given by (2.52): $m_f = \frac{f_s}{f_1}$

To recall, the fundamental component is given by (2.53): $V_{a1} = \frac{m_a V_{dc}}{2}$

The following example in Fig. 3.10 shows triangular PWM with $m_a = 0.9$ and $m_f = 33$:

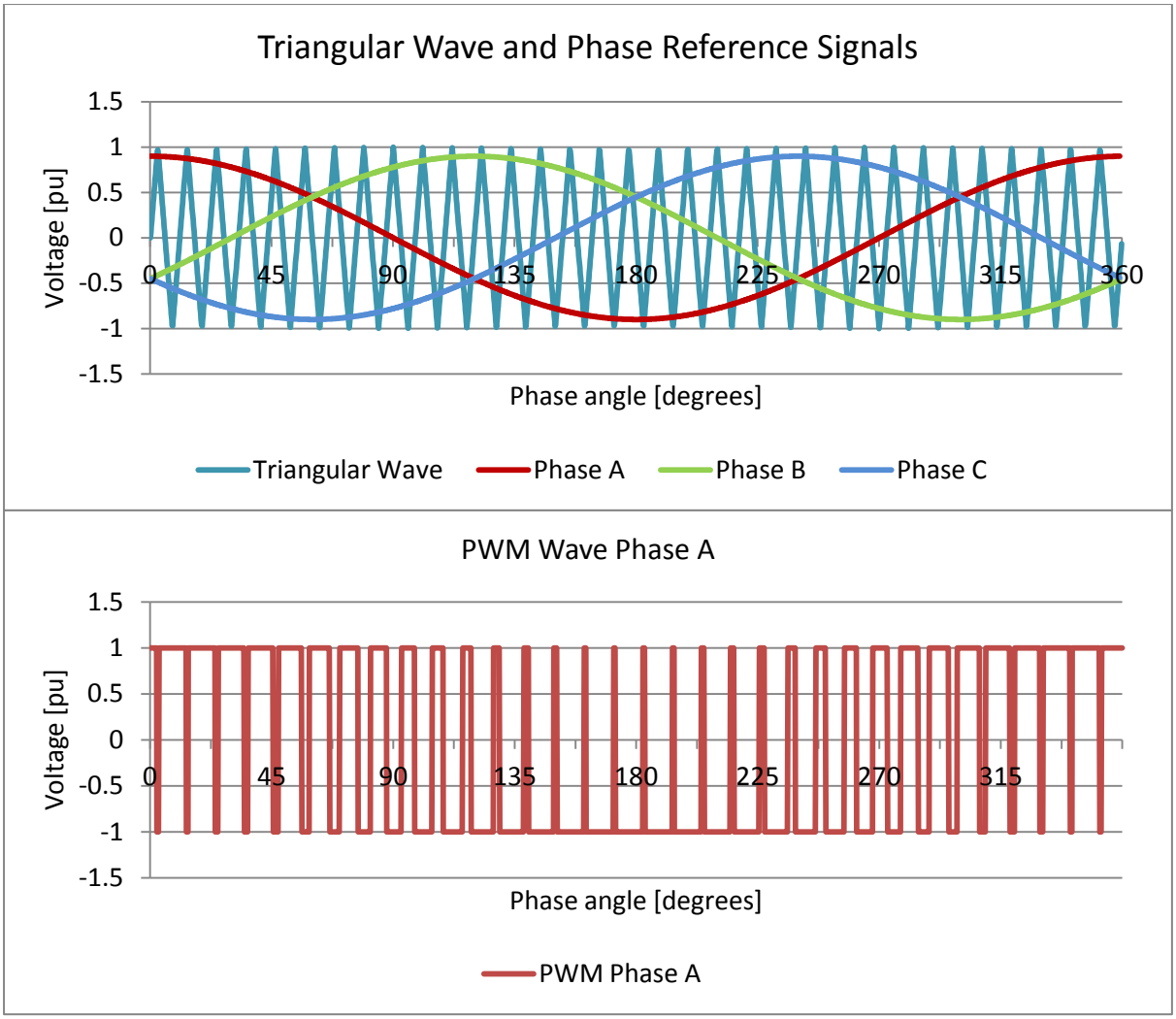

Fig. 3.10 PWM switching principle

Using the switching functions for k_a, k_b and k_c given by (2.45) – (2.47) defined for VSC's earlier in Section 2.6.3 gives the phase voltage wave shape as shown in Fig. 3.11 for phase A:

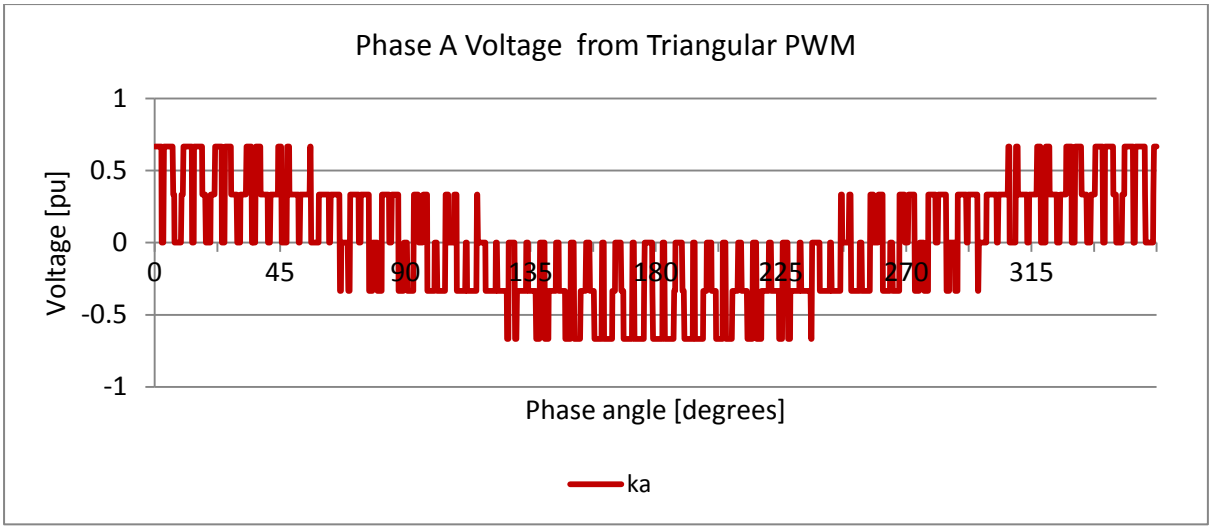

Fig. 3.11 VSC switching phase quantity

Switching at higher frequencies ($m_f > 21$) eliminates the problem of sub-harmonics at asynchronous PWM when the reference and triangular waves are not synchronised. This technique moves harmonic content to higher frequencies, but increases the switching losses and has a significant effect on high power applications. Triangular PWM produces harmonics at $(m_f), (m_f \pm 2), (m_f \pm 4), (2m_f \pm 1), (2m_f \pm 3), (2m_f \pm 5), (3m_f \pm 2), (3m_f \pm 4), (3m_f \pm 6), etc.$ [**28**] as shown in Fig. 3.12:

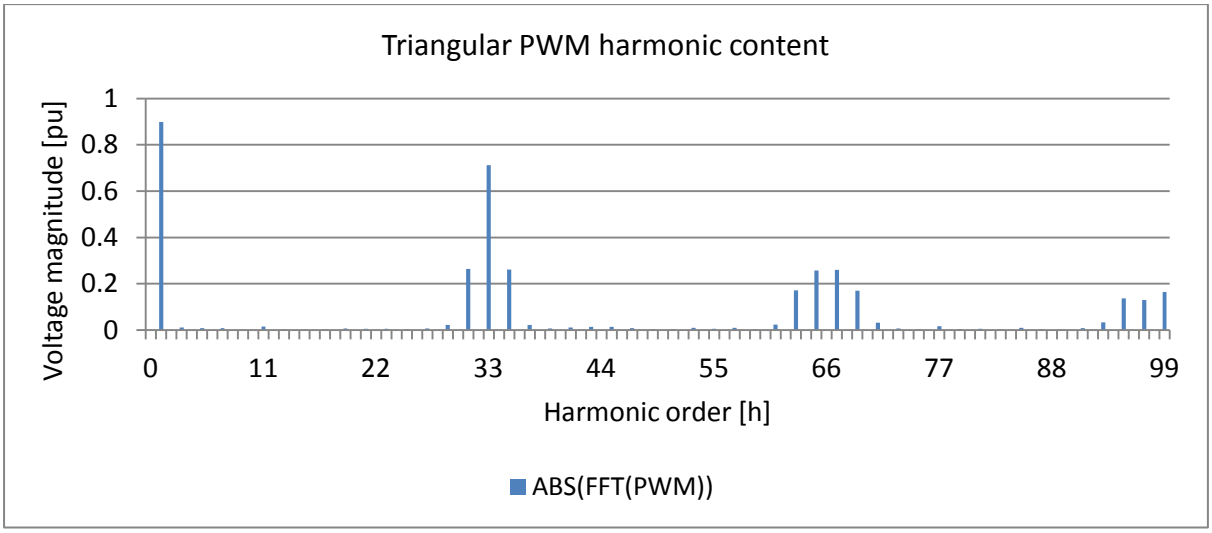

Fig. 3.12 Triangular PWM switching harmonic content

When investigating the harmonic content of the three phase quantities, multiples of the switching frequency and other zero sequence harmonic orders are suppressed. The fundamental component given by (2.53) of $V_{a1} = \frac{m_a V_{dc}}{2} = \frac{0.9}{2} = 0.45$ is also confirmed by Fig. 3.13:

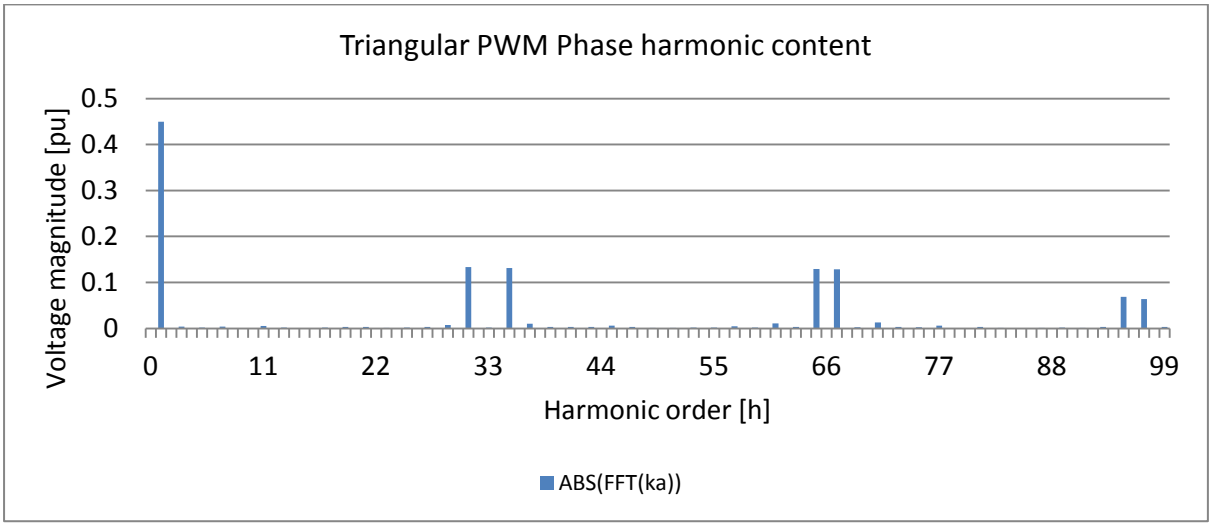

Fig. 3.13 Triangular PWM switching phase quantity harmonic content

Using saw-tooth PWM gives lower harmonic amplitudes, but wider clusters of harmonics. In the three-phase quantities, multiples of the switching frequency is greatly reduced as shown in Fig. 3.14:

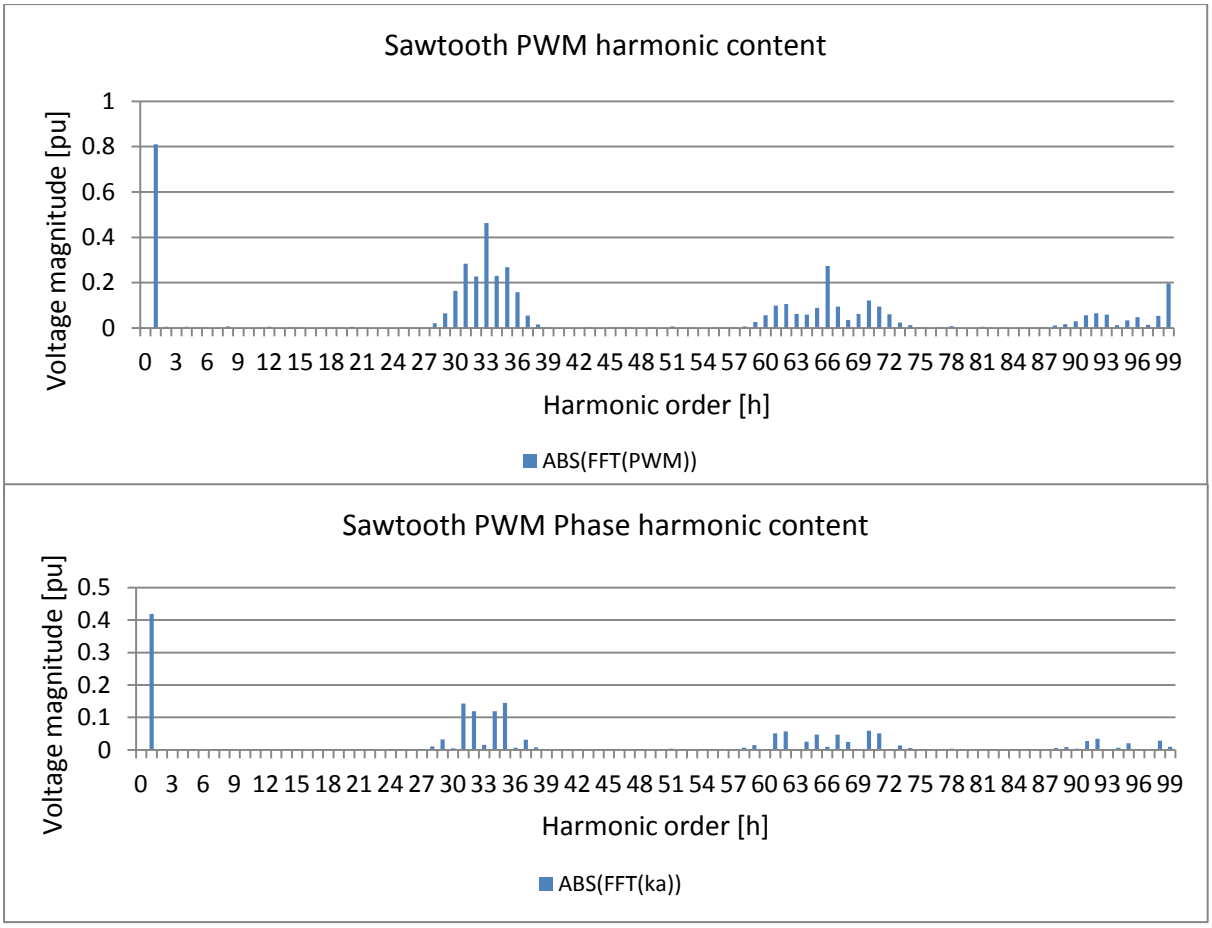

Fig. 3.14 Sawtooth PWM switching phase quantity harmonic content

3.2.3 Optimised Pulse Width Modulation

As discussed in Section 2.6.4.4, for high power applications, OPWM is more suited as it allows lower switching frequencies and thus lower losses, but with the capability of eliminating especially lower order harmonics. It also gives the advantage of a higher fundamental component when compared to normal PWM without third harmonic injection or when compared to PWM with third harmonic injection.

The principle behind OPWM, also known as programmed harmonic elimination, is that an output waveform that possesses half-wave symmetry is constructed by switching at specific angles during the cycle. The angles are determined by pre-determining for each desired modulation index what the firing angles need to be to cancel out certain harmonics. If the modulation ratio $m_f = n$, then the number of angles available to switch at are $\frac{n-1}{2}$. These angles are normally numbered $\alpha_1,\ \alpha_2, \ldots\ \alpha_{\frac{n-1}{2}}$. The equations that these angles have to fulfil

simultaneously are the formulas for the Fourier coefficients for the harmonic orders that are to be minimised, as well as the fundamental component or modulation index determination.

For example, to switch at 9 times the fundamental frequency, 3 harmonic orders can be eliminated and the modulation index can be set by solving the following equations simultaneously:

$$m_a = 0.94 = 1 - 2 * (cos\,\alpha_1 - cos\,\alpha_2 + cos\,\alpha_3 - cos\,\alpha_4)$$

$$h5 \approx 0 = 1 - 2 * (cos\,5\alpha_1 - cos\,5\alpha_2 + cos\,5\alpha_3 - cos\,5\alpha_4)$$

$$h7 \approx 0 = 1 - 2 * (cos\,7\alpha_1 - cos\,7\alpha_2 + cos\,7\alpha_3 - cos\,7\alpha_4)$$

$$h11 \approx 0 = 1 - 2 * (cos\,11\alpha_1 - cos\,11\alpha_2 + cos\,\alpha 11_3 - cos\,11\alpha_4)$$

To solve these equations, a non-linear solving program or iterative program has to be used. Both the programs Lingo64 and Excel were used to obtain solutions to minimise lower order harmonics. Below is an example of how to use Lingo64 to solve these equations:

```
MODEL:
! Find solutions for a1,a2,a3,a4;

 [MOD1] 1 - 2*(@cos(a1)-@cos(a2)+@cos(a3)-@cos(a4)) > 0.939;
 [MOD2] 1 - 2*(@cos(a1)-@cos(a2)+@cos(a3)-@cos(a4)) < 0.941;


 [_5th] (1 - 2*(@cos(5*a1)-@cos(5*a2)+@cos(5*a3)-@cos(5*a4))) < 0.01;
 [_7th] (1 - 2*(@cos(7*a1)-@cos(7*a2)+@cos(7*a3)-@cos(7*a4))) < 0.01;
 [_11th] (1 - 2*(@cos(11*a1)-@cos(11*a2)+@cos(11*a3)-@cos(11*a4))) < 0.01;
! [_13th] (1 - 2*(@cos(13*a1)-@cos(13*a2)+@cos(13*a3)-@cos(13*a4))) < 0.01;
! [_15th] 1 - 2*(@cos(15*a1)-@cos(15*a2)+@cos(15*a3)-@cos(15*a4)) < 0.1;
! [_17th] 1 - 2*(@cos(17*a1)-@cos(17*a2)+@cos(17*a3)-@cos(17*a4)) < 0.1;
 [total] min = @abs(1 - 2*(@cos(5*a1)-@cos(5*a2)+@cos(5*a3)-@cos(5*a4))
)+@abs(1 - 2*(@cos(7*a1)-@cos(7*a2)+@cos(7*a3)-@cos(7*a4)) )+@abs(1 -
2*(@cos(11*a1)-@cos(11*a2)+@cos(11*a3)-@cos(11*a4)))+@abs(1 -
2*(@cos(13*a1)-@cos(13*a2)+@cos(13*a3)-@cos(13*a4)))+@abs(1 -
2*(@cos(15*a1)-@cos(15*a2)+@cos(15*a3)-@cos(15*a4)))+@abs(1 -
2*(@cos(17*a1)-@cos(17*a2)+@cos(17*a3)-@cos(17*a4)) );

 a1 < a2;
 a2 < a3;
 a3 < a4;
 a4 < 1.570796;

END
```

After some experimentation and a lot of iterations, Excel seems to give better solutions when evaluating the minimum sum of harmonics to be cancelled out. Below is an Excel example with OPWM functions to minimise harmonic orders 5 to 17 while switching 9 times per cycle

depicted in Fig. 3.15. The four angles available when switching 9 times per cycle have been determined at: $\alpha_1 = 8.5°, \alpha_2 = 12.987°, \alpha_3 = 25.24°, \alpha_4 = 26.847°$

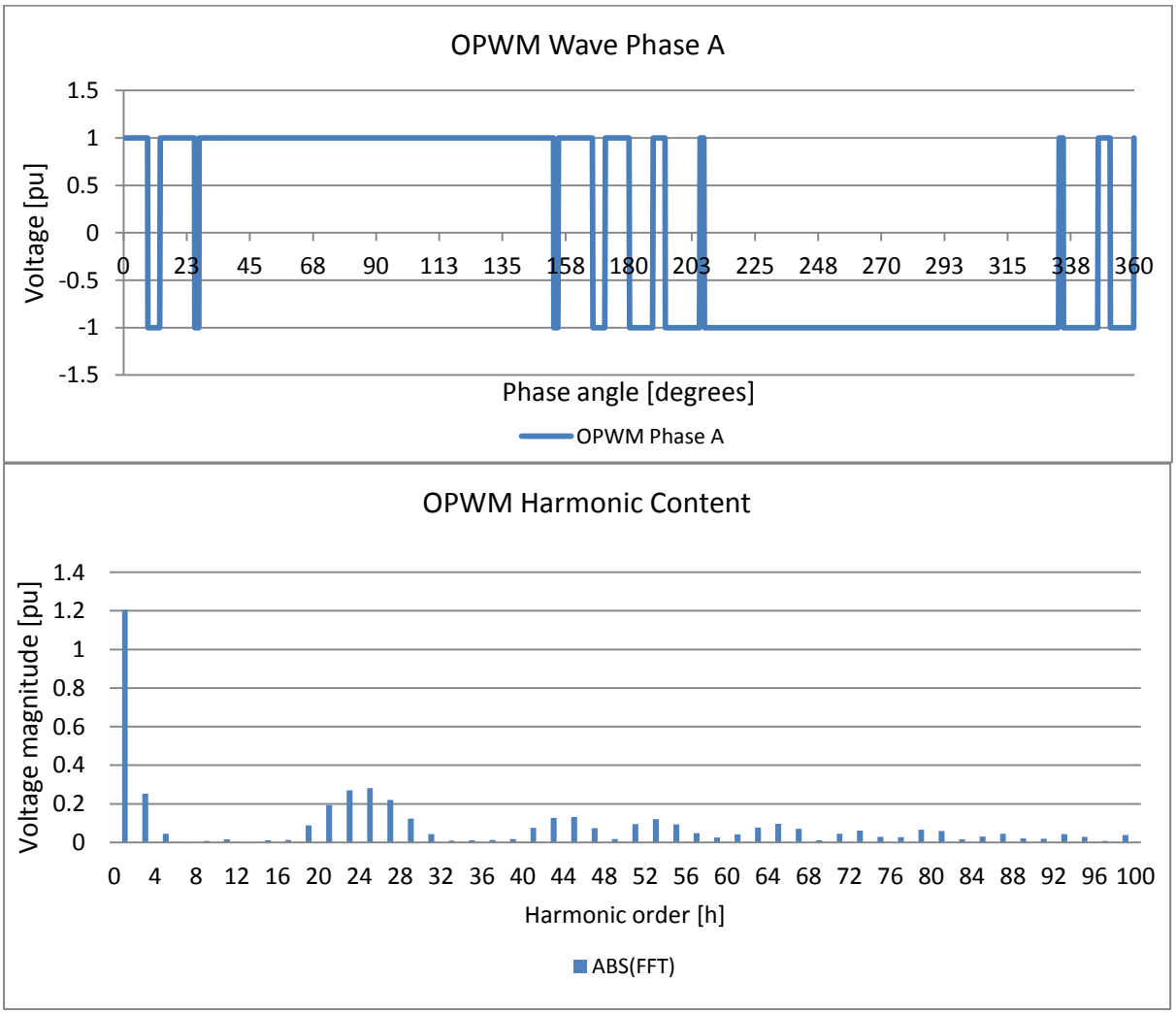

Fig. 3.15 OPWM switching and harmonic content

Investigating the three phase quantities and harmonic content, zero sequence harmonics also disappear. The fundamental component is set by the equation determining the modulation index to 0.94. Using (2.54), this gives the phase fundamental component of $V_{a1} = 0.94 * \frac{4}{\pi}\left(\frac{V_{dc}}{2}\right) = 0.6V_{dc}$ which is the square-wave fundamental component times the governed modulation index as shown in Fig. 3.16:

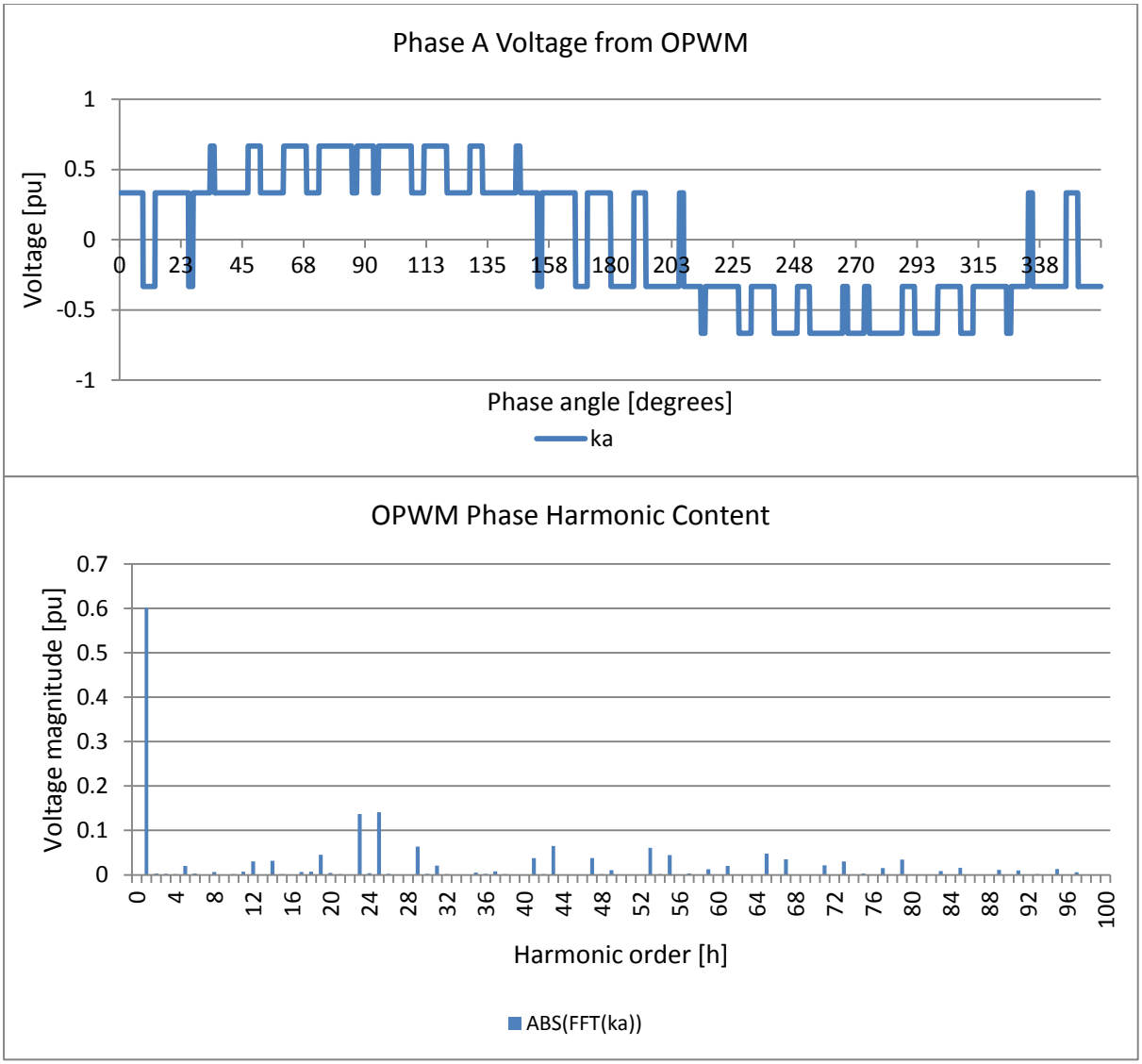

Fig. 3.16 OPWM switching and phase quantity harmonic content

To further investigate the influence that α angle variations have on the harmonic content and to get a better feeling of the simultaneous non-linear equations, a Matlab figure was created by plotting the harmonic amplitudes for harmonic components 3,5,7,9,11,13 and 15 while varying either of three α angles between zero and 90 degrees. From this plot in Fig. 3.17 it can be seen that a perfect cancellation solution does not exist, but only a "best-fit" solution since the "valleys" or zero amplitude crossings do not fall in a perfectly straight line as the harmonic order increases.

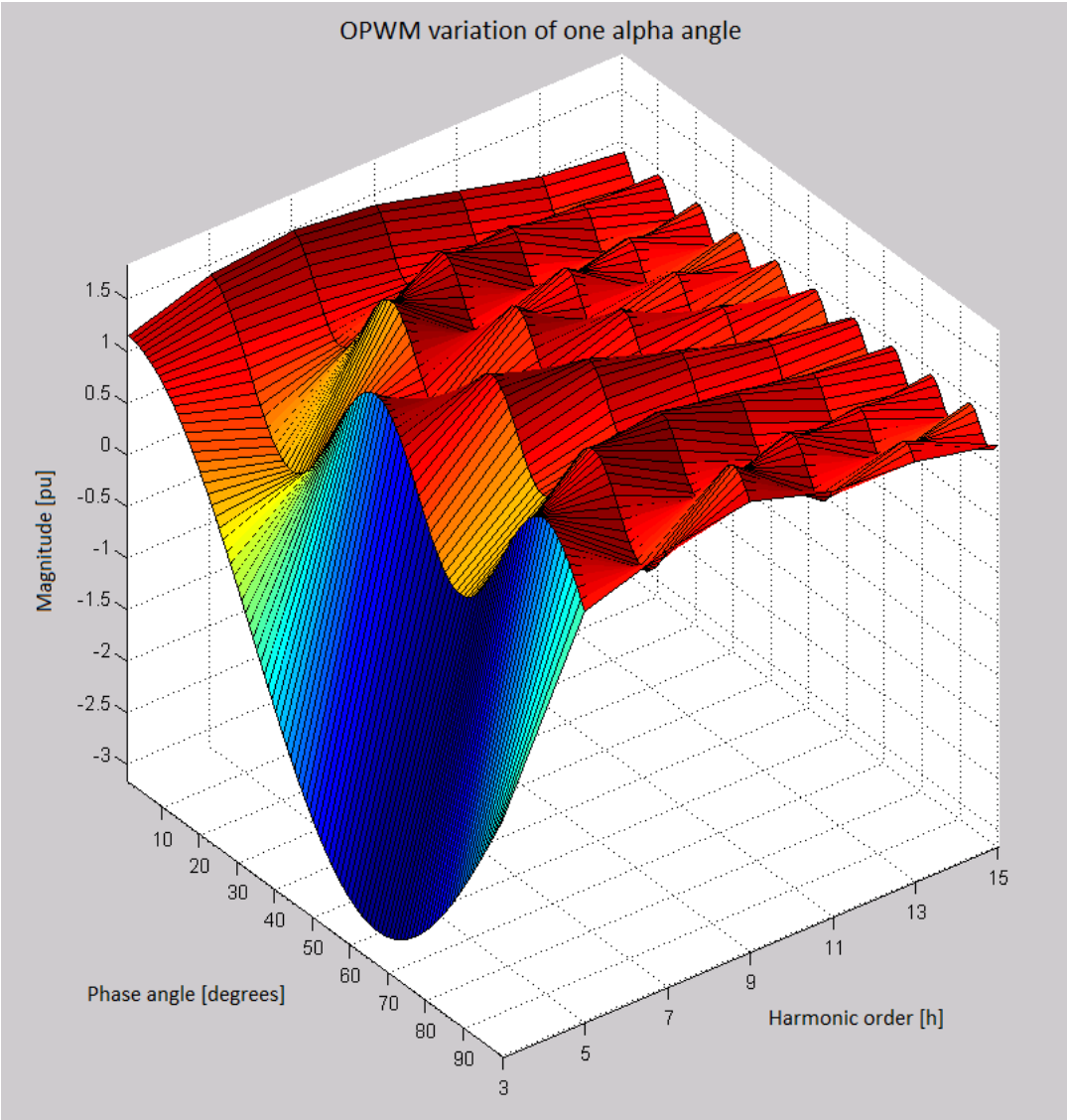

Fig. 3.17 OPWM solution angle variations

Fig. 3.18 shows a plot from the actual Gerus converter station switching in OPWM mode at 1150Hz, i.e. 23 times per cycle. Thus the control strategy can cancel out 10 lower order harmonics while maintaining the desired modulation index. The voltages and currents at PCC are shown, as well as the filter bus voltage, valve currents and DC voltage. A frequency analysis of the valve currents, as measured flowing through the valve before the midpoint phase split-off, is shown in Fig. 3.19 and indicates high 3rd and 9th harmonic orders, as well as a cluster of harmonics around the 32nd and 60th harmonic orders. When looking at the phase currents at the PCC as shown in Fig. 3.20, zero sequence harmonics have been suppressed as well as the cluster around the 60th harmonic by the HP60 filter. Only the 31st harmonic component still exists that is filtered out by the HP32 filter on the 400 or 330kV AC busbars.

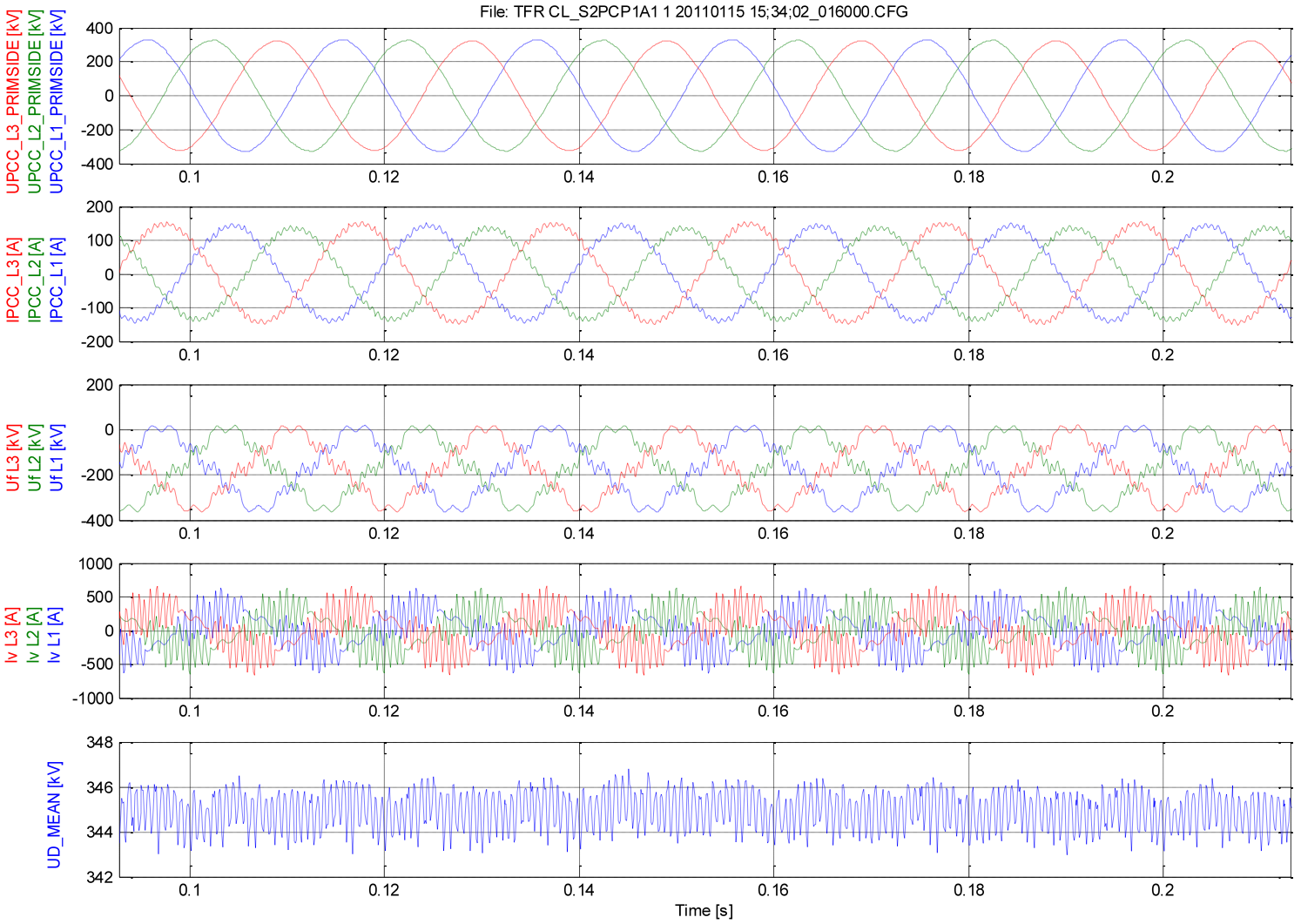

Fig. 3.18 Gerus converter station steady-state waveforms

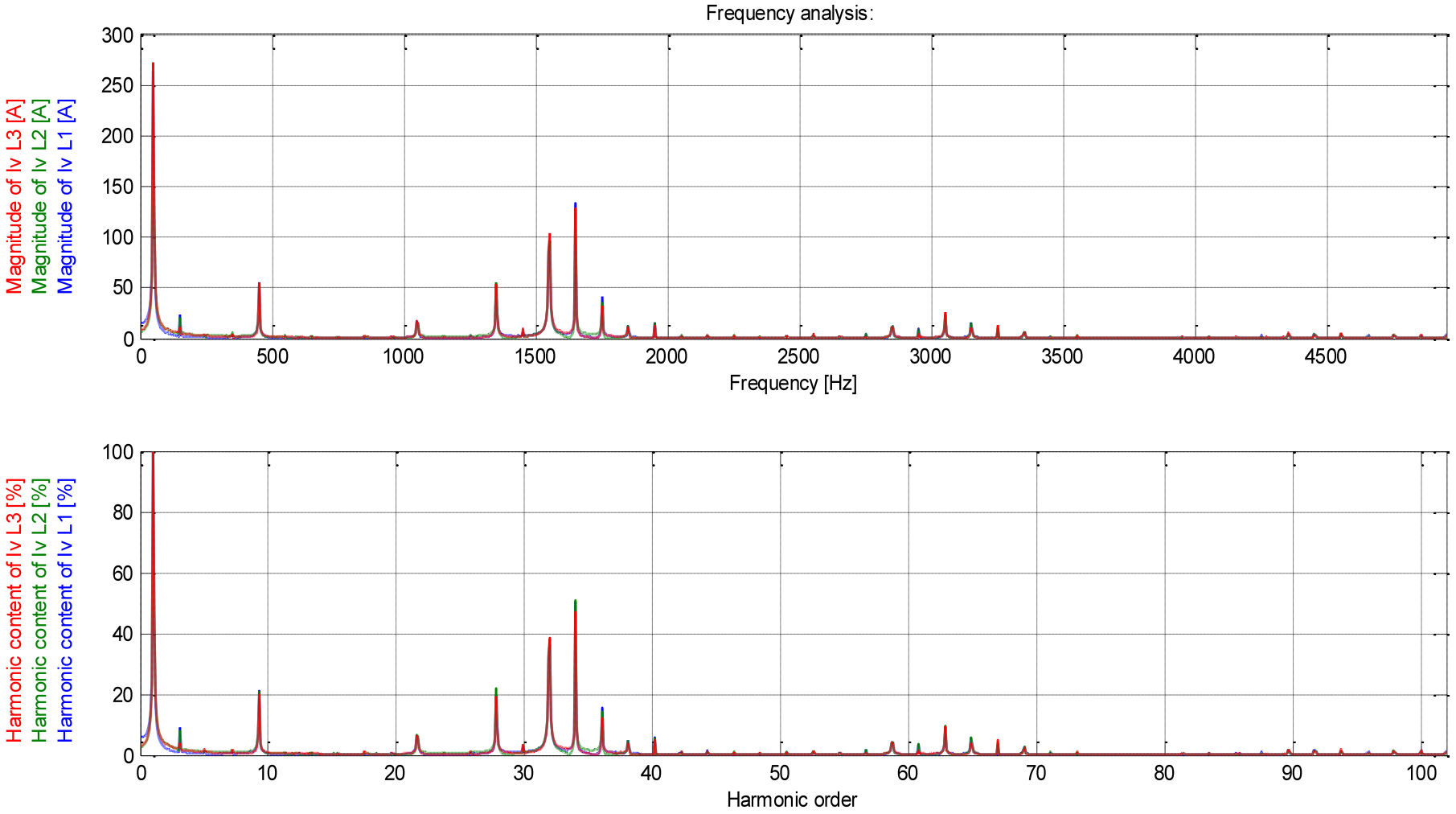

Fig. 3.19 Gerus converter station valve current harmonic content

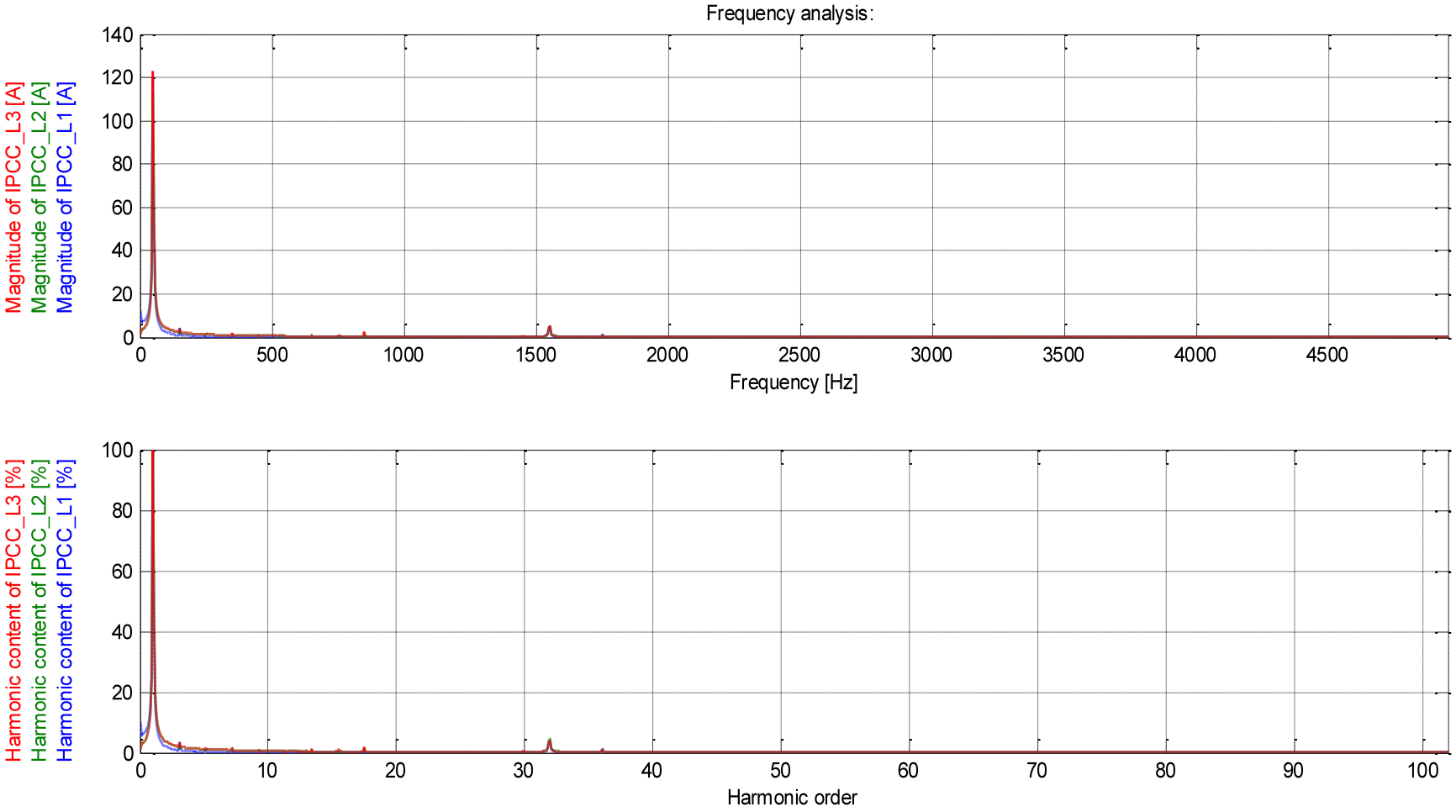

Fig. 3.20 Gerus converter station current harmonics at PCC

3.3 Alternating Current / Direct Current Harmonic interaction theory

3.3.1 Harmonic amplitude transfer ratio

Apart from the AC/DC harmonic interaction theory presented in Section 2.7.2 that centres primarily around harmonic cross-modulation and phase rotation, it would further be interesting to observe the amplitude ratios with which harmonic components are transferred between the AC and DC sides as this would help substantiate whether AC/DC harmonic interaction is a phenomenon to be reckoned with, or if its effects could be considered negligible.

One factor that would influence the harmonic amplitude transfer ratio (HATR) is the harmonic transfer equations from Section 2.7.2 (2.65), (2.67) and (2.69). Another important factor is the relationship to the relative fundamental component generation as determined by the specific switching scheme. The specific PWM method (e.g. PWM or OPWM strategy), modulation index, as well as other factors such as the external AC network frequency response and DC-side frequency response could possibly influence the effective or measured HATR from AC to DC or vice versa.

Another factor to consider is the simplification made in (2.61) whereby harmonic transfer is only considered with regards to modulation by the fundamental component. The higher order terms could also yield interesting results whereby introduced harmonics would also by modulated by the switching scheme's characteristic or pre-existing harmonics.

3.3.1.1 Harmonic amplitude transfer ratio (HATR) from DC to AC side

From Section 2.7.2.2, the side band harmonics that will be generated from any DC harmonic component has been derived, as well as their phase rotations.

From the same derivation in (2.65), the amplitude of the two AC side-band harmonics $U_{ach\pm1}$ can be seen for the basic VSC square wave switching operation where h indicates the DC harmonic order:

$$\left|U_{ach\pm1}\right| = \frac{U_{dch}}{\pi} \tag{3.18}$$

Let the harmonic amplitude transfer ratio (HATR) be given by the relationship

$$HATR = \frac{\left|U_{ach\pm1}\right|}{U_{dch}}. \tag{3.19}$$

This result yields that for a three-phase square-wave switching scheme and similarly for an OPWM switching scheme:

$$HATR = \frac{1}{\pi} \approx 0.318 \tag{3.20}$$

The HATR for a three-phase PWM switching scheme can be derived by using the relationship between the theoretical values for the fundamental components of a square wave switching scheme and a PWM switching scheme.

As was given earlier by (2.54), the fundamental component for a square wave switching scheme is given by:

$$U_{a1sqr} = \frac{4}{\pi}\left(\frac{U_{dc}}{2}\right) = 0.637U_{dc}$$

The fundamental component for a PWM switching scheme is given by (2.53):

$$U_{a1pwm} = \frac{m_a U_{dc}}{2}$$

Using the relationship between (2.53) and (2.54) yields the following result:

$$\frac{U_{a1pwm}}{U_{a1sqr}} = \frac{m_a U_{dc}}{2} * \frac{\pi}{2U_{dc}} = \frac{\pi m_a}{4} \tag{3.21}$$

To calculate the AC-side harmonic magnitudes, the basic VSC switching operation formula multiplied by the fundamental component ratio above yields:

$$\left|U_{ach\pm1}\right| = \left(\frac{U_{dch}}{\pi}\right) * \left(\frac{U_{a1pwm}}{U_{a1sqr}}\right)$$

$$= \frac{U_{dch}}{\pi} * \frac{\pi m_a}{4}$$

$$= \frac{m_a U_{dch}}{4} \tag{3.22}$$

Substituting (3.22) into (3.19) yields that for a three-phase triangular-wave PWM switching scheme:

$$HATR = \frac{m_a}{4} = 0.25m_a \tag{3.23}$$

In general, the two sidebands of the AC-side harmonics' amplitudes transferred from the DC side will for any switching scheme be given by:

$$\left|U_{ach\pm1}\right| = U_{dch} * HATR \tag{3.24}$$

Section 4.3 uses the proposed HATR figures as derived above and tests these in different simulation environments to establish their validity and applicability.

3.3.1.2 Harmonic amplitude transfer ratio from Alternating Current side to Direct Current side

From Section 2.7.2.3, it can be seen that if any of the two AC sideband harmonics are present, a single DC harmonic will be created with an amplitude ratio of:

$$|I_{DCh}| = \frac{3}{2}\left(\frac{2}{\pi}.I_{ACh}\right) = \frac{3}{\pi}\,I_{ACh} \tag{3.25}$$

This gives an effective AC to DC HATR of $\frac{3}{\pi}$ and seems to be independent of the switching technique or modulation index.

Section 4.3 uses the proposed HATR figure as derived above and tests this in different simulation environments to establish their validity and applicability.

In practice, the AC voltage- and current harmonics presented to the VSC are related by the system impedance at that specific frequency and transferred to the relevant DC-side frequency depending on the AC-side harmonic phase rotation. Depending on the DC-side frequency response and DC capacitor size, DC harmonics can be attenuated or filtered out. The remaining DC-side harmonic is transferred back to the AC side depending on the scheme specific HATR.

The effective cross-modulated voltage harmonics seen at the point of common coupling (PCC) on the system-side of the converter reactor or converter transformer is strongly influenced by the system impedance at those specific frequencies. Therefore low fault level systems are much more prone to AC/DC harmonic interaction. In general, OPWM schemes will show a larger total interaction transfer ratio than PWM switched schemes due to the larger DC to AC HATR. The effect of third harmonic injection on PWM schemes' HATR has not been investigated.

The diagram in Fig. 3.21 shows the AC-side and DC-side harmonics of a VSC scheme. A 13th harmonic PPS is introduced on the AC side and translates due to the fundamental component to a (13-1)th or 12th harmonic on the DC side as two sidebands. The 12th harmonic on the DC side translates back to an 11th harmonic NPS on the AC side.

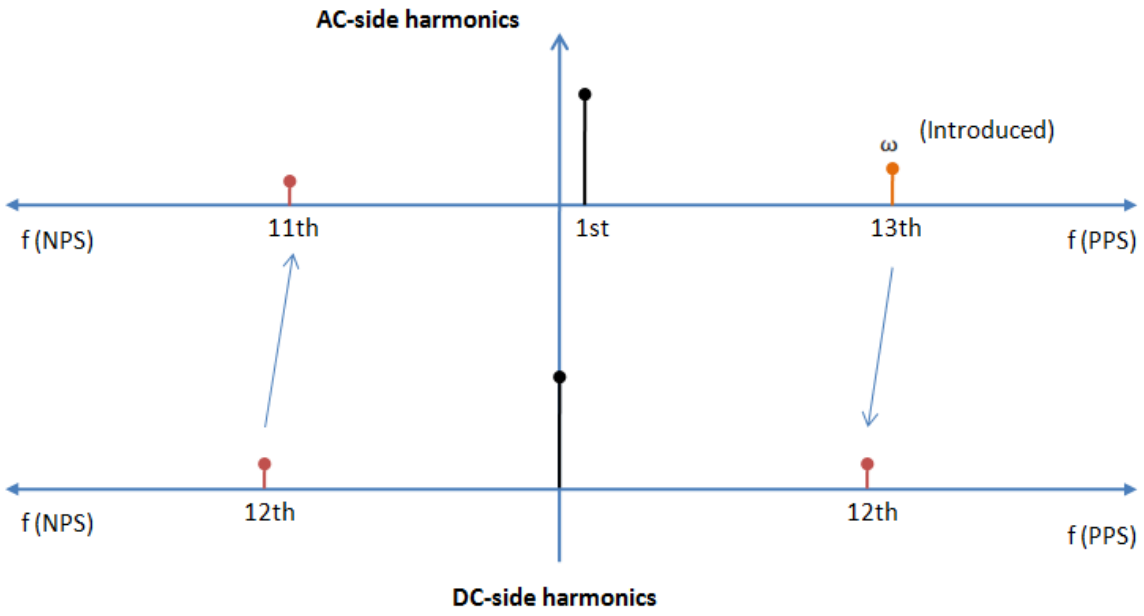

Fig. 3.21 Harmonic transfer due to modulation by fundamental component

3.3.2 Modulation by scheme characteristic harmonics

The fundamental component of the VSC scheme is designed to be the largest and therefore contributes the most to AC/DC harmonic interaction. Yet, it should be noted that the characteristic or pre-existing harmonics of the scheme will also play a role although to a lesser or even negligible extent.

If the simplification in (2.61) is not done, it can be shown that the higher order terms depending on their amplitudes will modulate DC-side harmonics to new AC harmonics as follows using (2.65). Instead of considering the fundamental component ω_1 , each characteristic harmonics that would normally be produced can be considered independently as ω_n . This would yield:

$$\boldsymbol{u_{vn}(t)} = (-1)^{\frac{n+3}{2}} * \left(\frac{2U_{dc0}}{\pi n} e^{j(\omega_n t - n\delta)} + \frac{U_{dch}}{\pi n}.e^{j((\omega_n+\omega)t-n\delta)} + \frac{U_{dch}}{\pi n}.e^{j((\omega_n-\omega)t-n\delta)}\right) \quad (3.26)$$

This result shows that each DC-side harmonic will be transferred to the AC side at two sidebands at ω_n radians apart from the DC harmonic. As shown as an example in Fig. 3.22, if a scheme characteristically generates a relatively large 5^{th} harmonic NPS by design and a new

AC-side 13th harmonic PPS is introduced, apart from the 12th harmonic DC side component and AC-side 11th harmonic NPS harmonic produced by cross-modulation due to the fundamental component, additional harmonics will be produced on the AC side at (12-5=7) 7th harmonic as well as at (12+5=17) 17th harmonic due to the 12th harmonic DC component. The phase rotation of the generated harmonics will depend on the phase rotation of the generated characteristic 5th harmonic. If the 5th harmonic is characteristically with NPS, the phase rotations will be opposite to those produced by the normal PPS fundamental component.

The same 13th harmonic (PPS) will also produce a smaller 18th harmonic DC component due to the generated NPS 5th harmonic and cross-modulate to a relatively small 23rd harmonic on the AC side with NPS. If the 18th harmonic DC component has any significant amplitude, it will again modulate back to the AC side also with the fundamental component to a 19th harmonic PPS and 17th harmonic NPS. Depending on the existing 17th harmonic, the new superimposed value will depend on the relative phase angles of the two generated 17th NPS harmonics.

These statements are further demonstrated by simulation in Section 4.4 to provide more clarity.

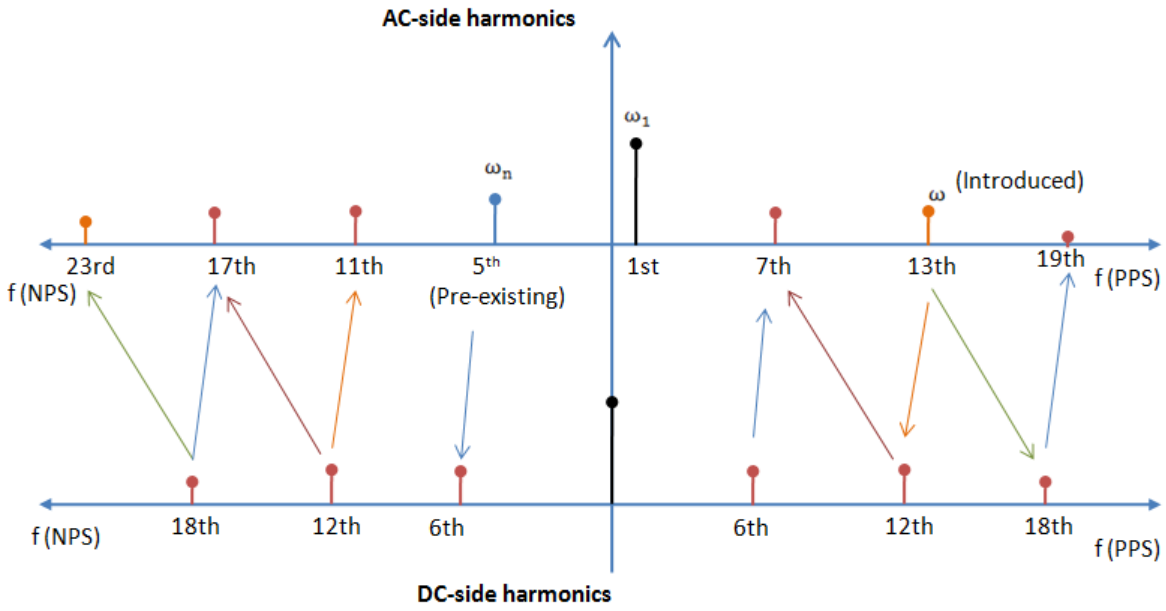

Fig. 3.22 Harmonic transfer due to modulation by scheme characteristic harmonics

4 Harmonic interaction simulation and modelling techniques

4.1 Modelling of NamPower and ZESCO transmission networks

Section 2.8 described the various modelling- and simulation techniques especially pertaining to EMT- and harmonic studies. In order to study harmonic interaction phenomena, these principles are important to obtain accurate results especially at higher frequencies.

For the complete NamPower network and southern ZESCO network, all transmission lines with tower geometries and frequency dependant parameters, transformers, generators, filter banks, SVC's and HVDC VSC have been modelled according to the principles described in Section 2.8 so as to be valid both load flow-, harmonic load flow-, RMS dynamic-, EMT dynamic studies and impedance versus frequency sweeps. The modelling of double circuit lines in DigSilent PowerFactory however have the limitation that only a lumped line parameter model can be selected as opposed to the preferred distributed model. Fortunately, in the network vicinity where studies were conducted, no double circuit lines exist that would influence the frequency response or EMT results. The Eskom network connected to the Namibian network has been modelled as an external grid with appropriate fault level, X/R ratio, inertia or acceleration time constant and secondary frequency bias in MW/Hz.

For EMT studies in DigSilent PowerFactory, a simplified HVDC VSC model excluding certain controllers is used in order to simulate valve switching instants but does not replicate the exact switching techniques employed in the PSCAD model, RTDS or real life scheme. This model is valid and effective to illustrate the principles of AC/DC harmonic interaction, but will not produce the exact same harmonic amplitude results as compared to the scheme's recorded Transient Fault Records (TFRs) when attempting to reconstruct a real life harmonic cross-modulation and resonance case.

Therefore, the case study example in Chapter 5 employs a DigSilent PowerFactory network model that is accurate for impedance versus frequency sweeps, EMT study for line energisation and time domain frequency analysis and checking of load flow results. A PSCAD HVDC VSC model developed by the manufacturer of the HVDC scheme is used to reconstruct the real life case study and confirm the preliminary PowerFacory results.

4.2 Development of Electromagnetic Transient mode harmonic voltage and current sources

As the purpose of modelling the interconnected AC networks and HVDC VSC scheme is to study AC/DC harmonic interaction, an essential component would be a harmonic voltage- or current source to provide controlled AC-side generation of harmonic components of known amplitude and phase rotation.

Although DigSilent PowerFactory has standard harmonic sources, these only operate in harmonic load flows and not in RMS/EMT simulations. In order to simulate AC/DC interaction, an EMT simulation is required to incorporate a detailed model for IGBT valve firing. The problem is thus that harmonic sources would not be taken into account and AC/DC harmonic interaction would not be visible in DigSilent PowerFactory simulations.

The solution was to create both harmonic voltage- and current sources by creating a composite model that incorporates either the standard AC voltage source with two terminals that can be put in series with the network to super-impose voltage harmonics, or the standard AC current source with one terminal to be put in parallel with a busbar. The parallel-connected harmonic current source effectively models a harmonic load that will translate to voltage harmonics according to the system frequency dependant impedance. The standard voltage source or current source components are then fed by a DigSilent simulation language (DSL) script to output the desired harmonic content during EMT simulations at the desired amplitudes and phase angles as governed by the chosen input parameters.

The first step is to create the library objects that will be referred to by the element objects. A frame is created that houses the standard “Iac” or “Vac” element type, as well as a block containing the DSL signal generator script. Although only creation of a harmonic current source is shown, the process for the harmonic voltage source is similar. The two blocks are connected by three signals that are named after the Iac or Vac internal variables designating the phase currents or voltages as shown in Fig. 4.1:

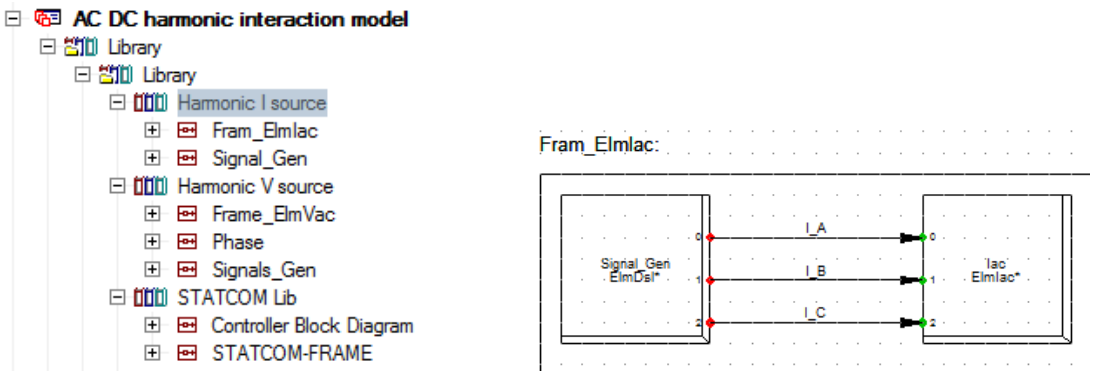

Fig. 4.1 Harmonic current source library type

The second step is to create the DSL script that will feed the Iac or Vac element. The "Signal_Gen" DSL element is set up with the correct parameters and internal variables and the simple script is entered as shown in Fig. 4.2. The phase angle for each phase (Pha, Phb and Phc) is defined as multiples of $\pi/3$ to make easy to enter a PPS (0, 4, 2) or NPS (0, 2, 4) rotation as shown in Fig. 4.3.

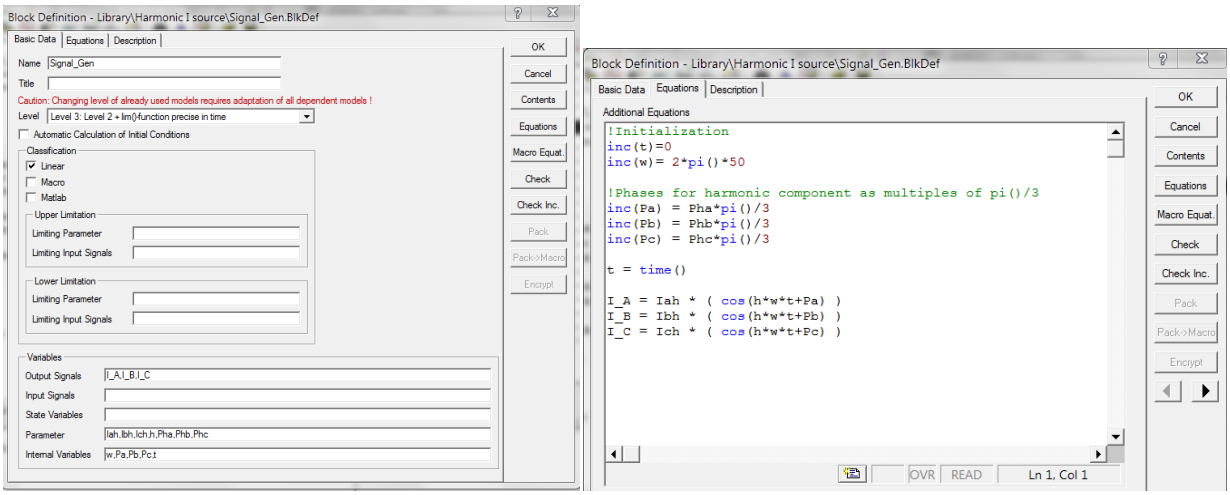

Fig. 4.2 Harmonic current source DSL script

After the library objects have been created, the elements objects in the active grid can be created and linked to the library items. The desired parameters defined in the DSL script can be entered into the DSL parameter page shown in Fig. 4.3:

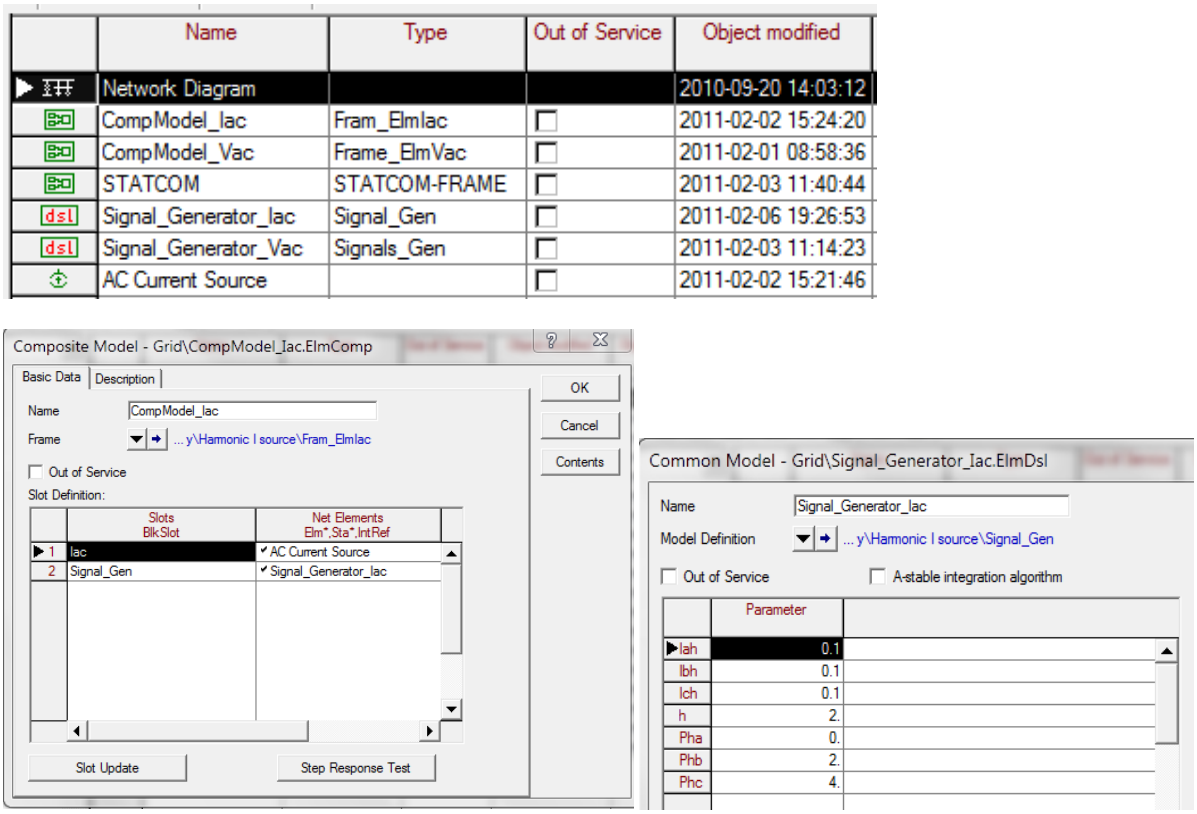

Fig. 4.3 Harmonic current source element type and frame

Fig. 4.4 shows the current- or voltage source outputs from the parameters entered in Fig 4.3. The parameters yield an output waveform with the peak amplitude at 0.1kA, harmonic order at 2 and the phase angle parameters yield negative phase rotation:

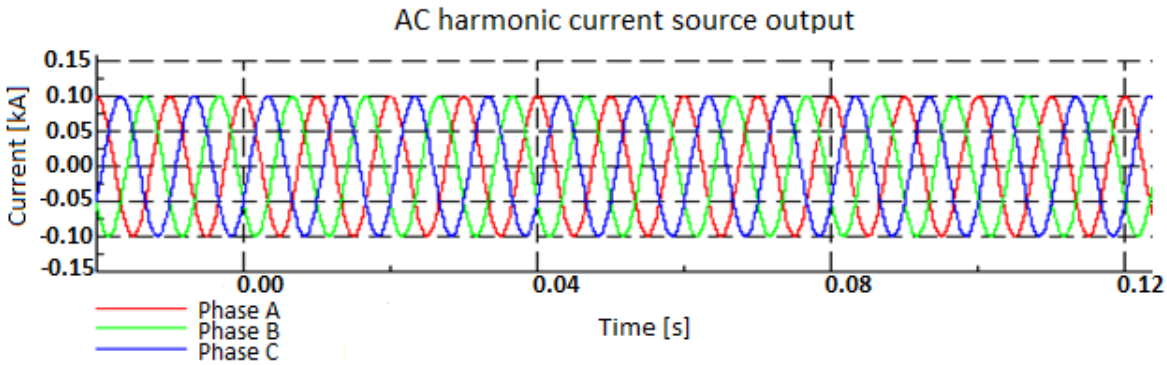

Fig. 4.4 Harmonic current source output of negative phase sequence, 2nd harmonic

The result is a harmonic current or voltage source that is easily configurable and can now be used in EMT simulations together with detailed VSC models to simulate AC/DC harmonic interaction.

4.3 Harmonic Interaction models

4.3.1 Mathematical model in Excel

An Excel model has been built using the switching functions (2.45)-(2.47) derived in Section 2.6.3. The model incorporates the addition of a harmonic of specified order and magnitude to be superimposed on the DC voltage. A FFT is done before and after the DC-side harmonic activation and then a harmonic sequence analysis as is done on the three phase quantities to confirm the phase rotation of the AC side harmonics. The results should confirm the mathematical theory presented in Section 3.3.1.

The sampling rate is set at 2048 samples per cycle or 102.4kHz to eliminate some of the unwanted effects of the FTT as discussed in Section 2.8.9.2.

First, a normal triangular PWM switching scheme at 33rd harmonic with modulation index equal to 1 is presented in Fig. 4.5 and analysed.

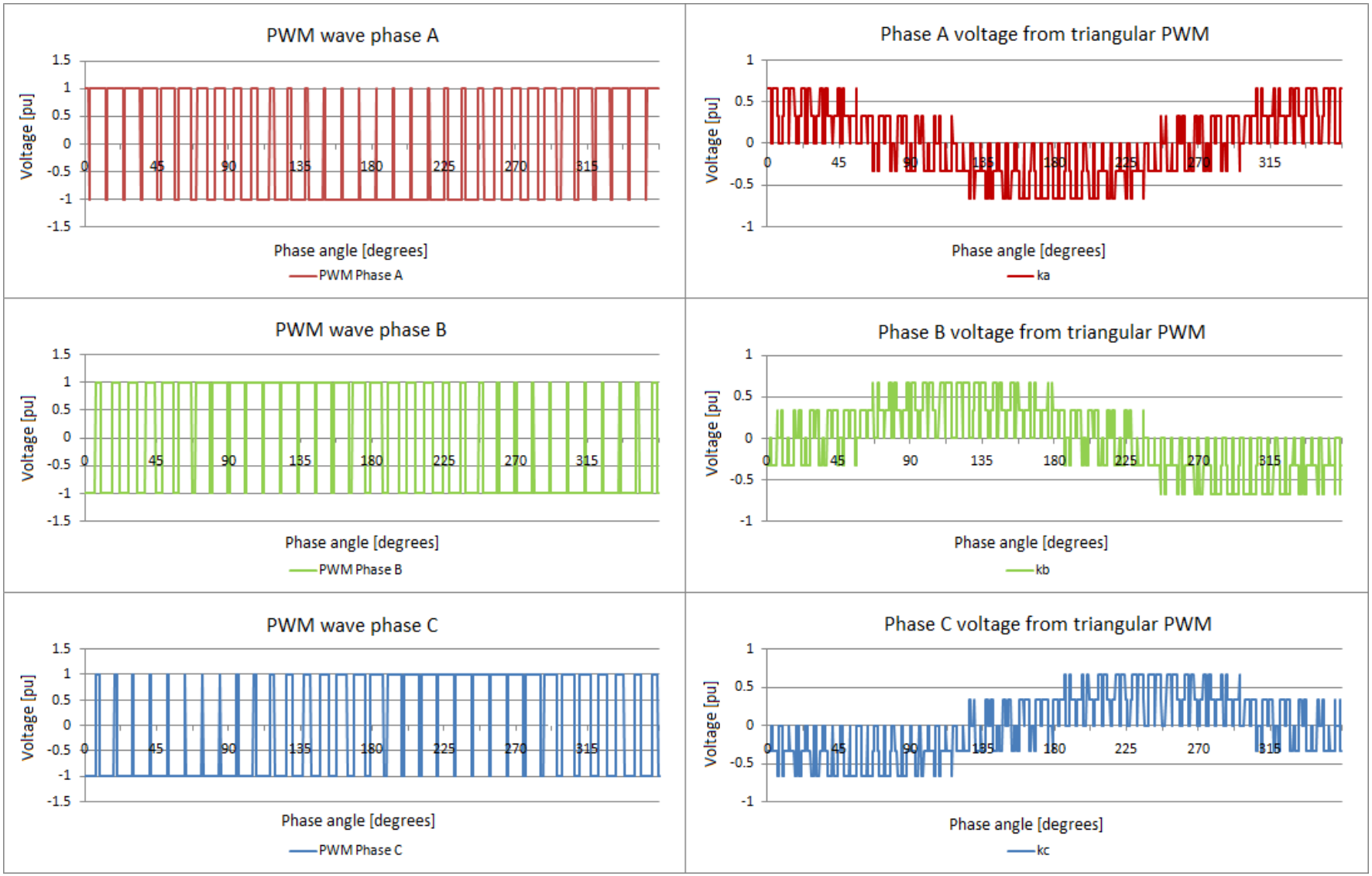

Fig. 4.5 VSC model PWM and phase quantity switching waveforms

The representation of the harmonic sequence components of the phase quantities in Fig. 4.5 for lower order harmonics is shown in Fig. 4.6. A relatively high switching frequency is chosen not to have dominant lower order harmonics so that additional harmonic components can easily be identified.

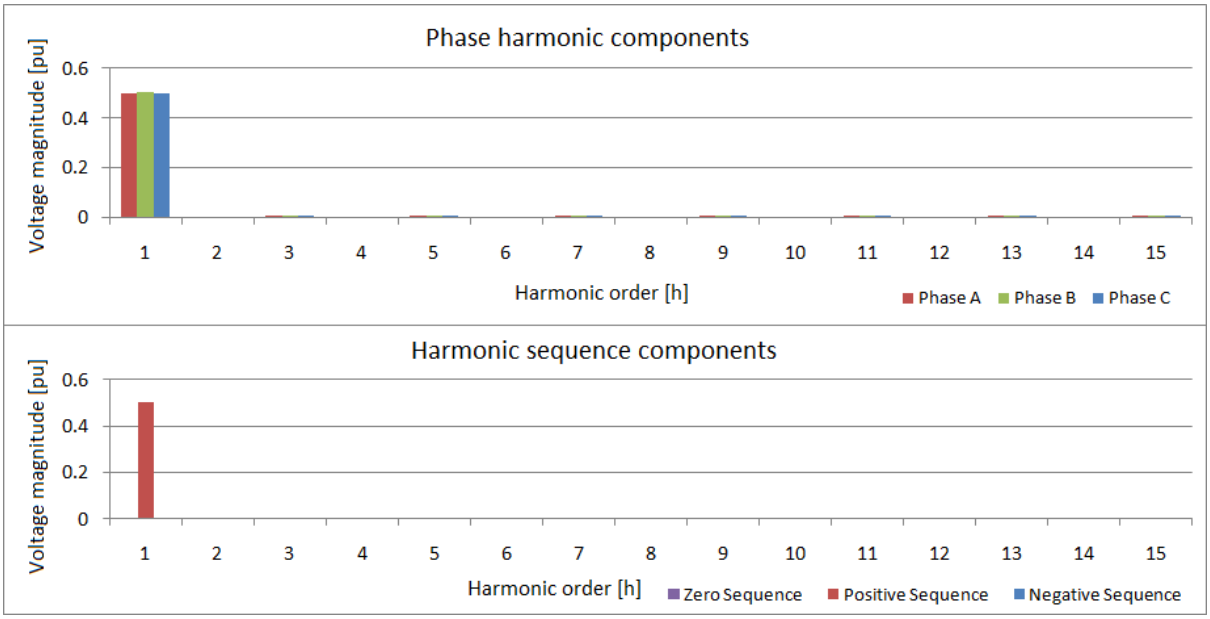

Fig. 4.6 Excel VSC model lower order harmonics

It is clear from Fig. 4.6 that no lower order harmonics of substantial magnitude are present other than the fundamental component. Now a 6th harmonic is added to the DC voltage with amplitude of 0.1 for demonstration purposes as shown in Fig. 4.7:

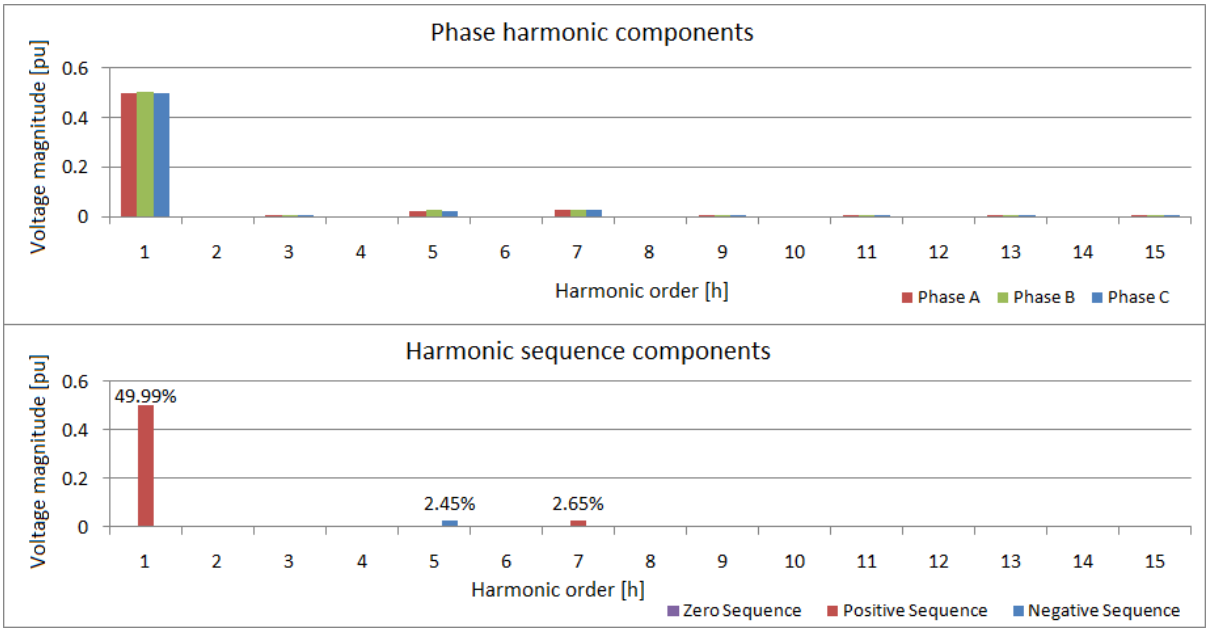

Fig. 4.7 Excel VSC model with 6th harmonic DC component

The 6th harmonic on the DC side is transferred to the AC side as a 5th harmonic with negative phase sequence and a 7th harmonic with positive phase sequence. According to (3.22) and (3.24) for a triangular PWM three-phase switching scheme, the transferred harmonic amplitude would be:

$$\left|U_{ach\pm1}\right| = U_{dch} * HATR = 0.1 * 1 * 0.25 = 0.025 = 2.5\%$$

This agrees with the simulated values in Fig. 4.7.

The next example shows a 3rd harmonic on the DC side with the same amplitude of 0.1, generating non-characteristic (even) harmonics on the AC side and also confirms the HATR of the previous example. A 2nd harmonic with negative phase sequence and a 4th harmonic with positive phase sequence is generated on the AC side with amplitude 0.025 or 2.5% as expected as shown in Fig. 4.8:

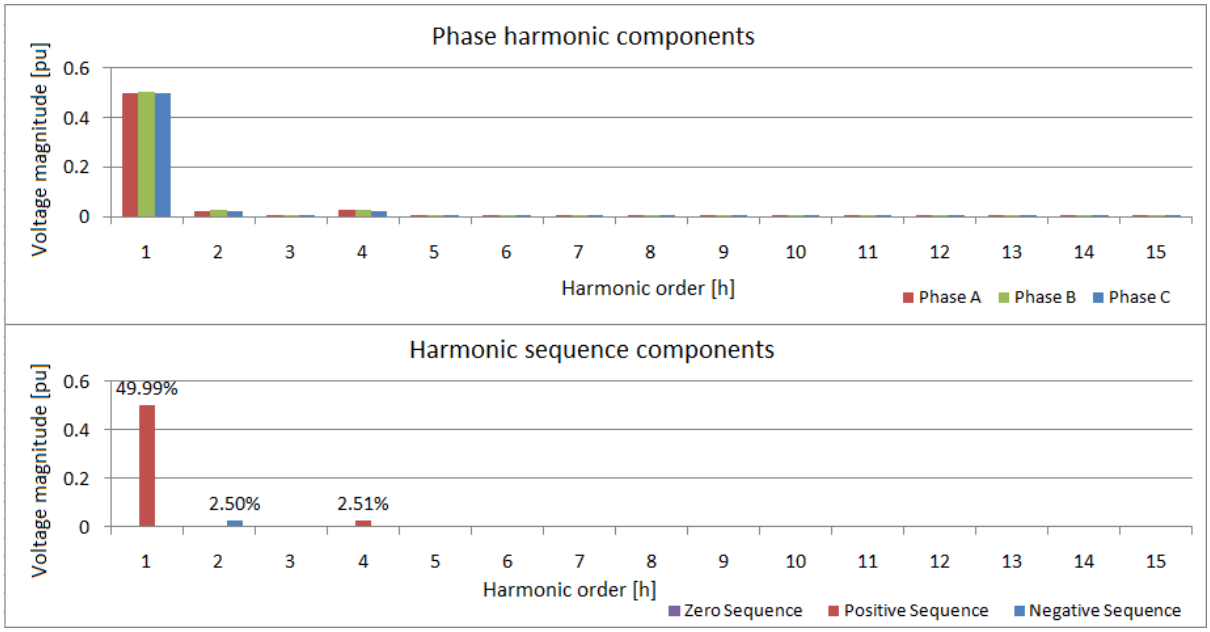

Fig. 4.8 Excel VSC model with 3rd harmonic DC component

The small differences in amplitude between the expected theoretical values and simulation values especially for odd harmonic orders are thought to be due to the FFT process, the conversion to sequence components, or small residual components from the triangular PWM harmonics. Taking a closer look at the pure triangular PWM at 33rd harmonic sequence components with no DC-side harmonic component added and excluding the fundamental component reveals that this could be the case as shown in Fig. 4.9. The phase angles of the existing harmonic component and that of the transferred harmonic component need to be taken into account as they would not add arithmetically, but would be a sum of two vector components. Thus the resultant harmonic amplitude could be slightly more or less than the expected value.

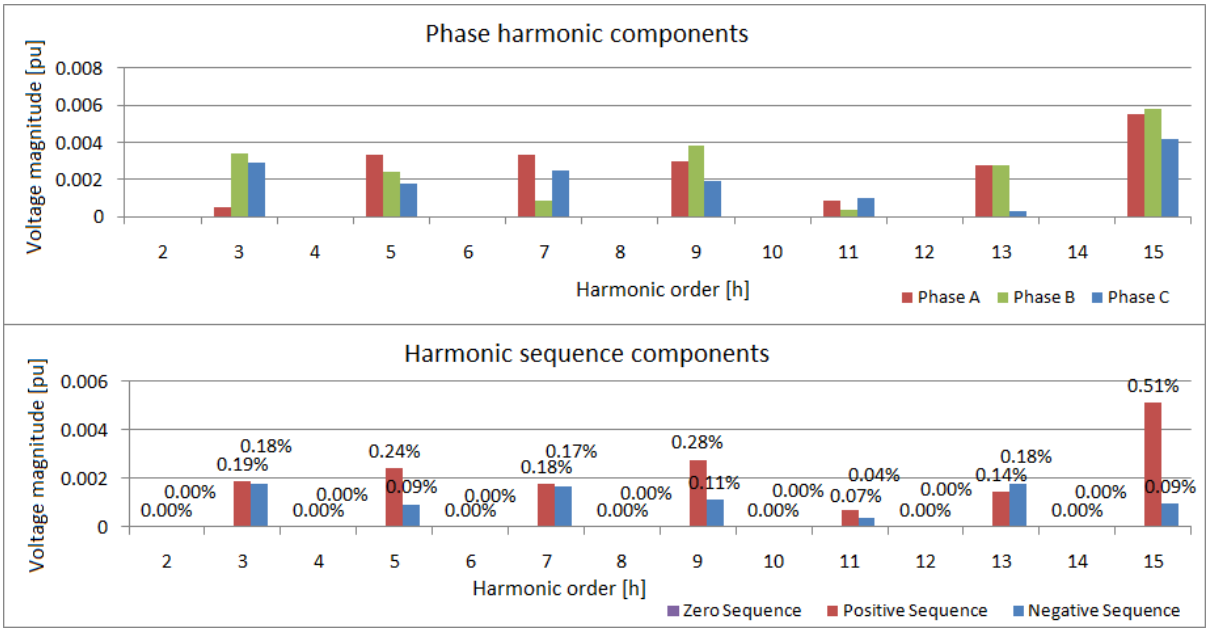

Fig. 4.9 Excel VSC model residual harmonic components

The harmonic amplitude transfer ratio for a PWM switching scheme depends mainly on the fundamental component amplitude. If a modulation index of 0.8 is used, the harmonic amplitude transfer ratio will be less by a factor 0.8. This has been tested by many different examples not listed here. The harmonic amplitude transfer ratios (HATR) as defined from the DC to the AC side for VSC's are revisited and given by:

For a three-phase square-wave switching scheme (3.20):

$$HATR = \frac{1}{\pi} \approx 0.318$$

For a three-phase triangular-wave PWM switching scheme (3.22):

$$HATR = \frac{m_a}{4} = 0.25 m_a$$

The two sidebands of the AC-side harmonics' amplitudes transferred from the DC side are given by (3.24):

$$U_{ach\pm1} = U_{dch} * HATR$$

For a three-phase OPWM switching scheme the same HATR applies as for a square-wave switching scheme. To confirm this statement for OPWM, a 13th harmonic of amplitude 0.1 was added to the DC voltage of a three-phase OPWM switching scheme that has been programmed to minimise all odd harmonic components below 17th harmonic with modulation index at 0.946.

Except for this specific case's OPWM characteristic 5th harmonic due to the OPWM solution implemented and the possible addition of a small residual harmonic components at both the 12th and 14th harmonics (although not expected for even harmonics), the fundamental and harmonic amplitudes should be as follows:

$$U_{ac1} = \frac{2}{\pi} * 0.946 = 0.6022 = 60.22\%$$

$$U_{ac12} = U_{ac14} = U_{dc13} * 0.318 = 0.1 * 0.318 = 3.18\%$$

These results are confirmed by the harmonic sequence analysis results in Fig. 4.11 derived from the time domain waveform shown in Fig. 4.10:

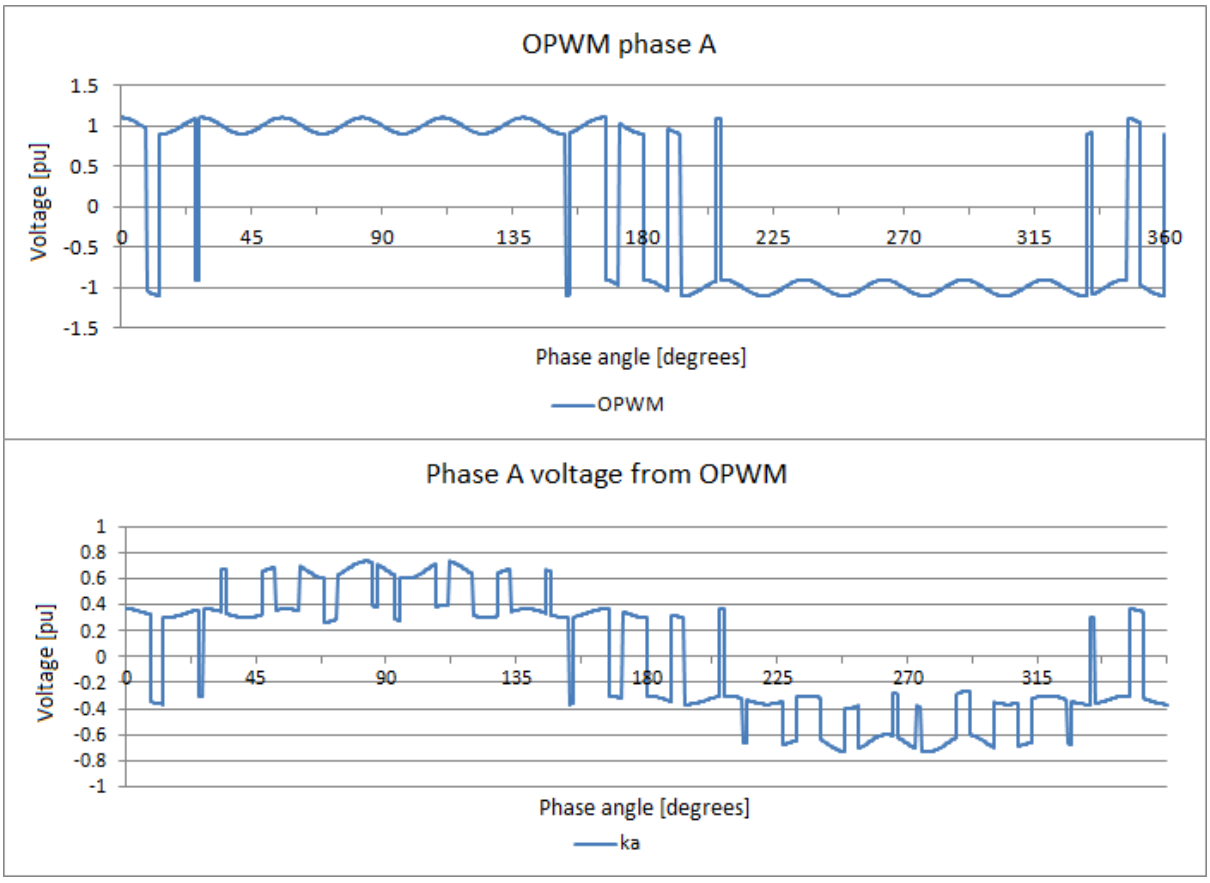

Fig. 4.10 Excel VSC OPWM model switching with 13th harmonic DC

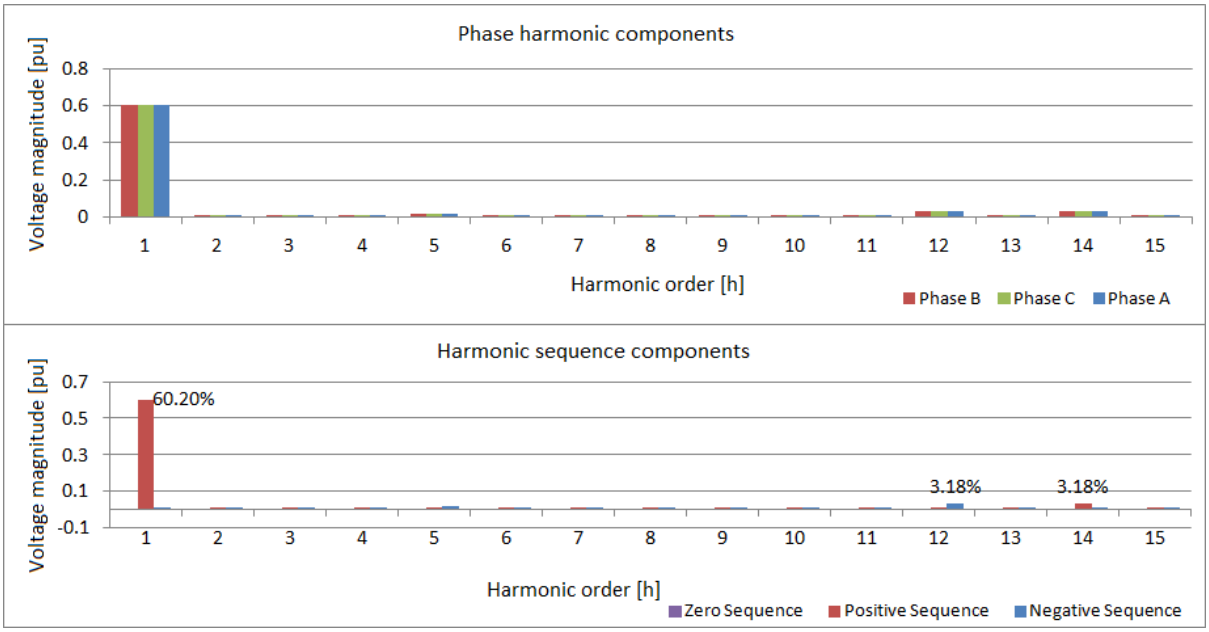

Fig. 4.11 Excel VSC OPWM harmonic components with 13th harmonic DC

A VSC converter will thus have a higher AC/DC harmonic interaction in OPWM mode than in a normal PWM mode. As stated earlier, the effect of PWM with third harmonic injection on the HATR has not been investigated.

The transfer of harmonic components from the AC to DC side will be discussed in the next section.

4.3.2 DigSilent PowerFactory harmonic interaction results

A DigSilent PowerFactory model was built to resemble a basic VSC terminal with DC capacitance. In this case, a simple 10MVA STATCOM was modelled using the standard PWM Rectifier/Inverter element with one DC connection. A switching frequency of 4kHz with sinusoidal PWM was selected so as to move the switching frequency far away from the lower harmonic orders. An EMT harmonic current source as developed in Section 4.2 was deployed on the 33kV busbar as shown in Fig 4.12. A series AC harmonic voltage source was also developed and tested but not activated for the following examples. Experiments were also done with a second harmonic current source connected to be able to simulate two different AC-side harmonic components.

The external grid has been set to have a low fault level of 250MVA so as to allow visible voltage harmonics to exist due to the harmonic current injection by the harmonic current source. The harmonic current source was then set to inject a specific harmonic order with

either negative or positive phase sequence at suitable amplitude that would give a notable harmonic voltage component of between 0.01pu and 0.1pu. Although it was tested, zero phase sequence harmonic generation was not selected for an example because it is not transmitted to the DC side of a VSC as proven earlier. The VSC control mode was set to AC/DC voltage control and the voltage set-point was set to slightly above 1.1pu in order to have the modulation index close to 0.75.

The time step and simulation output was set to 1µs and the FFT results were calculated using 4069 samples per period to retain good frequency resolution. Different sampled cycles in the records was compared to ensure no differences occur.

To compare the simulation results with (2.67), the harmonic currents at the VSC terminals and DC-side harmonic currents were measured. Because the STATCOM is connected to an external grid, the grid's source impedance will influence the voltage harmonics as it would provide an impedance path to sink the current harmonics flowing from the VSC. Therefore, considering current harmonics should give a better view on the HATR. Fig. 4.12 shows the single line diagram with load-flow results:

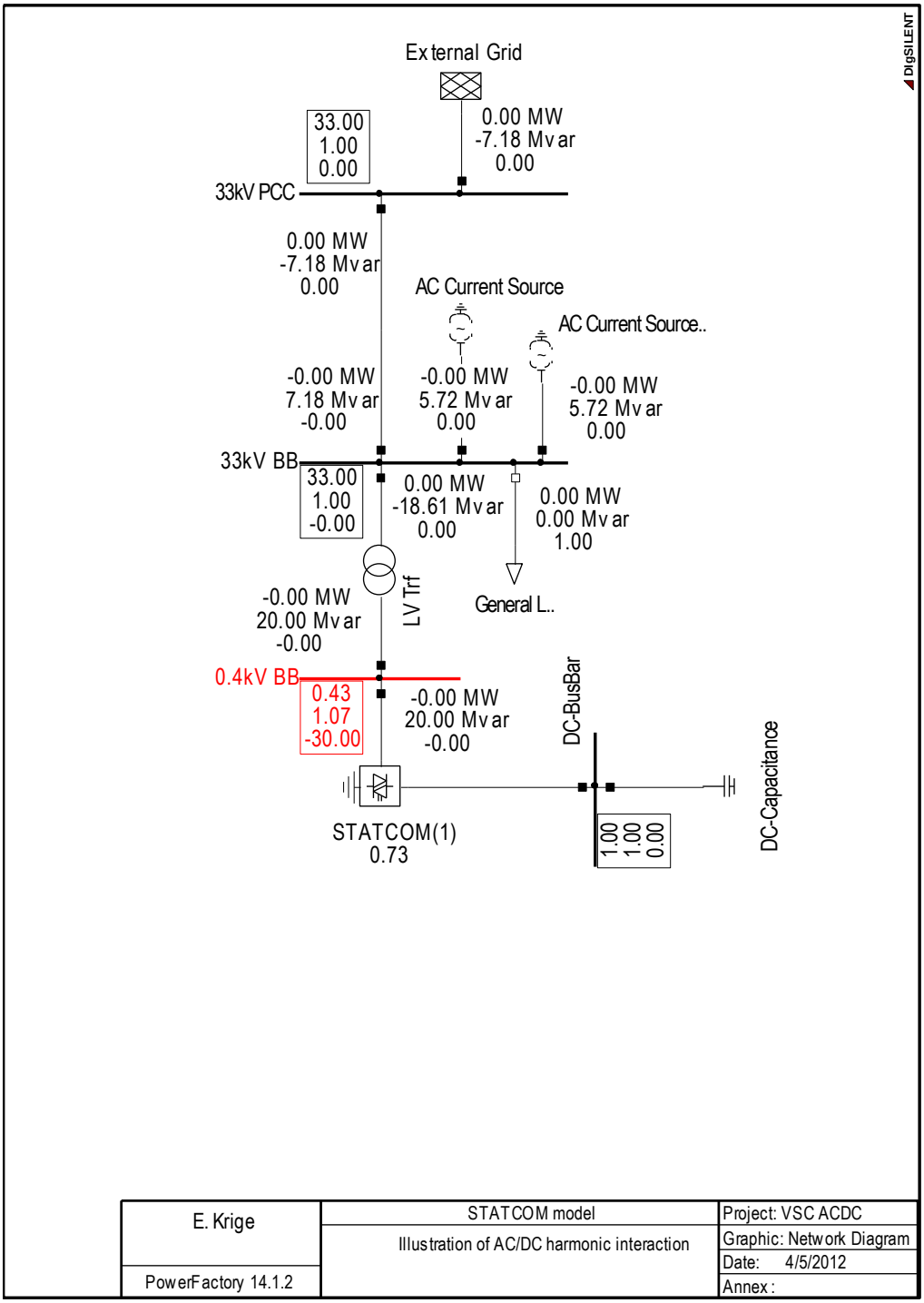

Fig. 4.12 PowerFactory STATCOM model single line diagram

4.3.2.2 Example 1:

The first example shown in Fig. 4.13 monitors the AC-side and DC-side harmonic components when a 5th harmonic with positive phase sequence (non-characteristically) is injected on the 33kV busbar:

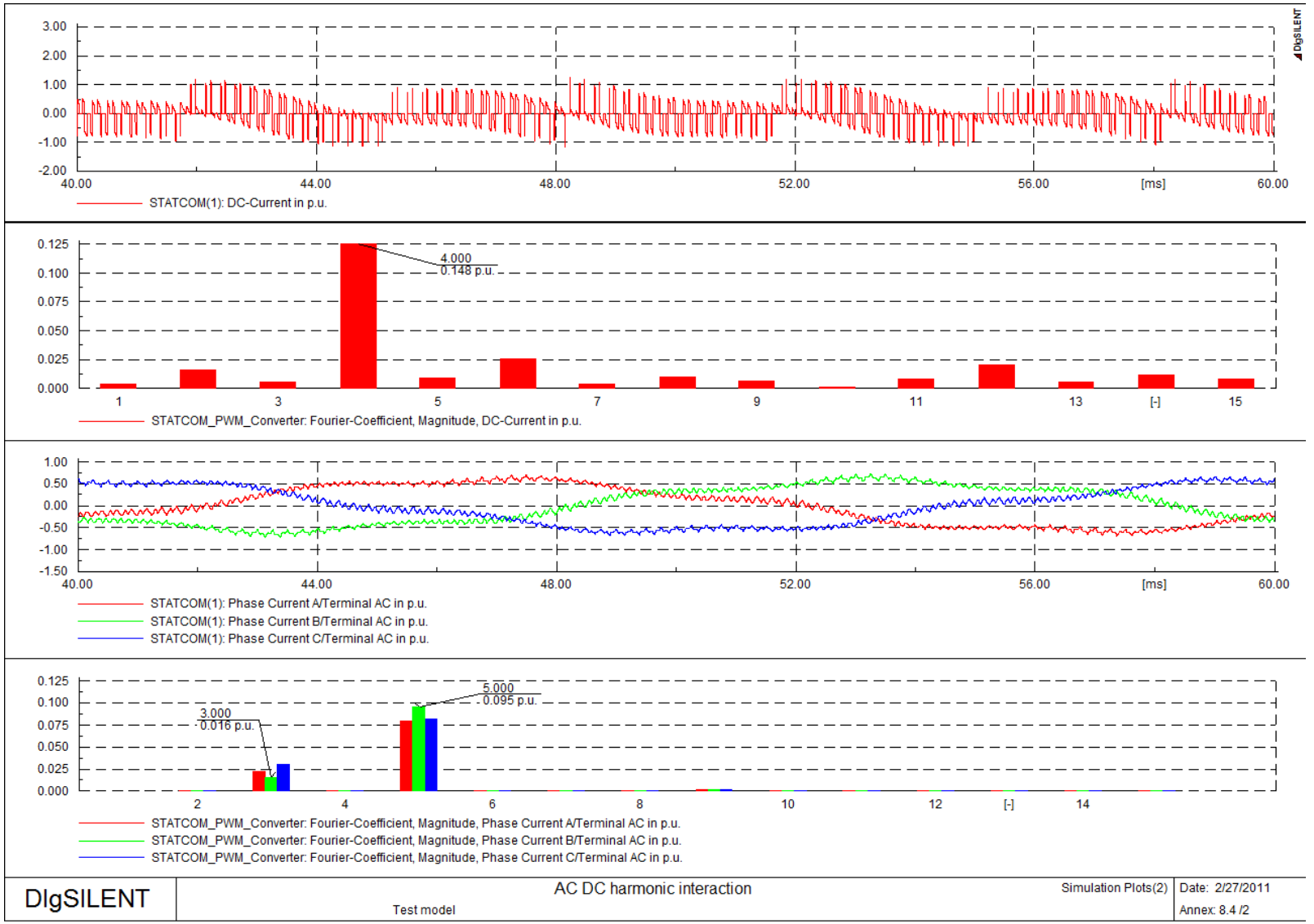

Fig. 4.13 PowerFactory model harmonic components with 5th harmonic PPS injection

The results in Fig. 4.13 show that the 5th harmonic with positive phase sequence yields a 4th DC harmonic component and cross-modulates back to the AC side as a 3rd harmonic with negative phase sequence, following the rules from Section 2.7.2.4. According (3.22) and (3.25), the amplitude of the new AC harmonic for a three-phase PWM switching scheme should be equal to $I_{ACh2} = I_{ACh1} * \frac{3}{\pi} * 0.25 m_a = 0.095 * \frac{3}{\pi} * 0.25 * 0.738 = 0.0167 pu$. The measured simulation value is 0.016pu. The phase rotations of the two harmonics have been confirmed by exporting the PowerFactory magnitude and phase information to Excel and running it through the same harmonic sequence analyser as used previously.

4.3.2.3 Example 2:

The next example in Fig. 4.14 shows a 7th harmonic with positive phase rotation (characteristically) that cross-modulates back as a 5th harmonic with negative phase sequence. The new harmonic amplitude should be equal to $I_{ACh2} = I_{ACh1} * \frac{3}{\pi} * 0.25 m_a = 0.084 * \frac{3}{\pi} * 0.25 * 0.738 = 0.0148 pu$. The measured simulation result is 0.014pu.

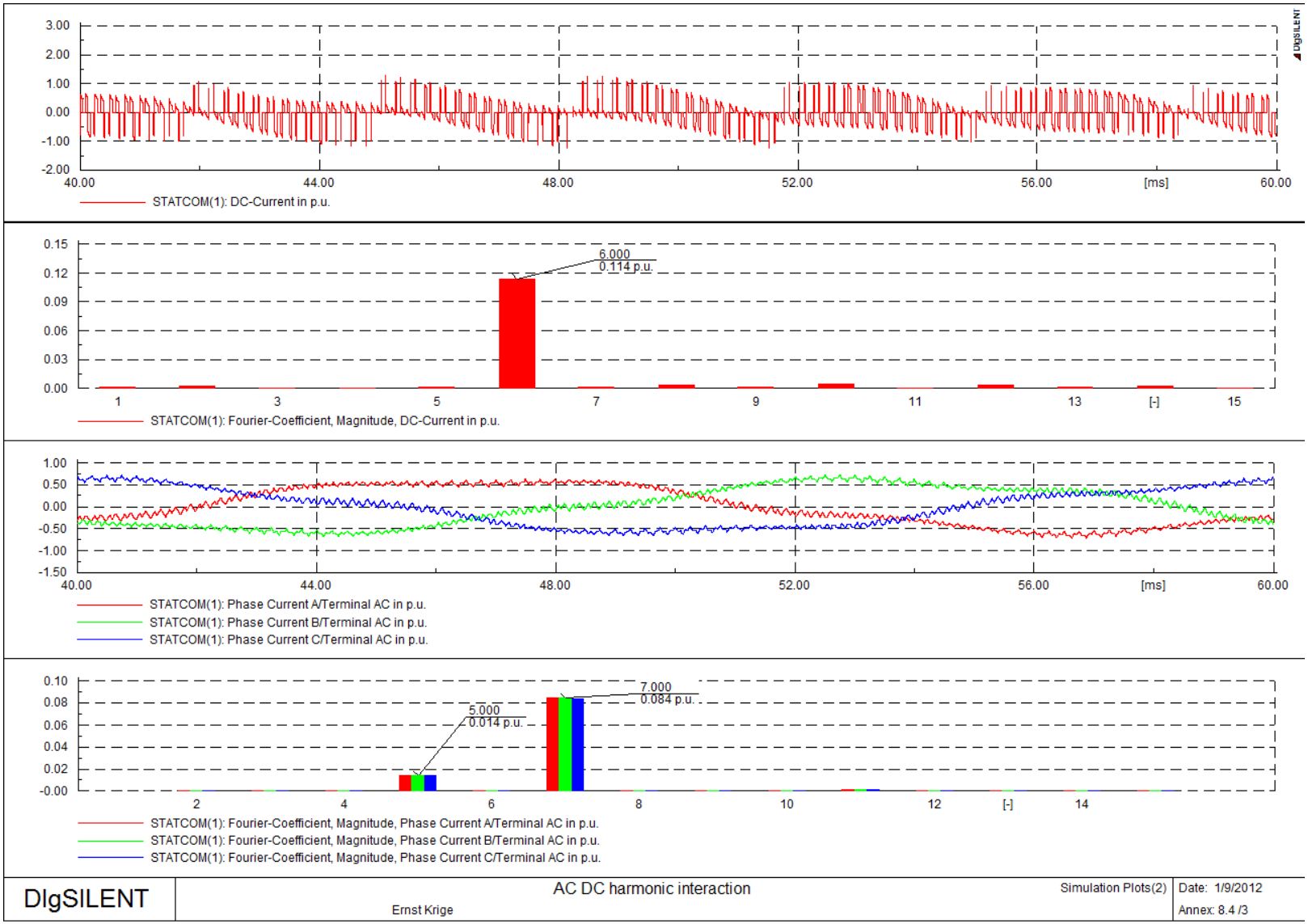

Fig. 4.14 PowerFactory model harmonic components with 7th harmonic PPS injection

Fig. 4.15 below confirms the expected harmonic sequence components as exported to the Excel harmonic sequence component analyser:

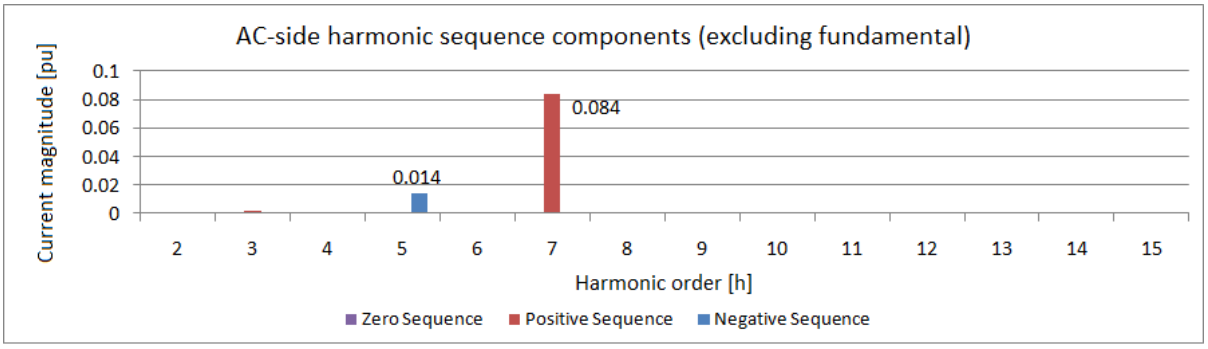

Fig. 4.15 Harmonic sequence components with 7th harmonic PPS injection

4.3.2.4 Example 3:

The last example shows a 4th harmonic NPS injection that cross-modulates to a 6th harmonic PPS. The new harmonic amplitude should be equal to $I_{ACh2} = I_{ACh1} * \frac{3}{\pi} * 0.25 m_a = 0.082 * \frac{3}{\pi} * 0.25 * 0.732 = 0.014 pu$**.** The measured simulation result is 0.013pu. Compare this with the PSCAD example in Section 4.3.3.1.

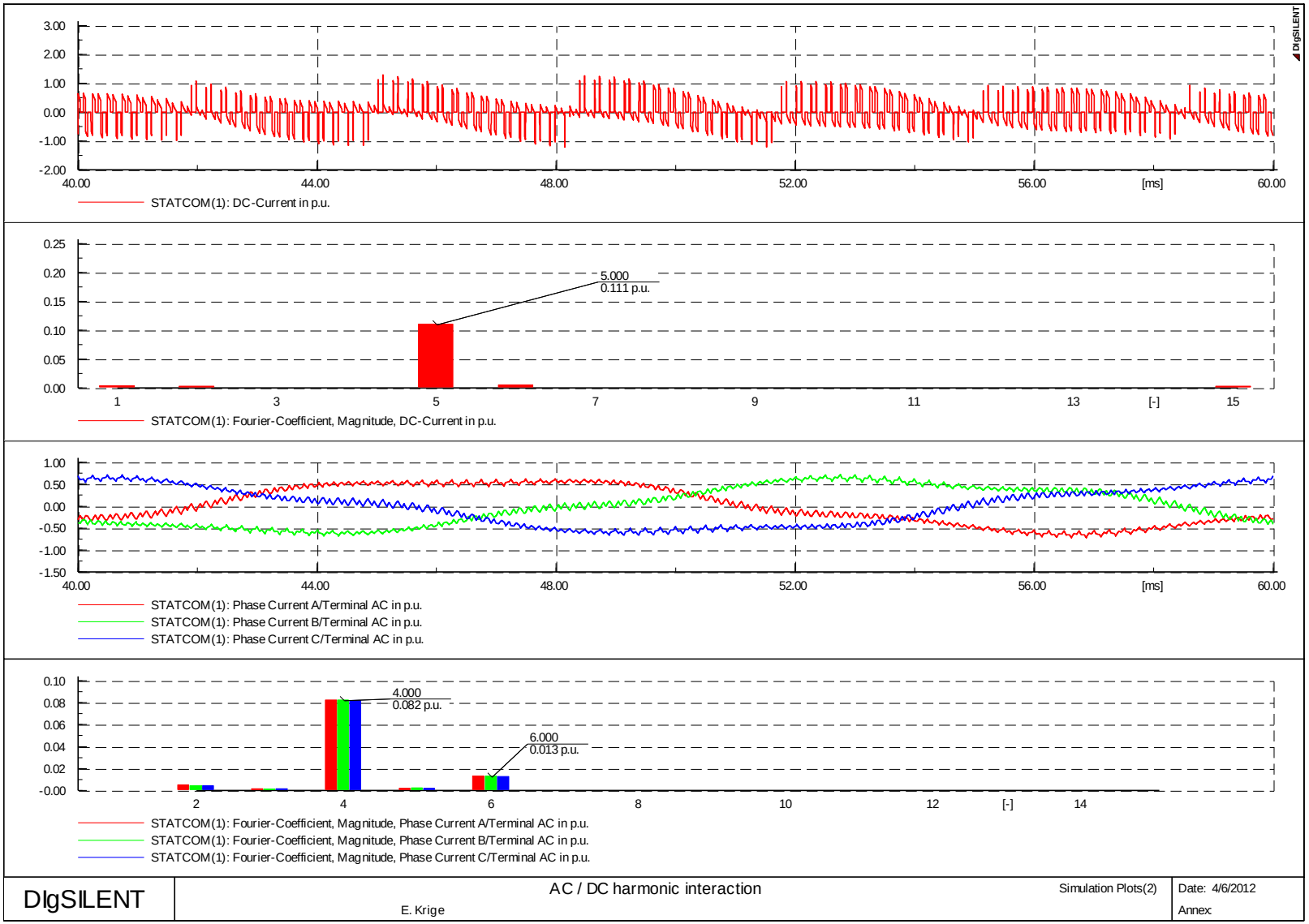

Fig. 4.16 PowerFactory model harmonic components with 4th harmonic NPS injection

The Excel harmonic sequence analysis confirms the 4th harmonic NPS and 6th harmonic PPS phase rotations as shown in Fig. 4.17:

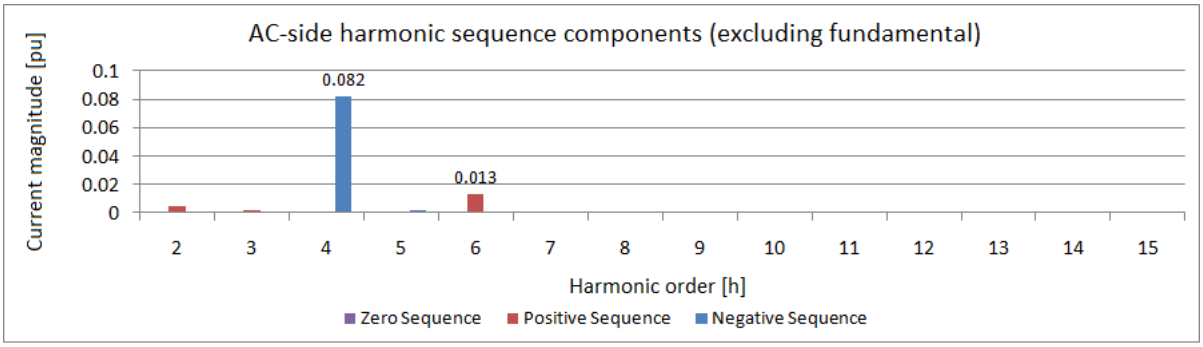

Fig. 4.17 Harmonic sequence components with 4th harmonic NPS injection

What was noted for other examples is that the cross-modulation amplitude factor seems to decrease with higher harmonic orders and is attributed to the measured DC voltage harmonic component decreasing as the injected frequency increases. The reason for this is thought to be the DC-side frequency response of the STATCOM model where the impedance decreases with $1/\omega$ because of the DC capacitance. This effect has not been noted in the Excel examples as no DC-side filtering is modelled in Excel.

4.3.3 PSCAD interaction results

The PSCAD model used to test AC/DC harmonic interaction is the actual detailed model that is also implemented in the CLI scheme and also the RTDS replica scheme. The time steps are set to 4µs to have accurate IGBT valve switching instants. In the model, the VSC is supplied via the DC line and connected to a passive network under light loading conditions where no other fundamental frequency sources exist. Harmonic voltage sources are connected on the AC-side of the VSC to each phase via the two 315MVA coupling transformer impedances at 220kV on the passive network side.

4.3.3.1 Example 1:

For this example, a 4th harmonic with negative phase sequence is injected under steady state conditions after 1 second and the time domain waveforms were analysed to determine the cross-modulation factors. The modulation index of the converter was measured at 0.78. The PSCAD results were exported to a Comtrade format and the Matlab program written as is

discussed in Section 5.1 was used to analyse these records and generate continuous harmonic sequence components versus time as shown in Fig. 4.18:

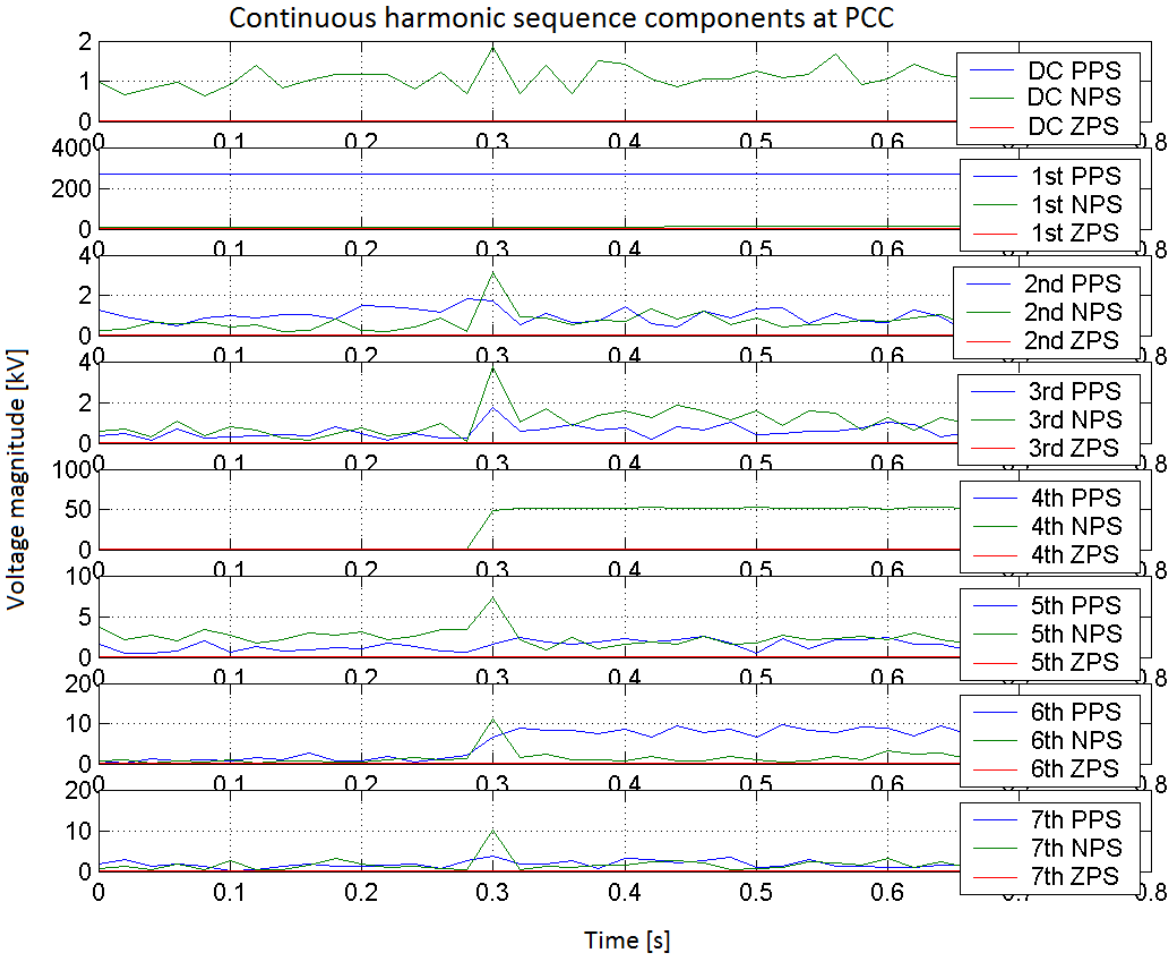

Fig. 4.18 PSCAD output analysed in Matlab harmonic sequence analyser

According to Section 2.7.2.4, (3.22) and (3.25), the amplitude of the new AC harmonic for a three-phase PWM switching scheme should be equal to $V_{ACh2} = V_{ACh1} * \frac{3}{\pi} * 0.25 m_a = 53 * \frac{3}{\pi} * 0.25 * 0.78 = 9.87 kV$. The measured simulation value varies around 9.7 kV. The phase rotations of the two AC-side harmonic components (4th NPS and 6th PPS) are also confirmed by the Matlab harmonic sequence analyser as expected.

This complete AC/DC/AC HATR = 9.7/53 = 0.183 compares well with the similar 3rd DigSilent PowerFactory example in Section 4.3.2.4 of HATR = 0.013/0.082 = 0.159 where the ratio of the two examples' HATRs should be in the same range as the ratio of the two examples' modulation indexes:

$HATR_{PF}/HATR_{PSCAD} = 0.159/0.183 = 0.87$

$m_{aPF}/m_{aPSCAD} = 0.732/0.78 = 0.938$

The relatively small difference in ratios (less than 10%) confirms that the harmonic interaction from AC to DC and back to AC compares fairly well between the two packages for this example. The reason why voltage harmonics could be considered and measured as opposed to current harmonics in the PowerFactory examples is that in PSCAD the HVDC scheme was run in a passive network condition without any other AC-side source impedance connected that would influence voltage harmonics.

As with DigSilent PowerFactory, the DC-side filtering for higher order harmonics was also noted in PSCAD, thus reducing the effective AC/DC/AC HATR because of reduced DC-side voltage harmonics. The DC-side capacitor sizing does play a role in the DC-side filtering and observed HATR especially for higher order harmonics and may need to be investigated further.

4.4 Alternating Current / Direct Current harmonic interaction: Modulation by scheme characteristic harmonics

As discussed in Section 3.3.2, harmonic content presented to the VSC scheme from the AC side will not only be transferred and modulated to the DC-side and back by the fundamental component, but also by scheme characteristic harmonics.

The following PowerFactory example shows a 13th harmonic PPS injection with assuming a pre-existing scheme characteristic 5th harmonic NPS. In Section 3.3.2, Fig. 3.22 suggests what harmonic orders should be formed according (3.26).

The graph in Fig. 4.19 shows the simulated DC-side and AC-side harmonic orders generated:

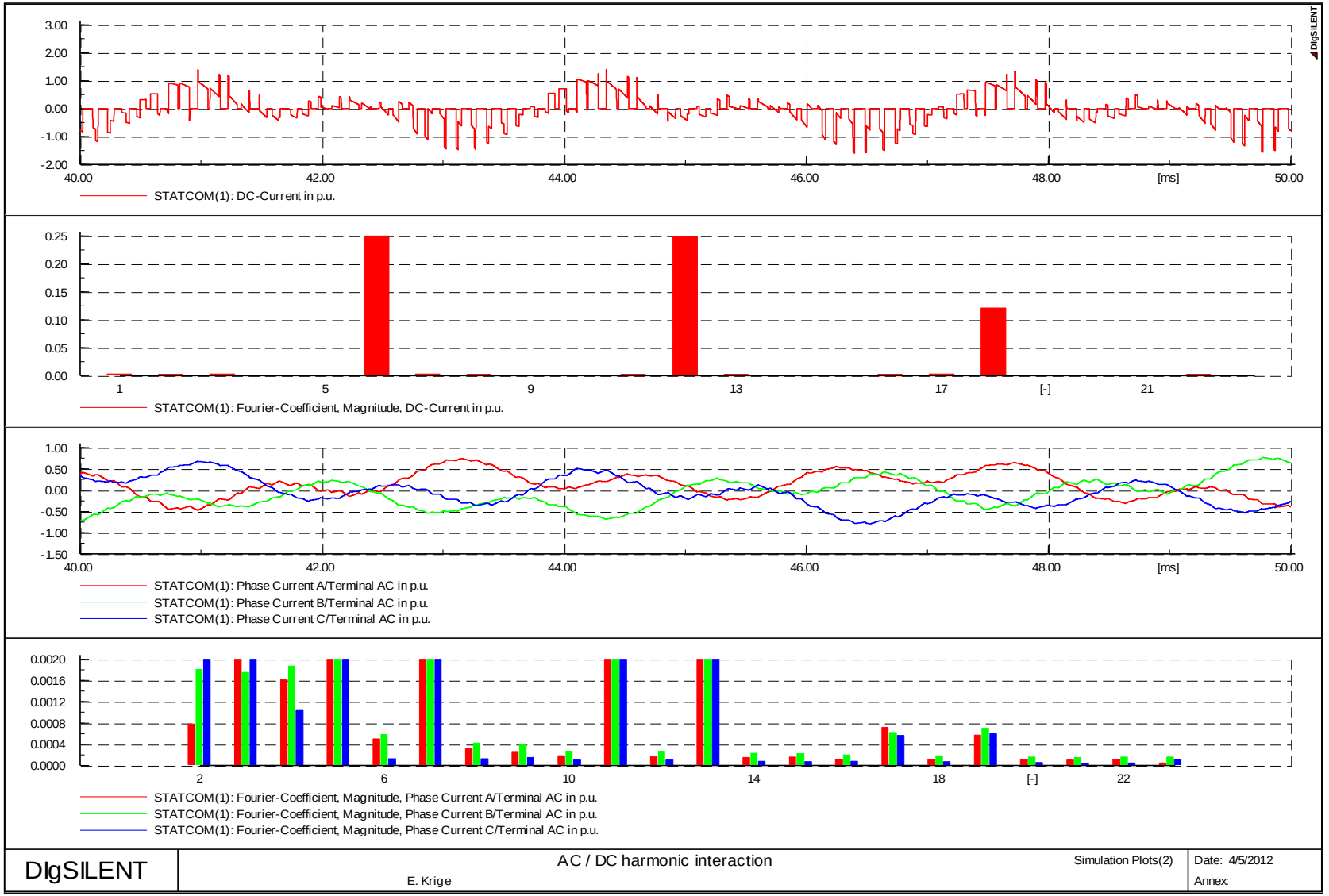

Fig. 4.19 Harmonic transfer by scheme characteristic 5th harmonic during 13th harmonic PPS injection

The DC-side and AC-side harmonic sequence components are confirmed by the Excel sequence analyser as shown in Fig. 4.20:

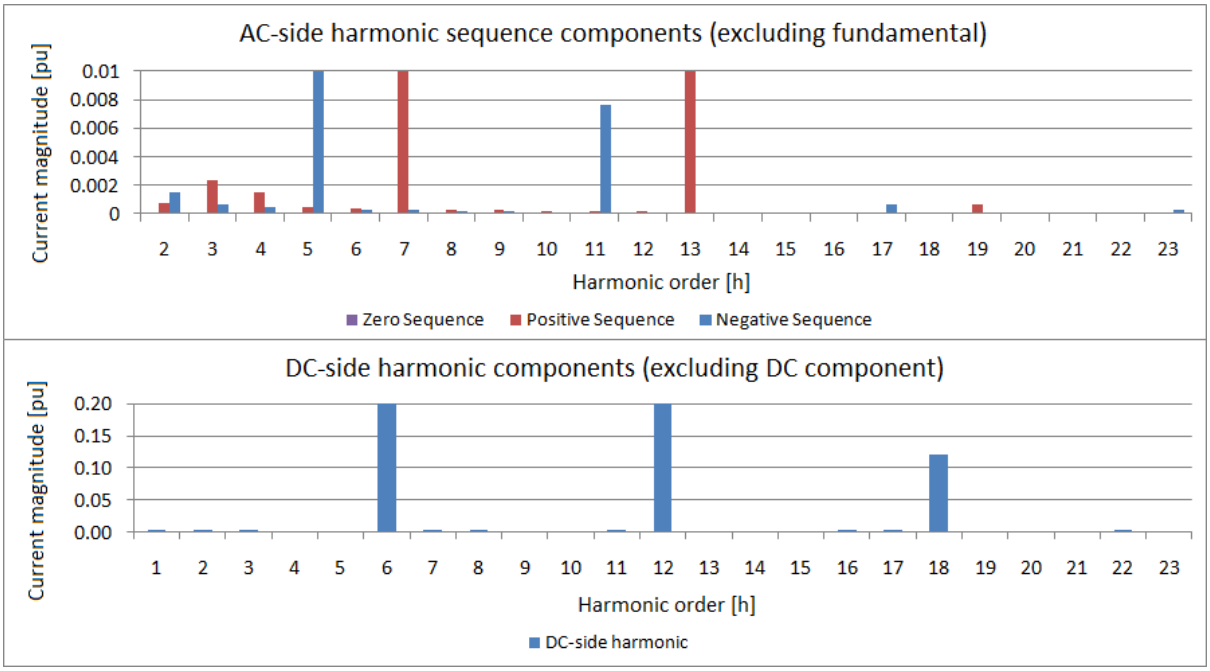

Fig. 4.20 Harmonic sequence components, transfer by scheme characteristic 5th harmonic during 13th harmonic PPS injection

Because of the DC-side filtering of higher order harmonics, the amplitudes of the 17th, 19th and 23rd harmonics are comparatively small compared to the lower order harmonics and the graph zooming level is increased. Despite this, the orders generated correspond to the theory presented in Section 3.3.2 and as proposed by Figure 3.22. An Excel model where higher order harmonics are not suppressed, the theoretical harmonic orders and relative magnitudes can be seen more clearly as shown in Fig. 4.21:

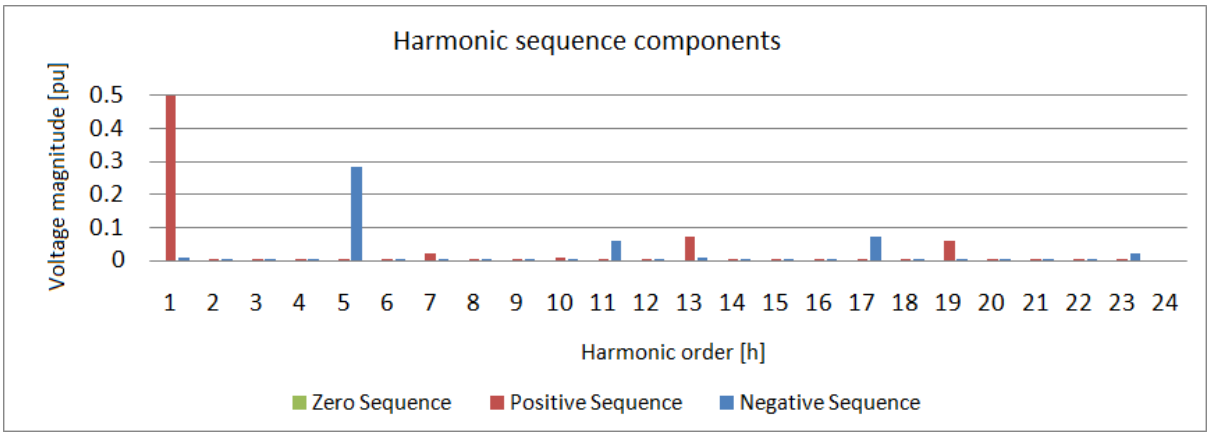

Fig. 4.21 Harmonic sequence components in Excel model, transfer by scheme characteristic 5th harmonic during 13th harmonic PPS injection

5 Harmonic Interaction case study analysis

5.1 Case background and methodology

This case study analyses the events of 05/10/2010 on the CLI connection with the ZESCO system where after energising a passive network, a resonance condition occurred causing the HVDC scheme to trip due to an AC harmonic overvoltage.

At 23:16, the Zambezi converter station went into passive network mode with the Southern ZESCO network after cascade tripping of generation and transmission equipment at the Victoria Falls Power Station. The 220kV Sesheke – Zambezi 1 line also tripped with this disturbance.

After the HVDC scheme supplied the passive local load at Zambezi substation with Katima Mulilo load for 10 minutes, the 220kV Sesheke Zambezi breaker was closed, energizing Sesheke substation including the 220kV Sesheke – Livingstone line with 15MVAR line reactor. This condition led to a resonance condition with high lower order harmonic content and subsequent overvoltage of 1.25 per unit causing the Zambezi converter station to trip on overvoltage. Supply to Zambezi was restored and the CLI was back to normal at 03:51 on 06/10/2010.

The aim of this case study is to determine the cause of the resonance condition and subsequent over-voltages that occurred. To do this, the frequency response of the AC network is done with DigSilent PF to determine which sensitive parallel and series resonant points exist. After this, an EMT study is performed to reveal the network energisation currents that would be characteristic of the line and reactor energisation. The harmonic content analysis of the inrush currents with sequence analysis is then done to establish the harmonic orders, amplitudes and phase rotations that would be characteristic of the line and reactor inrush condition. The theoretical analysis done in Chapters 2 and 3 on AC/DC harmonic interaction can then be utilised to ascertain how these harmonic orders would cross-modulate via the VSC terminal to give rise to new harmonic orders on the AC side. These newly cross-modulated harmonic orders can then be checked against the network frequency response for sensitivity. This would lead to possible reasons for the observed resonance condition.

In order to confirm the theoretical analysis and to consider possible solutions to the problem, a simulation in PSCAD or the RTDS can be done to replicate the case and to confirm the

results. The detailed model that exists for the CLI in DigSilent PowerFactory model is sufficient for loadflows, frequency sweeps and RMS dynamic simulations. An EMT simulation model with valve firing is only available in PSCAD and RSCAD for the RTDS. Therefore simulations that require detailed VSC time domain analysis will be done in PSCAD or in the RTDS.

An important source of information is the event list registered at the NamPower National Control Centre. This information is used to correlate GPS time-stamped events originating from the substation automation system with the recorded TFRs to be able to help identify the effects seen on the TFR waveforms. (See the events list in Appendix B).

Another vital source of information are the TFRs from the Zambezi converter station that recorded the relevant voltages, currents and digital channels during the disturbances and can be used as input data to perform a harmonic sequence analysis of the waveforms during each stage of the abnormal condition. Because the record is stored in Comtrade format, a Matlab file capable of importing a Comtrade file and doing a harmonic sequence analysis was used as a tool for the analysis. This tool from the author of [**10**] is mathematically similar to the Excel harmonic sequence analyser that was created for the other examples in this thesis.

However, the Matlab code of this tool had to be modified by the author of this thesis in order to be able to continuously plot different harmonic sequence components over time. For this a loop was created to step a window of one period at a time and to register all the harmonic sequence components for that period. Outside the loop, plots of the recorded harmonic sequence components are executed. In this way, continuous harmonic interaction and saturation effects can be seen against time. (See Matlab program code in Appendix A).

From the transient fault records of this case study it can be seen the waveform shapes change from one 50Hz cycle to the next. To be able to monitor continuous harmonic sequence components of a transient condition that changes from cycle to cycle, it was decided to only look at one fundamental cycle at a time and letting the DFT or FFT assume an infinite periodicity of the waveform. Although the sampling rate of the TFR's are sufficient at 200 samples per cycle or 10kHz to monitor up to the 100^{th} harmonic order in theory, any inter-harmonic distortion would be transformed to the two adjacent integer multiples of the fundamental component with some possible additional spectral leakage. Because of the fact that the inverse DFT or FFT would reproduce the original waveform, this possibility was accepted in order to be able to apply the common tools used that do not really cater for inter-

harmonic distortion such as the DigSilent Power Factory's FFT function, the Matlab continuous harmonic sequence analyser and the Excel FFT harmonic sequence analyser.

The harmonic cross modulation theory would yield the same results using (2.65), (2.67) and (3.26) whether the additional frequency components are integer multiples of the fundamental component or not. Thus an inter-harmonic distortion treated as two separate major harmonic components that are integer multiples of the fundamental, each consisting of its PPS and NPS components, would yield the same harmonic interaction results in the time domain as when a single non-integer multiple of the fundamental component would be applied. Determining the sequence components of a three-phase unbalanced transient inter-harmonic component in order to determine which cross-modulation rules apply would be more difficult to accomplish. Because harmonic components are theoretical constructs that can be considered independent from each other and because the principle of super-position applies, the assumptions above are considered valid.

5.2 Network configuration and frequency response

For the 220kV line and reactor energisation a scan of impedance versus frequency is done for the specific network configuration. The network was modelled in DigSilent PowerFactory as shown in Fig. 5.1 and Fig. 5.2 and the network impedance was determined for a frequency sweep from 10Hz to 1000Hz using distributed line parameters and unbalanced loadflow iterations as shown in Fig. 5.3. The model includes the HVDC link with exact parameters, filter banks, local transformers, loads and exact line parameters such as conductor type, bundle spacing, tower geometry, phase conductor sag, earth conductor sag, etc.

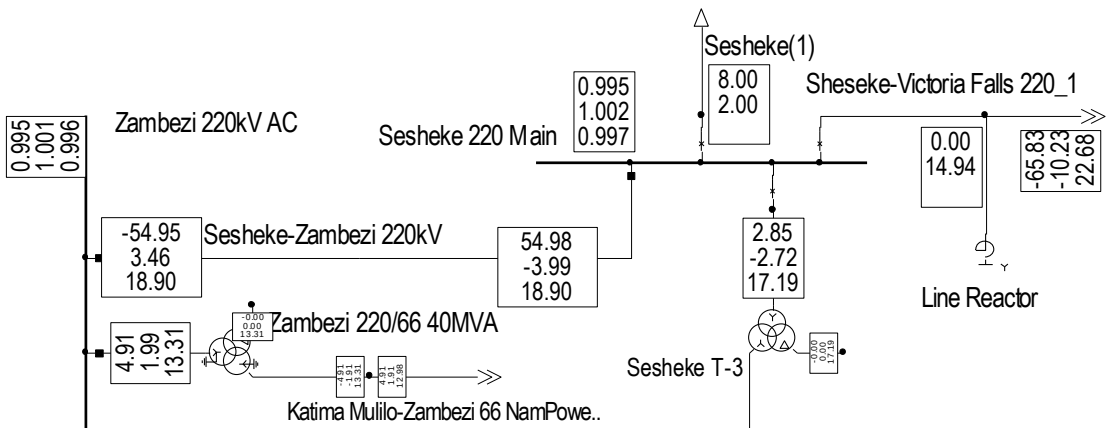

Fig. 5.1 NamPower and ZESCO interconnector

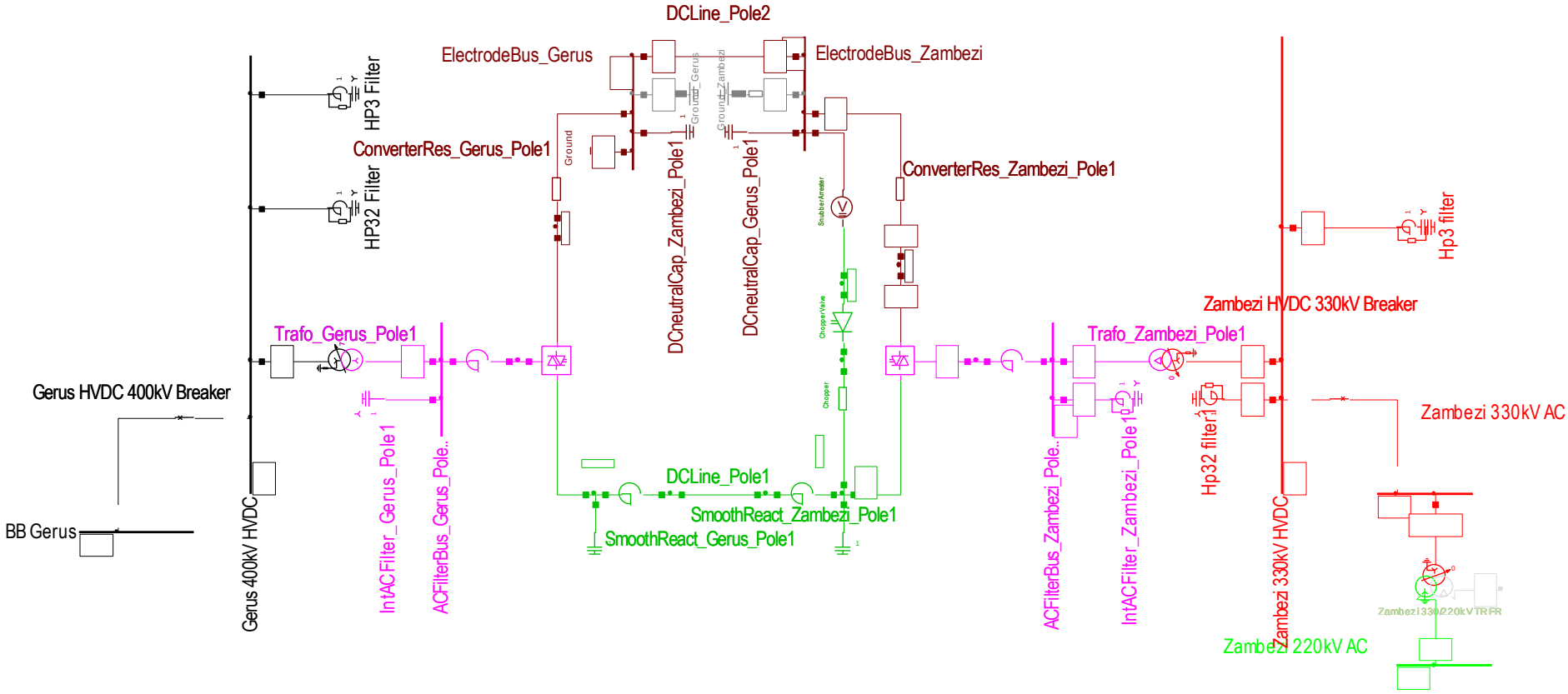

Fig. 5.2 CLI HVDC model single line diagram (Courtesy NamPower / ABB)

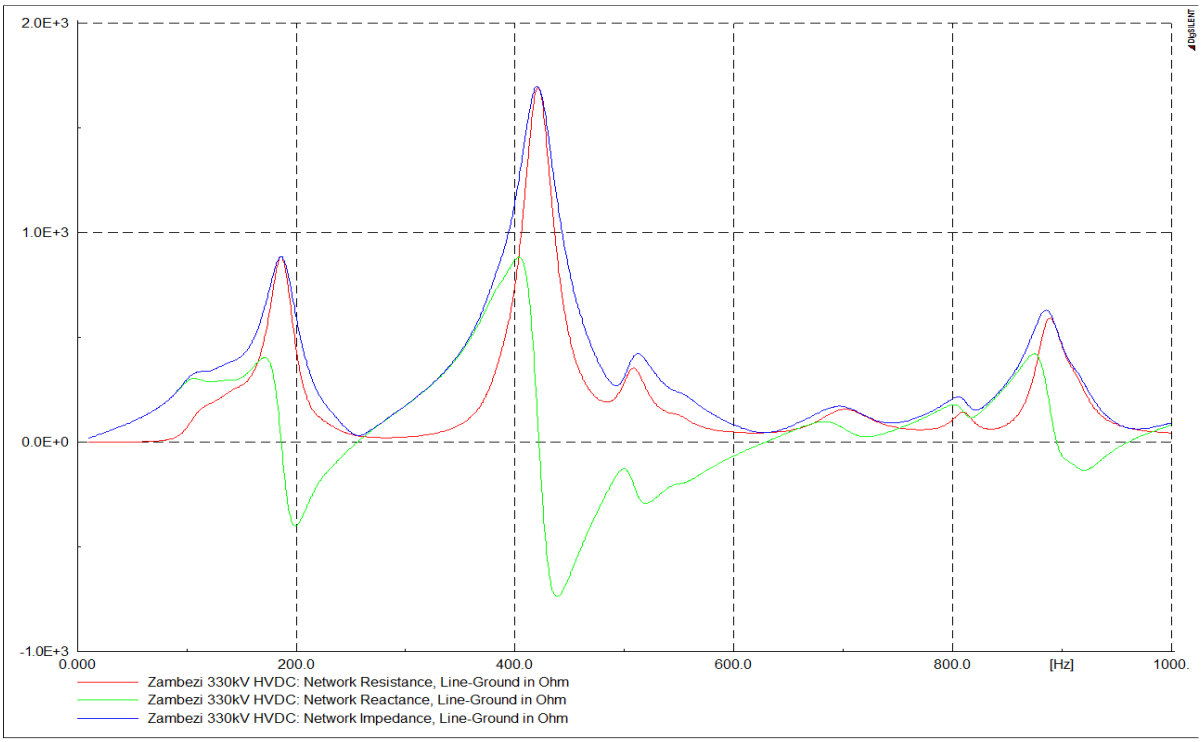

Fig. 5.3 Passive ZESCO network frequency response

The frequency response of this network configuration shows a parallel resonance point close to the 4th harmonic order, a series resonance point close to the 5th harmonic order and other dominant parallel resonance points close to the 9th and 17th harmonic orders. The major players in these resonance points are the open-ended 224km long 220kV line between Sesheke and Victoria Falls with 15MVAR line reactor and the HVDC scheme source impedance with connected filter banks. Under normal circumstances, a parallel resonance point close to the even-numbered 4th harmonic order would not be a great concern. However, in this case it could prove to be an aspect to be reckoned with.

5.3 Simulated line and reactor energisation analysis

Since the local Katima Mulilo load was already energised by the HVDC converter station, the inrush currents of the 220kV Sesheke Victoria Falls line with line reactor was investigated by using a DigSilent EMT simulation to determine the nature of the inrush currents as it would be without the VSC but only a normal external grid with equivalent source impedance and is shown in Fig. 5.4:

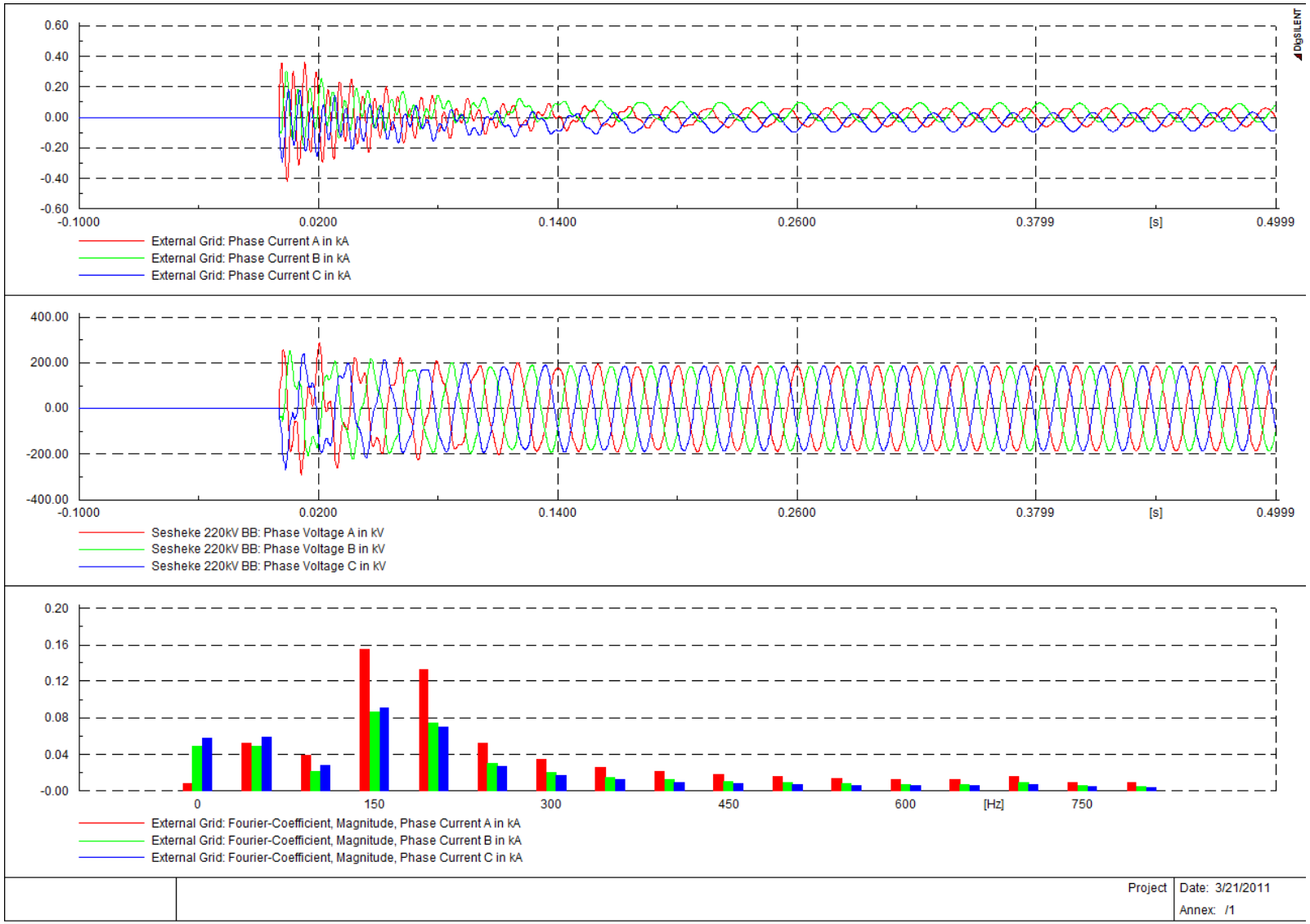

Fig. 5.4 220kV Sesheke VicFalls line energisation

The inrush currents were analysed in the frequency domain to reveal dominant harmonic components. Among these, the 3rd and 4th harmonics were notably higher than the rest during the transient condition. A proper harmonic sequence analysis of the current wave shapes would give insight as to how these harmonic orders would cross-modulate via the VSC. The continuous harmonic sequence analyser as developed for this thesis in Matlab was used and yielded the following results as shown in Fig. 5.5:

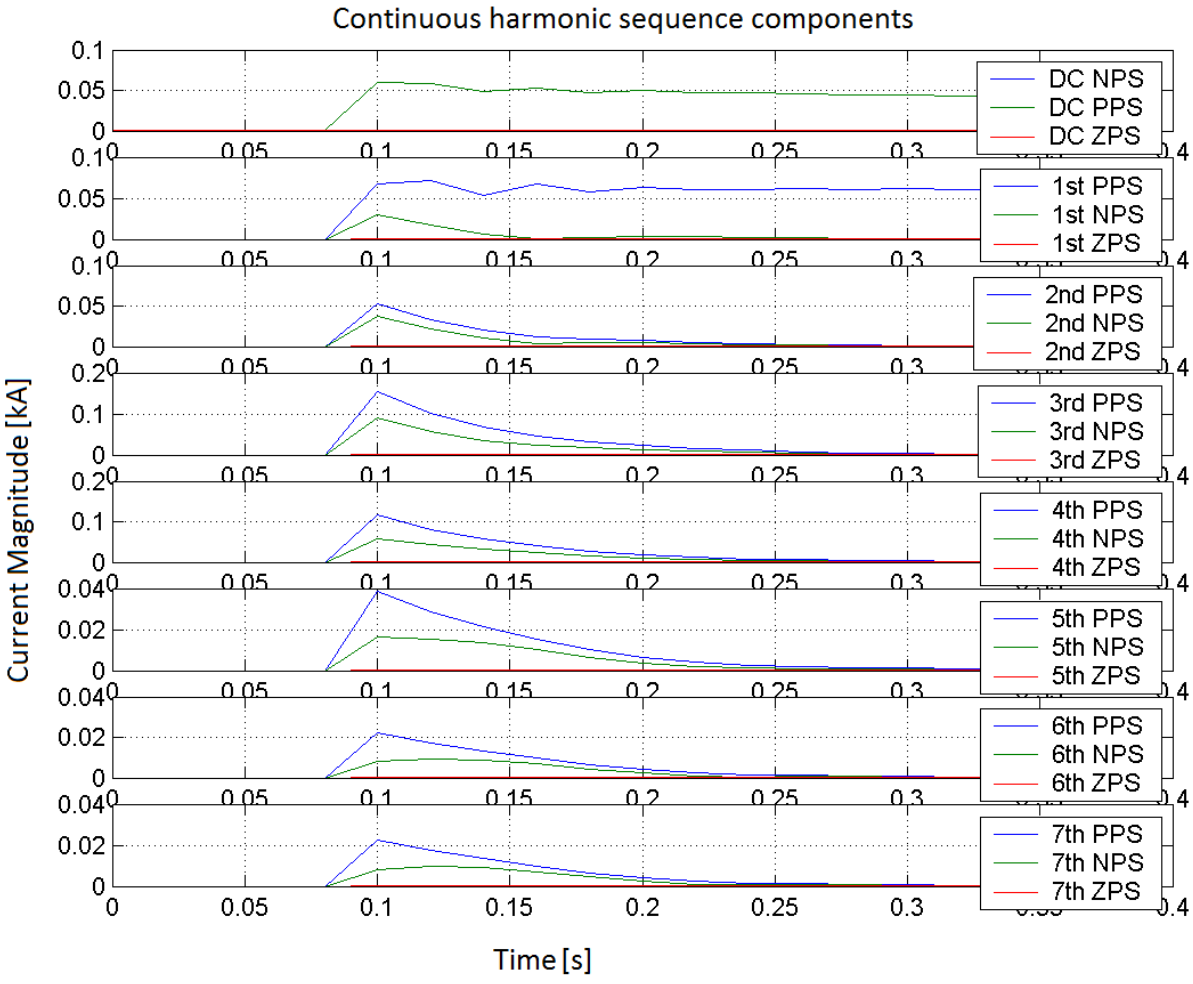

Fig. 5.5 Line energisation harmonic sequence components

The phase sequence of the high 3rd and 4th harmonic orders can be identified as mostly PPS but also with notable NPS components. Note the slow decaying DC component that contains almost equal stationary NPS and PPS. These, together with the 2nd harmonic PPS and NPS presence will have a definite effect on cross-modulated VSC harmonics.

Table 5.1 lists the expected cross-modulation effects as also shown in Fig. 2.23:

Table 5.1 Expected harmonic cross-modulation

Original AC-side harmonic	DC-side harmonic	New AC-side harmonic	Original AC-side harmonic	DC-side harmonic	New AC-side harmonic
DC PPS/NPS	1st	2nd PPS	4th NPS	5th	6th PPS
1st PPS	DC	-	5th PPS	4th	3rd NPS
1st NPS	2nd	3rd PPS	5th NPS	6th	7th PPS
2nd PPS	1st	DC PPS/NPS	6th PPS	5th	4th NPS
2nd NPS	3rd	4th PPS	6th NPS	7th	8th PPS
3rd PPS	2nd	1st NPS	7th PPS	6th	5th NPS
3rd NPS	4th	5th PPS	7th NPS	8th	9th PPS
4th PPS	3rd	2nd NPS			

When observing this network configuration's sensitivity to 4th harmonic, as well as the presence of 4th harmonic during the line and reactor energisation, it can already be seen that a 4th harmonic resonance condition is possible. When further taking into account the presence of 2nd harmonic NPS and 6th harmonic PPS that could further boost the 4th harmonic PPS, a 4th harmonic resonance can be considered very probable.

Furthermore, when taking into account the magnitude of the DC components present that can further cause saturation effects in all transformers and reactors, all harmonics from 2nd to 6th is further boosted and cross-modulated by the VSC scheme. The combination of these effects gives a reasonable explanation for a parallel resonance condition where small exciting current harmonics would give rise to large voltage harmonics.

5.4 Actual line and reactor energisation analysis (23:27.24)

Fig. 5.6 shows the actual energisation waveforms as recorded by the HVDC control and protection system. Note the similarity of the inrush currents to the EMT simulation in Fig 5.4. The only difference is that the harmonic content does not damp out, but increases due to the network's sensitivity and VSC cross-modulation further exciting those harmonic orders such to register an overvoltage condition which trips the converter station.

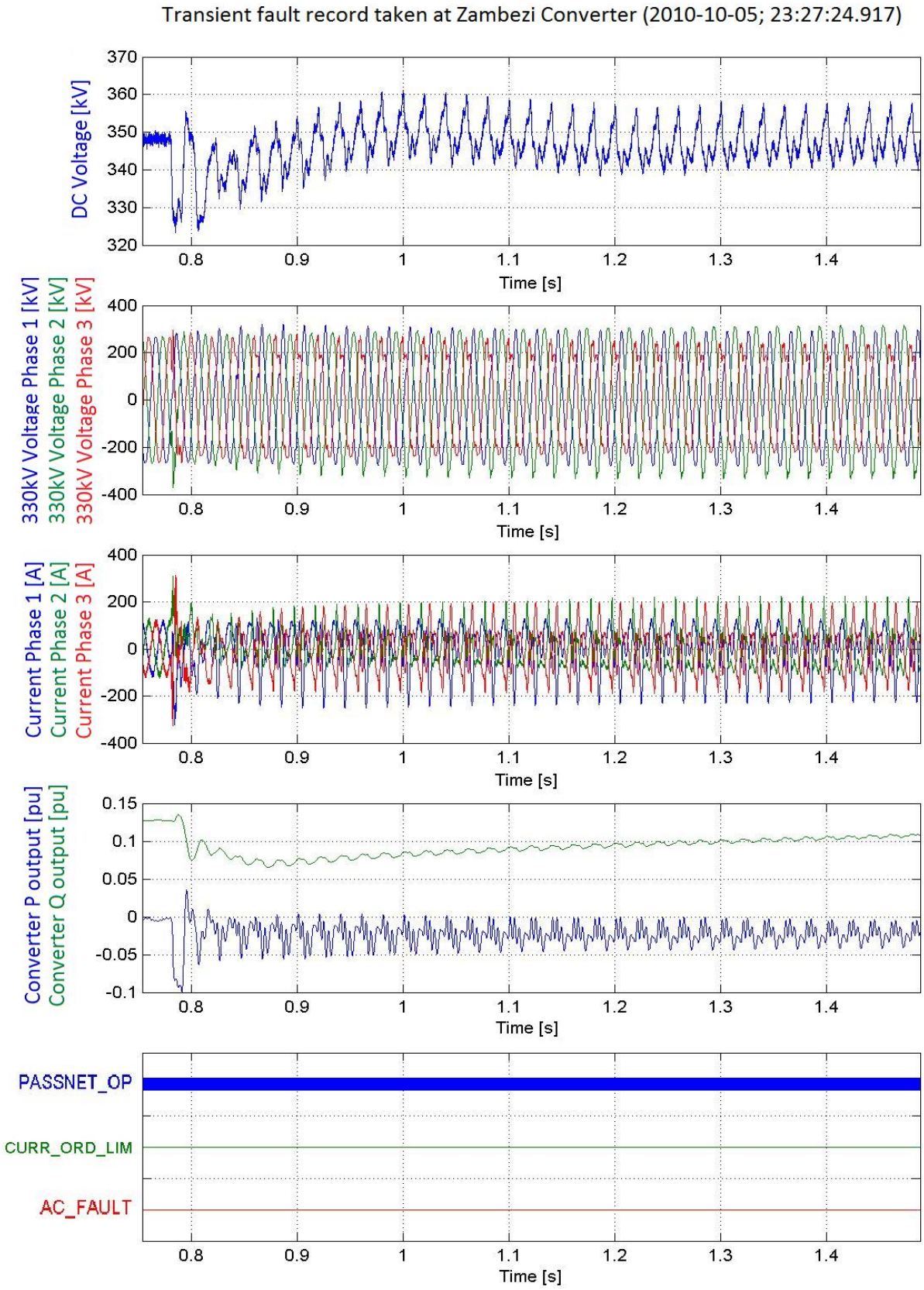

Fig. 5.6 Actual line energisation plots

The frequency response of the voltage waveforms from Fig. 5.6 as shown in Fig. 5.7 shows the expected high 3rd and 4th harmonics. Note the relatively high 9th harmonic that makes sense when looking at the network frequency response and the parallel resonance point close to the 9th harmonic previously in Fig. 5.3.

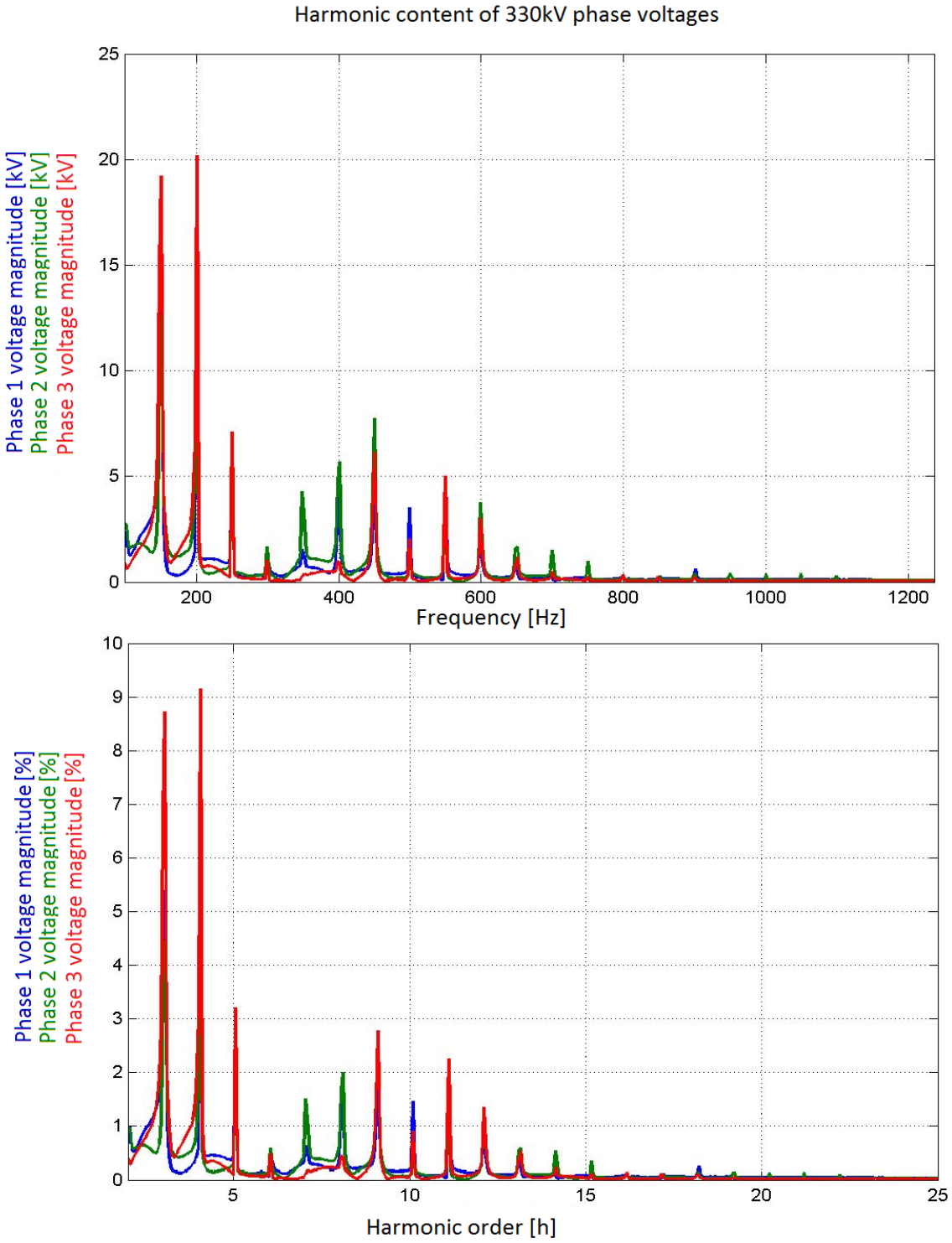

Fig. 5.7 Actual line energisation AC-side harmonic components

The DC-side harmonics shown in Fig. 5.8 reveal a high fundamental component, as well as high 2nd - 6th harmonic orders. These harmonic are cross-modulated from the AC-side harmonic content as a result of the inrush current DC offset and other inrush and saturation harmonic orders.

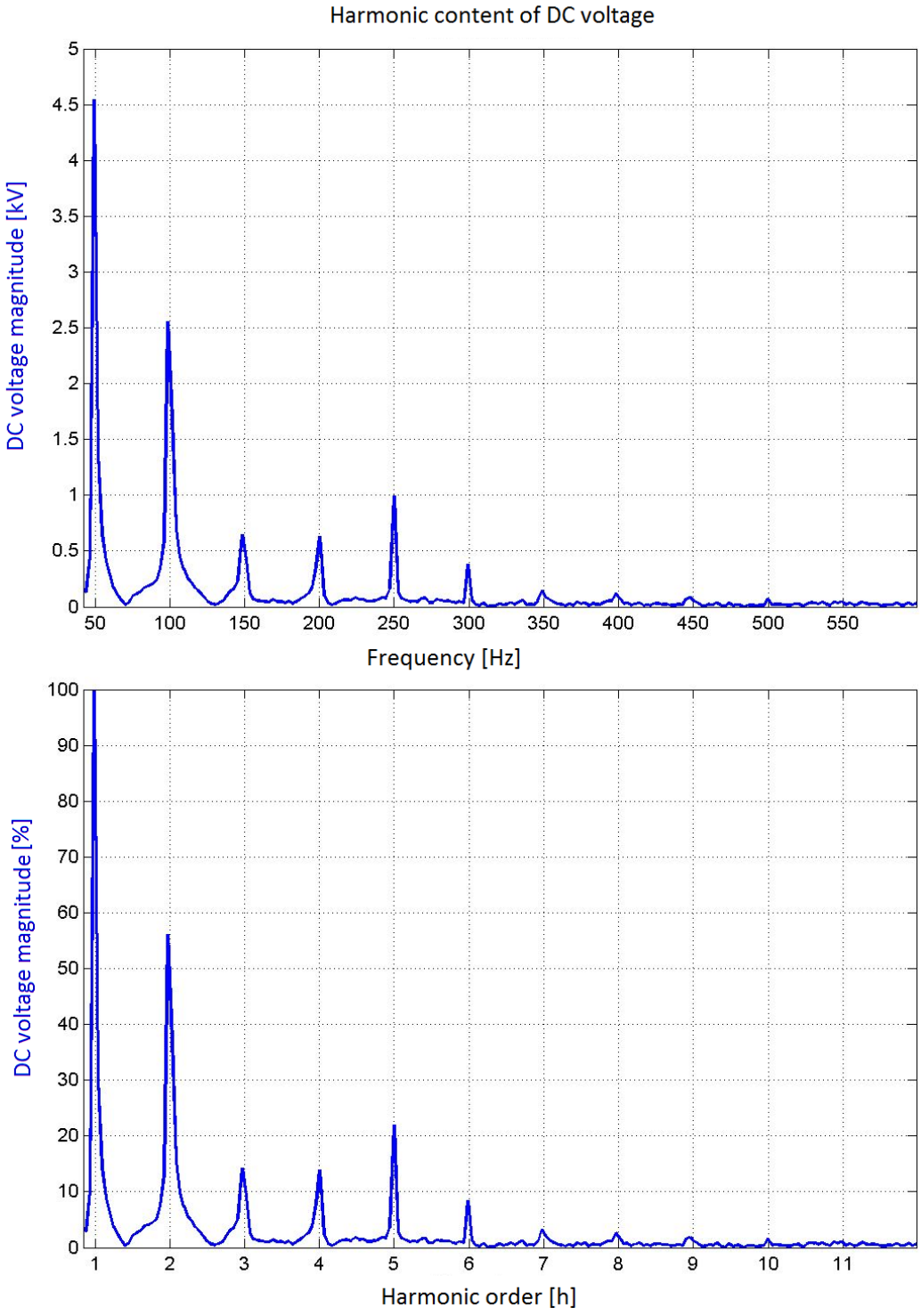

Fig. 5.8 Actual line energisation DC-side harmonic components

A continuous harmonic sequence component analysis of the recorded TFR reveals the following results as shown in Fig. 5.9:

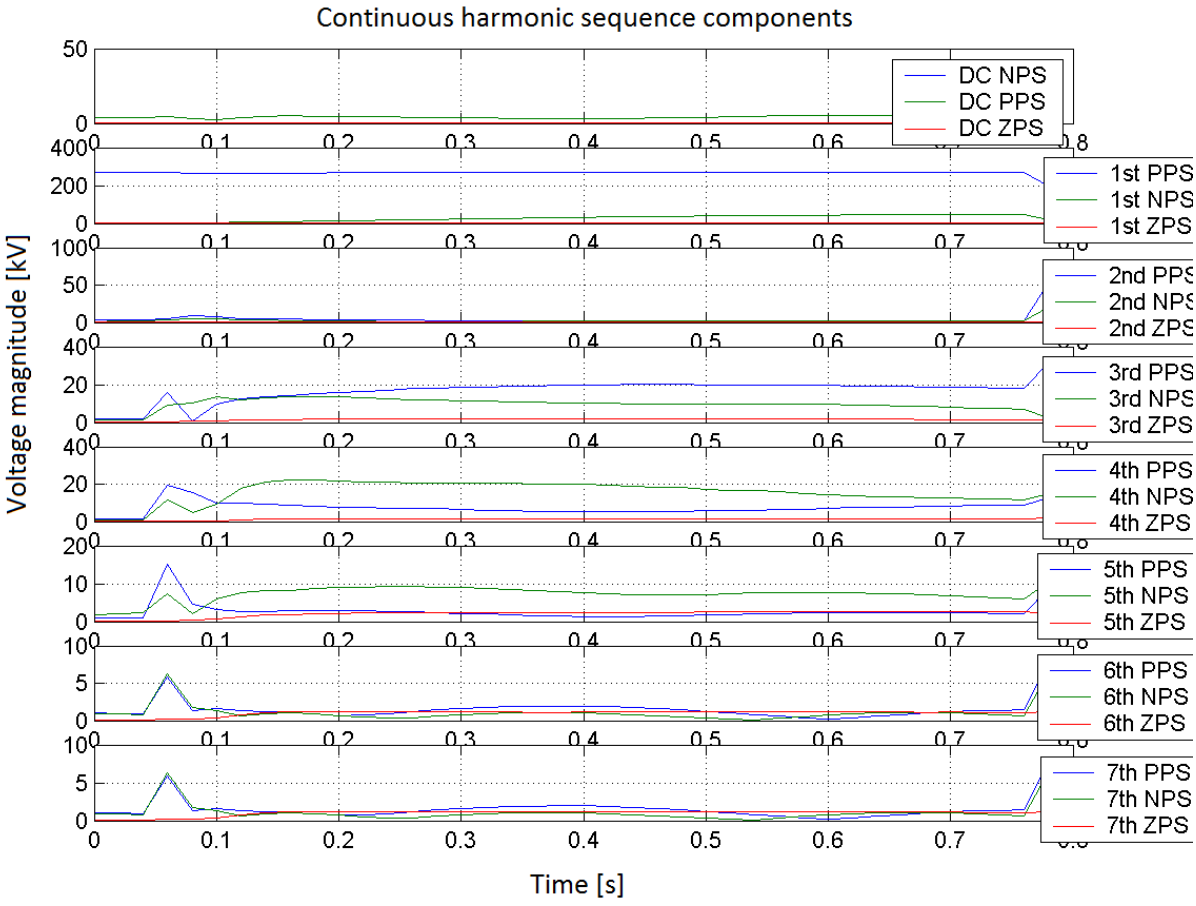

Fig. 5.9 Actual line energisation continuous harmonic sequence components

The constant presence of DC NPS and PPS with 2nd harmonic PPS explains DC-side fundamental component. This effect could prolong transient and saturation conditions and give rise to more harmonic content.

The increasing fundamental NPS component corresponds to the high DC-side 2nd harmonic and increasing 3rd harmonic PPS. When investigating the HP3 filter that is supposed to cater for 3rd harmonic PPS, it is found to be tuned at 115Hz which is closer to 2nd harmonic. Thus the 3rd harmonic is not sufficiently damped but is allowed to grow.

The initial inrush currents contain all harmonic orders from 2nd to 7th. The initial presence of 4th harmonic PPS and NPS, boosted by more 4^{th} harmonic content originating from cross-modulated 6th harmonic PPS and 2nd harmonic NPS interacts with the network parallel resonance point that is close to 4th harmonic. Although the 4th harmonic NPS declines slightly over time, the 4th harmonic PPS increases keeping the total 4th harmonic content

fairly stable although slightly increasing. This correlates with a slightly increasing DC-side 3rd harmonic. This exchange of NPS and PPS content is still to be examined.

The total harmonic content added to the fundamental component over the time period fulfils the over-voltage tripping condition of the converter station at 1.25pu after 400ms.

5.5 PSCAD Electromagnetic Transient simulation

An EMT study was also conducted in PSCAD with the same detailed model that is used in the RTDS system with the results shown in Fig. 5.10. The difference in this case is that the energisation load selected to the various substations' loading points is the normal load which is about 50MW compared to the 5MW energisation load in the actual case. The reasoning behind this is to see if energising the line with normal load connected beforehand would help to damp out some of the harmonic distortion effects.

The simulation time step was selected at 4µs as this gives a balance between high bandwidth and valve firing accuracy, i.e. 125 times faster than valves switching at around 2kHz and the amount of time consumed to complete a single simulation run of 2 to 5 seconds.

The detailed Caprivi Link model was used with the line parameters for the 220kV Zambezi Sesheke line, 220kV 15MVAR line reactor, local transformers and loads, etc. Energising the line and reactor yielded very much the same results as the actual energisation records and DigSilent PF line energisation results when considering the line inrush current (320A peak) and general wave shapes. The PSCAD results were written to a Comtrade format file for easy external analysis.

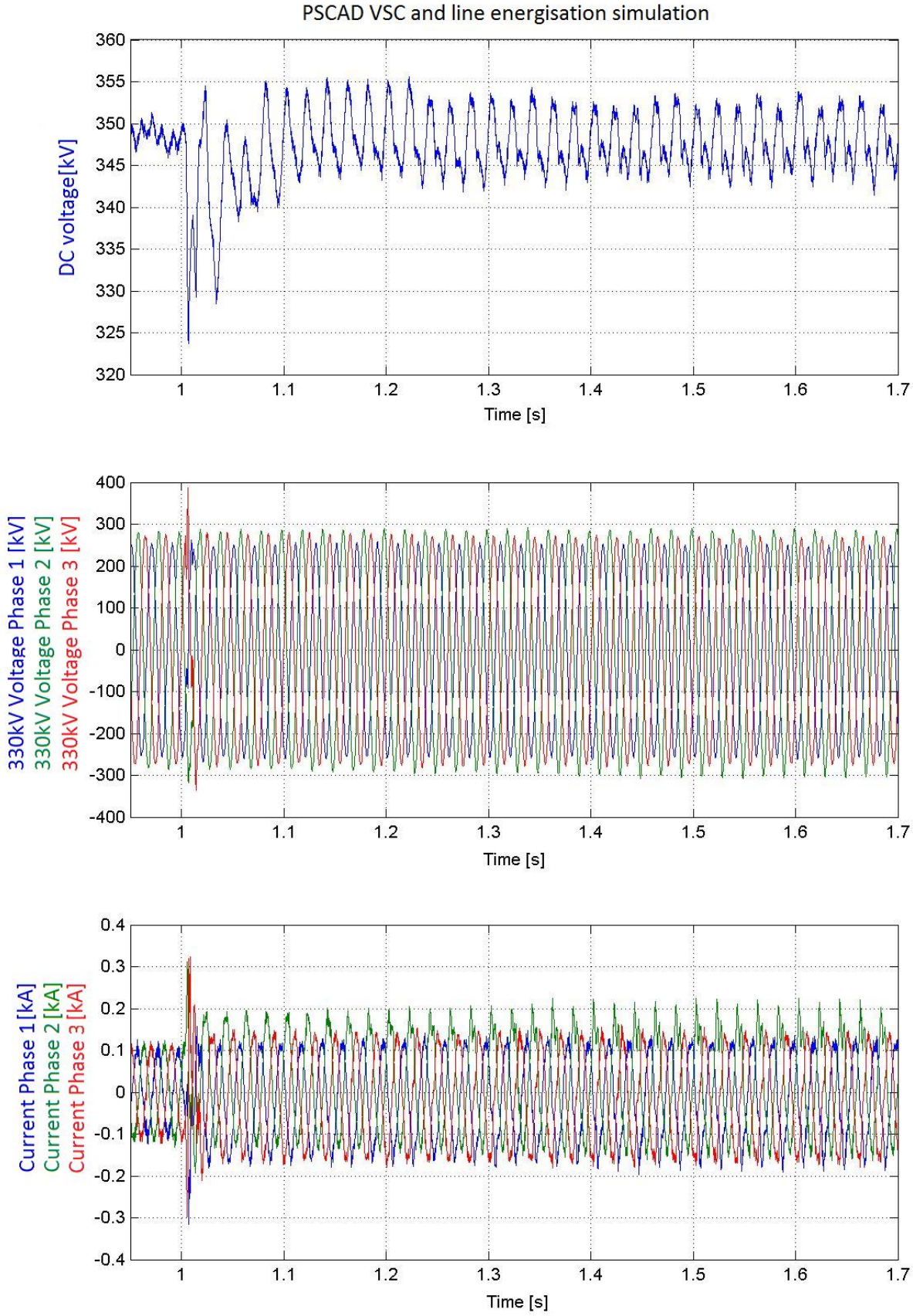

Fig. 5.10 PSCAD VSC line energisation simulation

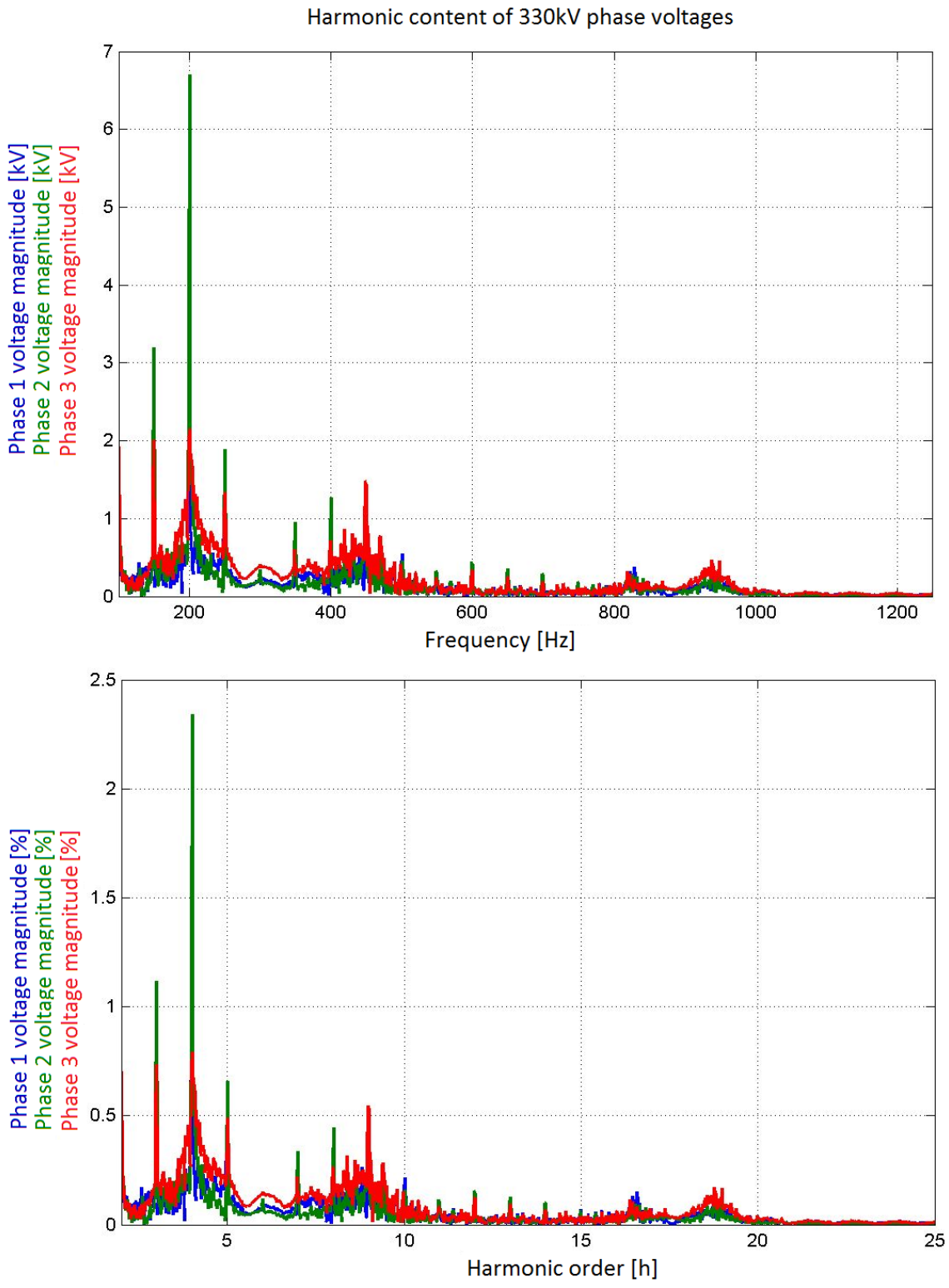

Fig. 5.11 PSCAD VSC with line energisation AC-side harmonic components

On closer inspection is evident that both the current and voltage harmonics are significantly less due to the damping effect of the added load. Although the inrush current of the line and line reactor is still the same, the continuation of the 3rd, 4th, 5th and 9th AC-side harmonics

as shown in Fig. 5.11 are less by a factor ranging from 6 to 9 and close to the limits stipulated in the South African National Recommended Standards (NRS-048-4) [**7**] for odd and even harmonic content. The DC-side harmonic content shown in Fig. 5.12 is less by a factor of roughly two. Another important point is that the harmonic content starts to slowly damp out over time which was not the case with the real life energisation.

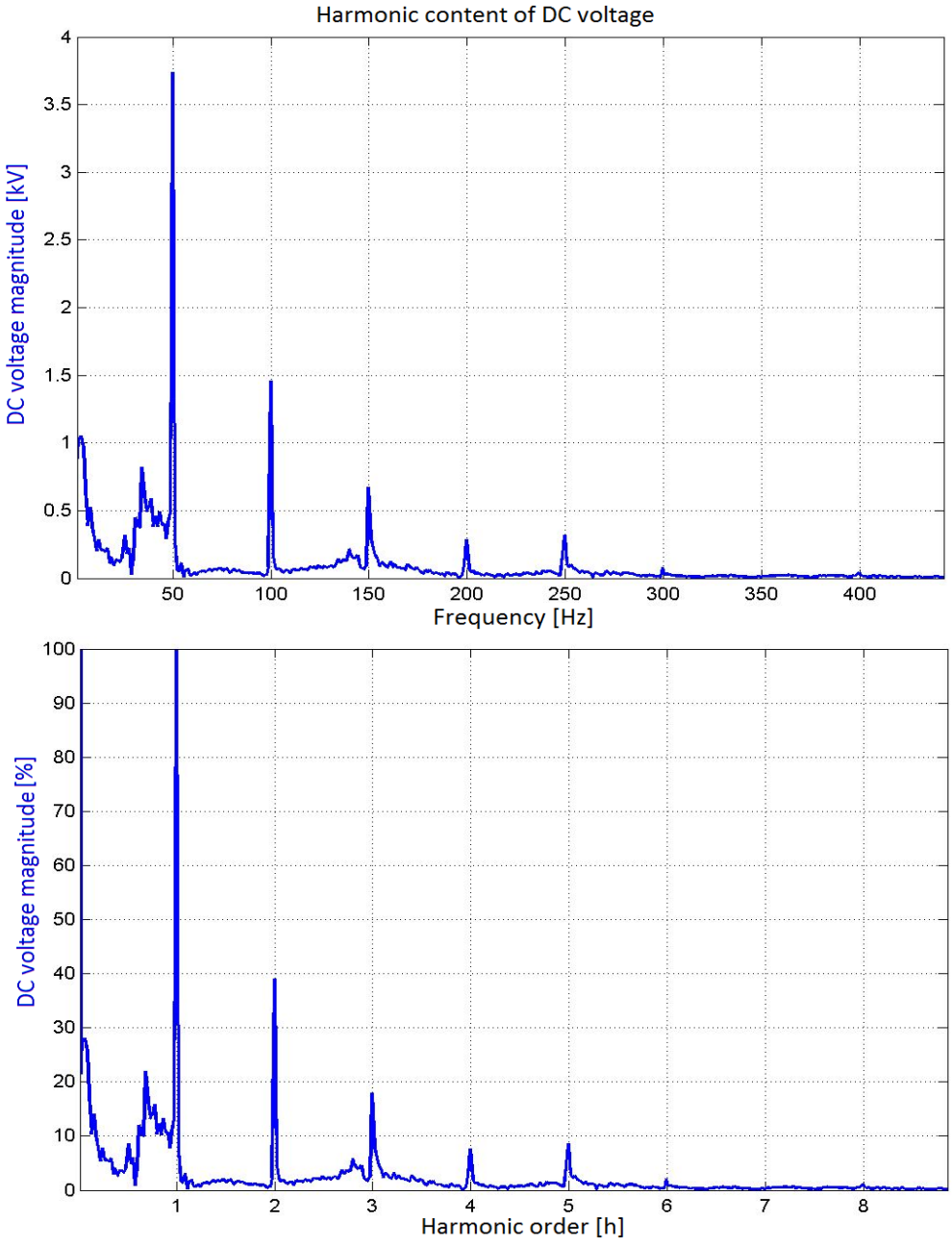

Fig. 5.12 PSCAD VSC with line energisation DC-side harmonic components

5.6 Case study conclusions and risk mitigation

A last check would be to compare the frequency response of the system with and without load to see what the effect on the parallel resonance points are. This frequency response comparison is shown in Fig. 5.13:

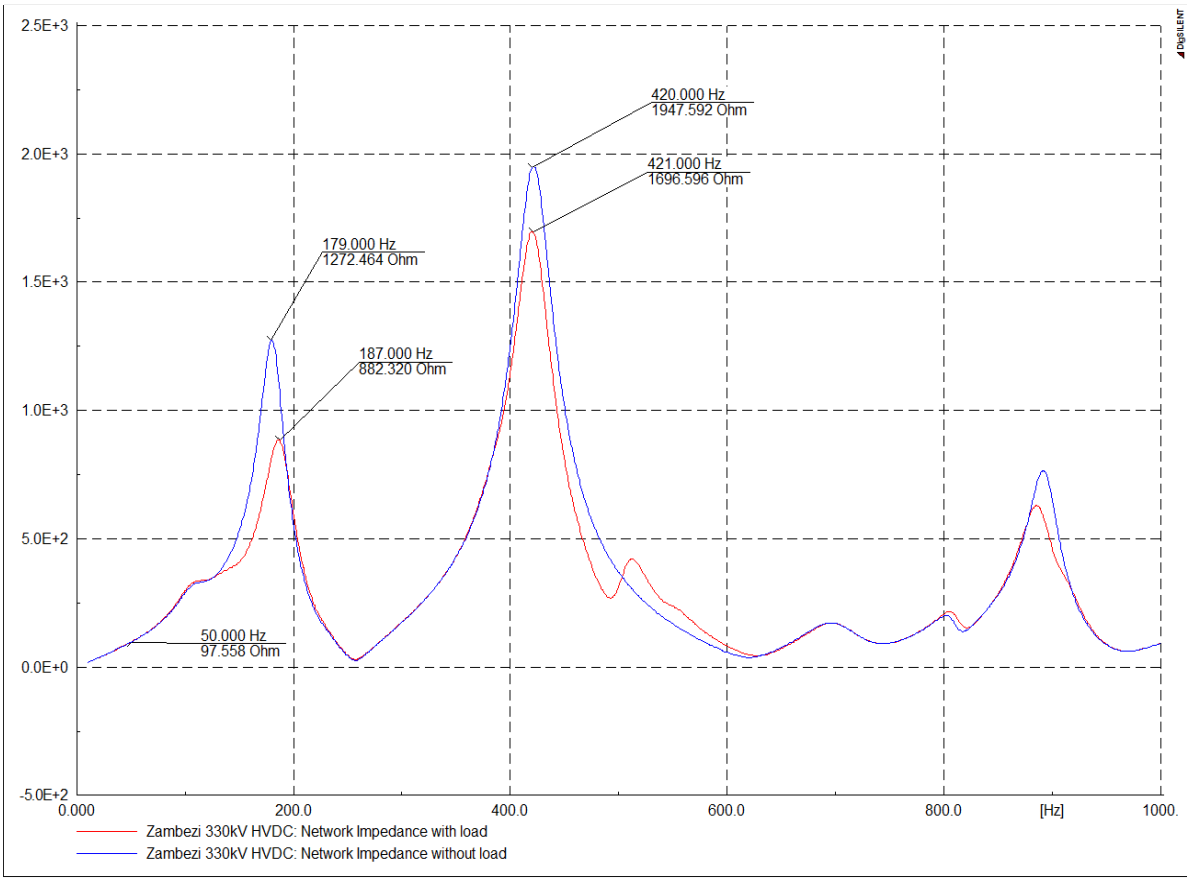

Fig. 5.13 Passive network frequency response with and without loading

From the impedance versus frequency scans of the passive network with and without load connected, it can be seen that with load, the first parallel resonance point moves slightly higher towards 4th harmonic and decreases in magnitude from 1272 Ohm to 882 Ohm.

When considering the rule of thumb for resonance points (Section 2.5.4) to fall within the guideline given by (2.25): $0.5|Z_{f_0}|\frac{f}{f_0} < |Z(f)| < 2|Z_{f_0}|\frac{f}{f_0}$, then 2*(97.558)(187/50) = 729.7 < 882 Ohm.

Thus the first parallel resonance point is likely to still cause some resonance as can be seen from the PSCAD simulation, but is likely to damp out and a lot less severe than the case without load where 2*(97.558)(179/50)=698.5 < 1272.5 Ohm where a distinct resonance condition can be observed.

When the voltage harmonics between the two cases are compared, it can be seen that with load less 3rd harmonic is observed in relation to the 4th harmonic. This can be attributed to the parallel resonance point moving closer to 4th harmonic and further away from 3rd harmonic.

The effects of harmonic cross-modulation by the VSC can be observed in both cases by the extra harmonic orders generated around 3rd and 4th harmonic according to the harmonic sequence components or the phase harmonics. The high fundamental component on the DC side of the VSC for both cases indicates a risk of transformer saturation by DC components produced by the VSC as a result of 2nd harmonic PPS inrush components.

The case of energising the network with load connected has been tested in real life as result of a situation in the ZESCO network that necessitated NamPower to energise the line and line reactor with the HVDC scheme. This time all loads were connected beforehand and after energising the line and reactor, no tripping occurred as with the first case and thus no records were generated indicating that any resonance condition damped out and did not grow to register an overvoltage trip.

In general, it is advised not to energise the 220kV Sesheke - Victoria Falls line with line reactor from the HVDC scheme due to the inrush harmonic components and cross-modulation by the VSC. If absolutely necessary, it can be done but with all loads connected where possible in order to bring more damping to the system.

Another mitigation technique would be to implement a modification to the HVDC control system to allow manual operation of one of the two filter banks at the Zambezi converter station. By switching in or out a filter intelligently, this would give some control over the parallel resonant point frequency and damping. The feasibility of such a solution needs to be studied further in more detail because it would imply removing the damping given by one of the filter banks and thereby possibly sharpening the existing network parallel resonant points.

6 Results and conclusions

6.1 Overview of results and conclusions

In conclusion, although a fairly wide range of related fields had to be discussed in order to lay the theoretical foundation and context for harmonic interaction between VSC HVDC and weak AC systems, the theory in Chapter 3 and the application thereof in Chapter 4 and 5 could be focussed on strongly and explored in reasonable detail.

In Chapter 1, certain key questions were raised as well as objectives to be met in order to be able answer these key questions. These objectives have been met by the various fields discussed in the literature study in Chapter 2 from VSC systems, HVDC systems, VSC switching theory and PWM switching techniques, power system harmonic principles, harmonic sequence components, AC/DC harmonic interaction, simulation techniques and simulation tools. This laid the foundation for Chapter 3 to further explore the fields of harmonic sequence components, phase rotation in the frequency domain, VSC switching, PWM and OPWM. The concept of HATR was introduced and the AC/DC HATR was derived for different switching techniques. A new perspective was given by the examination of harmonic cross-modulation by scheme characteristic harmonics. Chapter 4 made these theories more practical by showing ways to model and simulate AC/DC harmonic interaction and proving that the theories presented are valid. The case study in Chapter 5 confirmed that the real life results are in line with the theories and simulations results presented. This chapter aims to give a summary of these results and their significance to the industry.

The results and interpretations found in this thesis are spread throughout Chapters 2, 3, 4 and 5. Therefore a summary of the most important results are given in the next section.

6.2 Overview of important results

6.2.1 Harmonic sequence components

In Section 2.4.3, the harmonic dependent versus harmonic independent definition for the operator $\boldsymbol{a}$ and the validity for determining the sequence components of waveforms containing harmonic content according to [**31**] - [**34**] as well as by Fortescue in [**42**] was discussed and the case for a harmonic independent operator $\boldsymbol{a} = e^{j\frac{2\pi}{3}}$ was made. This

statement was further proved by the theory presented in Section 3.1.1 where the known characteristic phase rotations for harmonics generation were confirmed.

The static harmonic sequence analyser developed in Excel, as well as the continuous harmonic sequence analyser that was developed in Matlab, were based on the equations presented in Section 3.1.1. All the simulation results exported from DigSilent PowerFactory and PSCAD analysed in these two custom-made tools make perfect sense and align with the theories presented in Section 3.2 and 3.3.

6.2.2 Identification of potentially dangerous series and parallel resonant points

The rule of thumb presented in Section 2.5.3 and Figure 2.14 to identify potentially dangerous series or parallel resonance points by means of impedance versus frequency scans, where no literature could be found to support its validity or invalidity, was shown to be accurate in the conclusions of the case study in Section 5.6 at least for parallel resonance points.

The understanding of the evaluation of impedance versus frequency sweeps is crucial in any harmonic study including filter design. Movements in resonant points due to system contingencies and fault level variations, as well as impedance magnification studies when adding filter banks, is important to understand in order to avoid harmonic resonance problems. Line energisation frequencies and possible inter-harmonic resonance conditions also need to be considered.

6.2.3 Voltage Source Converter zero sequence elimination

The theory and equations presented in Section 3.2.1 to show that a VSC scheme does not produce or transfer zero sequence components was confirmed by simulation study results.

The DC components transferred to the AC side of the VSC due to a DC-side fundamental component are theoretically not of zero sequence order, but of equal stationary PPS and NPS components as shown in the Matlab continuous harmonic sequence analyser. In the phase domain, this relates to two positive DC phase quantities and one negative DC phase quantity of double the amplitude of the other two phases. This challenges assumption that AC transmission system DC components are only to be of zero sequence nature and is only true for perfectly balanced flows.

6.2.4 Alternating Current / Direct Current harmonic interaction theory

The harmonic interaction theory and harmonic amplitude transfer ratios (HATRs) presented in Section 3.3.1 for PWM and OPWM schemes were confirmed throughout Chapter 4 by various Excel examples, DigSilent PowerFactory examples and a PSCAD example. Scheme specific HATRs were confirmed and the attenuation for complete AC to DC to AC harmonic transfers for higher order harmonics were discussed and attributed to DC-side frequency response and DC-side filtering effect. The harmonic transfer rules were also confirmed by the case study in Chapter 5 as a real life example of AC/DC harmonic interaction and resonance with connected AC system. The role of the AC network frequency response with series and parallel resonance points' effect on harmonic interaction that was highlighted in Section 3.3.1 can clearly be seen in the case study and network frequency response.

The presentation of the HATR concept, the deduction of the HATR formula for PWM schemes and validity in simulations is a valuable concept for the study of AC/DC harmonic interaction for VSC schemes.

6.2.5 Alternating Current/Direct Current harmonic interaction for modulation by scheme characteristic harmonics

The assumptions made as presented in Section 2.7.2 and investigated in Section 3.3.2 has opened a new world of harmonic interactions that are generally not noted in real life due to the relatively low amplitudes of VSC scheme characteristic harmonics and AC-side harmonics presented to the VSC scheme. Although these effects will be negligible in most cases, they could start to play a role in case of low fault level AC systems coupled with a strong VSC HVDC scheme in conjunction with other harmonic loads in the vicinity. Harmonic amplification due to the presence of AC network series or parallel points could pose some interesting scenarios.

Therefore this theory is valuable to take note of and to keep in mind when investigating strange harmonic resonance cases involving VSC schemes and weak AC networks. The presence of network unbalance and negative phase sequence components on the AC network will also influence VSC positive phase sequence 3^{rd} harmonic generation and need to be kept in mind since 3^{rd} harmonic components are normally assumed to be of zero sequence order.

The theory and equation (3.26) presented to determine harmonic cross-modulation by components other than the fundamental component has been suggested in Section 3.3.2 and is

proved in concept by simulations performed in Excel and DigSilent PowerFactory in Section 4.4.

6.2.6 Modelling techniques and simulations

The modelling techniques and tools presented in Section 2.8 and Section 2.9 are further discussed in Section 4.1 and are validated by the fact that the theories presented, the simulations done for each theory and the case study results all line up very closely. This shows the reliability and exactness of the simulation packages used and gives some comfort to the concerns expressed in the beginning of Section 2.9.

However, the harmonic orders considered were limited to traditional lower order harmonics below 25^{th} harmonic. Although the results for higher order harmonics may also have been accurate, cognisance has been taken of the sampling rate (10kHz or 200 samples per 50Hz cycle) of the real life transient fault records and accurate comparability to software simulation outputs that may be of very high sampling rates (1MHz or 20000 samples per cycle) in order to gain accurate valve switching instants for harmonic interaction results.

6.2.7 Case study results

Although the case study results have been discussed in Section 5.6, it gives a satisfying conclusion to the important role system damping plays in the proliferation of power system harmonics and the importance of impedance versus frequency sweep studies.

It shows that although AC/DC harmonic interaction is an effect to be reckoned with especially with weak AC systems and that it does not only exist in theory. Yet the case study shows that it can be mitigated to some extent by understanding the connected AC systems and resonant sensitivities and it highlights that operational regimes can often be used to mitigate certain risks if they have not been identified during a design or conceptualisation process.

Often a harmonic integration study cannot beforehand, often a few years in advance, cater for all future developments and all possible contingencies. In that case, new ways need to be found to mitigate harmonic problems with the least cost implications such as operational regimes, filter banks, gradual increase in fault level as system develops, etc.

6.3 Future work on Alternating Current / Direct Current harmonic interaction

Although this thesis started to open the world of harmonic cross-modulation for VSC schemes, there are still many aspects that can be studied in order to make the picture of AC/DC harmonic interaction more complete:

- The relative phase angles of harmonic orders transferred from the AC- to DC side and back to the AC side can be investigated to determine if transferred harmonics will add in phase or in another relation to one-another especially when considering harmonic interaction due to scheme characteristic harmonics and other pre-existing AC-side harmonics.
- The HATR derivation for modulation by scheme characteristic harmonics can be investigated if deemed relevant for practice.
- The effect of third harmonic injection on PWM schemes' HATR can be investigated.
- HATR equations considering DC-side frequency response could be investigated to incorporate the typical effects of DC-side capacitance.
- Higher order harmonic measurement techniques is a separate field, but could be relevant considering that many higher order harmonic components are difficult to accurately measure in order to make good comparisons with simulation results.
- Control strategies and effect of OPWM to minimize harmonic content could be investigated to see if cross-modulated harmonic orders that are programmed to be eliminated by OPWM strategies are actually eliminated, or if harmonic cross-modulation bypasses this mechanism.
- Harmonic interaction can also be investigated for different VSC configurations especially considering multi-level bridge configurations.
- Frequency injections other that integer multiples of the fundamental components, such as frequencies in the SSR range can be investigated to determine the wide band response of VSC schemes as it relates to cross-modulation and frequency interaction.
- The development of software tools suitable for the continuous harmonic sequence analysis of multiple transient inter-harmonic distortions can be investigated. One option could be to use the DWT as the basis of analysis.

6.4 Recommendations and final conclusion

Although the pursuit of a deeper theoretical understanding of the mechanisms behind harmonic interaction is valid, sight should not be lost of the real life practical implications. Some aspects are very relevant and need to be taken into account. For other aspects, where the accuracy and dependability of field measurements become realistically doubtful and where the level of relative harmonic quantities become too small and insignificant to be meaningful, a reality check may be required. Yet, the point where theoretically interesting and practically relevant become mutually exclusive is not always so clear especially given the great variations in fault level and network characteristics encountered in transmission systems all over the world.

In conclusion, it can be said that power systems harmonic analysis and the search for solutions and mitigations is not always simple and straightforward and is by some considered not only a science, but also an art where at the end, years of experience in the field backed by a solid theoretical foundation is the best teacher.

7 References

[1] NamPower. (2011) Short term critical supply project. Presentation.

[2] T.G. Magg, E. Krige, M. Manchen, J. Wasborg, and J. Sundin, "Connecting networks with VSC HVDC in Africa: Caprivi Link Interconnector," in *IEEE PES PowerAfrica 2012 Conference and Exposition*, Johannesburg, 2012.

[3] AE-Africa. (2011, April) Alternative Energy Africa Publications. [Online]. http://ae-africa.com/read_article.php?NID=2889

[4] T.G. Magg, M. Manchen, J. Wasborg, E. Krige, and H. D. Mutschler, "Caprivi Link Interconnector: The first VSC HVDC power transmission with overhead lines," in *CIGRE B4 Colloquium*, Sydney, Paper 29, 20 October 2011.

[5] M. Bongiorno, S. Lundberg L. Harnefors, "Input-admittance calculation and shaping for controlled Voltage Source Converters," *IEEE Transactions on Industrial Electronics*, vol. 54, no. 6, December 2007.

[6] A. P. J. Rens, "Validation of popular non-sinusoidal power theories for the analysis and management of modern power systems," Ph.D. dissertation, Electrical Engineering, North-West University, Potchefstroom, South Africa, 2005.

[7] "SABS Standards Division, Electricity Supply - Quality of Supply, Part 4: Application practices for licensees," NRS048-4, Ed. 2, 2009.

[8] G. J. Wakileh, *Power Systems Harmonics, Fundamentals, Analysis and Filter design*. Germany: Springer, 2001.

[9] Index Mundi. [Online]. http://www.indexmundi.com/namibia/area.html

[10] Y. Jiang, "Active and Reactive Power Control for Transmission Systems with Voltage Source Converters," Ph.D. dissertation, Royal Institute of Technology, Stockholm, 1997.

[11] G. Reed, R. Pape, and M. Takeda, "Advantages of Voltage Sourced Converter (VSC) based design concepts of FACTS and HVDC-link applications," in *Power Engineering Society General Meeting, 2003, IEEE*, vol. 3, 2003.

[12] J. Arrillaga and N. R. Watson, *Power System Harmonics*, 2nd ed. Chichester, England: John Wiley & Sons, Ltd, 2003.

[13] E. Krige, NamPower Utility Experiences, available from author, 2004-2012.

[14] J. Arrilaga, *High Voltage Direct Current Transmission*, 2nd ed. London, United Kingdom: IEE Power and Energy Series 29, 1998.

[15] Wikipedia, The free encyclopedia. [Online]. www.wikipedia.com at 2011-11-09.

[16] P. Kundur, *Power System Stability and Control*, N. J. Balu (The EPRI Power System Engineering Series), Ed. United States of America: McGraw-Hill, Inc, 1994.

[17] J. D. Glover and M. Sarma, *Power System Analysis and Design*, 2nd ed. Boston: PWS Publishing Company, 1994.

[18] P.K. Steimer, H. Grüning, J. Werninger, and D. Schröder, "State of the art verification of the Hard Driven GTO Inverter development for a 100MVA Intertie," *IEEE Transactions on Power Electronics*, vol. 13, no. 6, pp. 1182 - 1190, 1998.

[19] J.P. Ballad, R.J. Bassett, and C.C. Davidson, "Power Electronic Devices and their impact for Power Transmission," in *6th International Conference on AC and DC Power Transmission, IEE Conference Publication No. 423*, 1996.

[20] L. Gyugyi, "Dynamic Compensation of AC Transmission Lines by Solid-state Synchronous Voltage Sources," *IEEE Transactions on Power Delivery*, vol. 9, no. 2, April 1994, pp. 904 - 911.

[21] E. Larsen, N. Miller, S. Nilsson, and S. Lindgren, "Benefits of GTO-based compensation systems for electrical utility applications," *IEEE Transactions on Power Delivery*, vol. 7, no. 4, pp. 2056 - 2064, October 1992.

[22] D.G. Holmes and T.A. Lipo, *Pulse width modulation for power converters: principles and practice*, M. E. El-Hawary, Ed. New Jersey, USA: IEEE Series on Power Engineering, IEEE Press, J. Wiley and Sons, 2003.

[23] D. L. H. Aik, "Methods for voltage and power stability analysis of emerging HVDC system configurations," in *International Conference on Power System Technology*, vol. 1, 2000, pp. 409-414.

[24] D.J. Melvold, T. Endo, and H.P. Lips, "Effects of operating configurations of multi-terminal HVDC systems on dc filter performance," *IEEE Transactions on Power Delivery*, vol. PWRD-2, no. 3, July 1987.

[25] K. Sadek, M. Pereira, D.P. Brandt, A.M. Gole, and A. Daneshpooy, "Capacitor Commutated Converter Circuit Configurations," *IEEE Transactions on Power Delivery*, vol. 13, no. 4, pp. 1257-1264, October 1998.

[26] "CIGRE Protocol for Reporting the Operational Performance of HVDC Transmissions Systems," Working Group 14.04, March 2008.

[27] "IEEE Guide for the Evaluation of the Reliability of HVDC Converter Stations," IEEE Std 1240-2000, R2006.

[28] N. Mohan, T. M. Undeland, and W. P. Robbins, *Power Electronics - Converters, Applications, and Design*, 2nd ed. United States of America: John Wiley & Sons. Inc, 1995.

[29] L. Carlsson; G. Asplund; H. Bjorklund; H. Stomberg;, "Recent and future trends in HVDC converter station design," in *IEE 2nd International Conference on Advances in Power System Control, Operations and Management*, Hong Kong, 1993, pp. 221-226.

[30] R. E. Betz, C. Townsend, T. J. Summers, and G. Mirzaeva, "Simultaneous estimation of sequence and harmonic components for StatCom applications," in *14th Annual Internation Power Electronics and Motion Control Conference, EPE-PEMC*, 2010, pp. T7-47 - T7-54.

[31] B. C. Smith, N. R. Watson, A. R. Wood, and J. Arrillaga, "A sequence components model of the AC / DC converter in the harmonic domain," *IEEE Transactions on Power Delivery*, vol. 12, no. 4, pp. 1736 - 1743, October 1997.

[32] M. T. Hartman, "The application of Fortesque's transformation to describe power states in multiphase circuits with non-sinusoidal voltage and currents," in *9th International Conference, Electrical Power Quality and utilisation*, Barcelona, October 2007, pp. 1-6.

[33] S. M. Deckman and E. F. Melo, "On-line evaluation of voltage quality indexes for harmonic distoration, flicker, and sequence components," in *8th International Conference on Harmonics And Quality of Power*, SP, Brazil, 1998, pp. 549 - 554, Vol1.

[34] A. Baggini, *Handbook of power quality*. Chichester, United Kingdom: John Wiley & Sons, Ltd, 2008.

[35] IEEE Interharmonic Task Force, "Interharmonics in Power Systems," Cigre 36.05/CIRED 2 CC02 Voltage Quality Working Group, 1997.

[36] L. F. Beites, J. G. Mayordomo, A. Hernandez, and R. Asensi, "Harmonics, interharmonics, and unbalances of arc furnaces: A new frequency domain approach," *IEEE Transactions on Power Delivery*, vol. 16, no. 4, p. 661, October 2001.

[37] J. Fourier, "The analytical theory of heat," Cambridge University Press, 1978.

[38] S. Haykin, *Introduction to analog and digital communications*. New York, United States of America: John Wiliey and Sons, Inc, 1989.

[39] J. A. Glassman, "A generalization of the Fast Fourier Transform," *IEEE Transactions on Computers*, vol. C-19, no. 2, pp. 105 - 116, February 1970.

[40] "IEEE Recommended Practice for Industrial and Commercial Power Systems Analysis," IEEE Std 399, 1997.

[41] F. Neves et al., "A Space-vector Discrete Fourier Transform for Detecting Harmonic Sequence Components of Three-Phase Signals," in *35th Annual Conference of IEEE Industrial Electronics*, 2009, pp. 3631 - 3636.

[42] C.L. Fortescue, "Method of Symmetrical co-ordinates applied to the solution of polyphase networks," *Transactions of the American Institute of Electrical Engineers*, vol. 37, no. 2, pp. 1027 - 1140, 1918.

[43] Y. M. Chen, "Passive filter design using genetic algorithms," *IEEE Transactions on Industrial Electronics*, vol. 50, no. 1, pp. 202-207, February 2003.

[44] F.Z. Peng, H. Akagi, and A. Nabae, "A new approach to harmonic compensation in power systems-a combined system of shunt passive and series active filters," *IEEE Transactions on Industry Applications*, vol. 26, no. 6, pp. 983 - 990, 1990.

[45] M.M. Zakaria Moustafa and S. Filizadeh, "Simulation of a VSC transmission scheme supplying a passive load," in *34th Annual Conference of IEEE Industrial Electronics*, 2008, pp. 942 - 946.

[46] J. Holtz, "Pulsewidth Modulation-A Survey ," *IEEE Transactions on Industrial Electronics*, vol. 39, no. 5, pp. 410 - 420 , 1992.

[47] J. E. Chen and T. J. Liang, "A Novel Algorithm in Solving Nonlinear Equations for Programmed PWM Inverter to Eliminate Harmonics," in *23rd International Conference on Industrial Electronics, Control and Instrumentation* , Ta-hsu Hsiang, Kaohsiung Country, Taiwan, 1997, pp. 698 - 703 vol.2.

[48] Z. Du, L.M. Tolbert, and J.N. Chiasson, "Harmonic elimination for multilevel converter with programmed PWM method ," in *39th IEEE Industry Applications Conference*, 2004, pp. 2210 - 2215 vol.4.

[49] A. M. Trzynadlowski, F. Blaabjerg, J. K. Pedersen, R. L. Kirklin, and S. Legowski, "Random Pulse Width Modulation Techniques for Converter-Fed Drive Systems - A Review," *IEEE Transactions On Industry Applications*, vol. 30, no. 5, pp. 1166 - 1175, September / October 1994.

[50] DigSilent GmbH, *PowerFactory Technical Documentation, Build 511*., March 2011.

[51] Manitoba HVDC Research Centre Inc, *Applications of PSCAD / EMTDC*., 2007.

[52] Z. Bo and L. Tiecheng, "Application of Nonlinear Dynamic on Ferroresonance," in *Engineering Conference*, Asia-Pacific, 2009, pp. 1-4.

[53] J. Watson, N.R. Arrillaga, "The Harmonic Domain Revisited," in *13th International Conference on Harmonics and Quality of Power*, Wollongong, 2008, pp. 1-9.

[54] W. Wiechowski, J. Lykkegaard, B. Bak-Jensen, and C. L. Bak, "Hybrid time/frequency domain modelling of nonlinear components," in *9th International Conference, Electrical Power Quality and Utilisation*, Barcelona, 9-11 October 2007, pp. 1-6.

[55] J. Arrillaga, A. Medina, M. L. V. Lisboa, M. A. Cavia, and P. Sanchez, "The harmonic domain: A frame of reference for power system harmonic analysis," *IEEE Transactions on Power Systems*, vol. 10, no. 1, pp. 443-440, February 1995.

[56] B.C. Smith, J. Arrillaga, A.R. Wood, and N.R. Watson, "A review of iterative harmonic analysis for AC-DC power systems," *IEEE Transactions on Power Delivery*, vol. 13, no. 1, pp. 180-185, January 1998.

[57] M.A.A. Lima, J.R. de Carvalho, D.V. Coury, A.S. Cerqueira, and C.A. Duque, "A method of dynamic resampling for DFT-based harmonic analysis under time-varying frequency conditions," in *14th International Conference on Harmonics and Quality of Power (ICHQP)*, 2010, pp. 1-6.

[58] M. A. Cody, "The Fast Wavelet Transform," Dr. Dobb's Journal, April 1992.

[59] Z Xiang and Y Lu, "A study of the fast wavelet transform method in computational electromagnetics," *IEEE Transactions on Magnetics*, vol. 34, no. 5, pp. 3323 - 3326, 1998.

[60] H. W. Dommel, "Digital computer solution of electromagnetic transients in single- and multiphase networks," *IEEE Transactions on Power Apparatus and Systems*, vol. PAS-88, no. 4, pp. 388 - 399, April 1969.

[61] RTDS Technologies Inc. [Online]. http://www.rtds.com at 2011-12-02

[62] Mathworks. [Online]. http://www.mathworks.com at 2011-12-02

[63] MathCad. [Online]. http:///www.ptc.com/products/mathcad/ at 2011-12-02

[64] Excel for Engineers. [Online]. http://www.engineers-excel.com at 2011-12-02

[65] Lindo64. [Online]. http://www.lindo.com/ at 2011-12-02

Appendix A – Harmonic sequence analyser code

```
% Precise Harmonic analyse for positive, negative and zero sequence

% components up to 30*F1 Hz, The sampling frequency should not be slower

% than F1*100 provided Ying Jiang_Häfner 200706


% Modified by E.Krige 20110315 for continuous harmonic sequence plots

% for harmonic components h=0,1,2,...11

clear

a=comtrade %load the TFR to be analysed

%

ss=7000; % select a starting point for harmonic analyse S=tstart/Tsample

Tsample=0.0001

Swin=30 %Total cycles to analyse

for count = 1:Swin

    Ss=Sss+((count-1)*200); % select a starting point for harmonic analyse S=tstart/Tsample

    Se=Ss+200 ; % manual setting (200=1period)

    Xp(count)=(count-1)*0.02 % Time axis from starting point

     upcat=a.aCh(9).d; % "1" should be the channel number in TFR for the analysed variable
     phase a

     uLa=upcat([Ss:1:Se]);

     upcbt=a.aCh(10).d; % "2" should be the channel number in TFR for the analysed variable
     phase b

     uLb=upcbt([Ss:1:Se]);

     upcct=a.aCh(11).d; % "3" should be the channel number in TFR for the analysed variable
     phase c

     uLc=upcct([Ss:1:Se]);

     tplot=[Ss:1:Se]*Tsample;

     ZuLa=fft(uLa)/length(uLa);

     ZuLb=fft(uLb)/length(uLb);

     ZuLc=fft(uLc)/length(uLc);

     %

     i=sqrt(-1);

     r1=cos(2*pi/3)+i*sin(2*pi/3);

     r2=cos(4*pi/3)+i*sin(4*pi/3);

     %

     ZLP=(1/3)*2*(ZuLa([1:12])+r1*ZuLb([1:12])+r2*ZuLc([1:12]));
```

```
ZLN=(1/3)*2*(ZuLa([1:12])+r2*ZuLb([1:12])+r1*ZuLc([1:12]));
ZLO=(1/3)*2*(ZuLa([1:12])+ZuLb([1:12])+ZuLc([1:12]));

Z1P(count)=abs(ZLP(1));
Z1N(count)=abs(ZLN(1));
Z10(count)=abs(ZLO(1));

Z2P(count)=abs(ZLP(2));
Z2N(count)=abs(ZLN(2));
Z20(count)=abs(ZLO(2));

Z3P(count)=abs(ZLP(3));
Z3N(count)=abs(ZLN(3));
Z30(count)=abs(ZLO(3));

Z4P(count)=abs(ZLP(4));
Z4N(count)=abs(ZLN(4));
Z40(count)=abs(ZLO(4));

Z5P(count)=abs(ZLP(5));
Z5N(count)=abs(ZLN(5));
Z50(count)=abs(ZLO(5));

Z9P(count)=abs(ZLP(9));
Z9N(count)=abs(ZLN(9));
Z90(count)=abs(ZLO(9));

Z6P(count)=abs(ZLP(6));
Z6N(count)=abs(ZLN(6));
Z60(count)=abs(ZLO(6));

Z7P(count)=abs(ZLP(7));
Z7N(count)=abs(ZLN(7));
Z70(count)=abs(ZLO(7));

Z8P(count)=abs(ZLP(8));
Z8N(count)=abs(ZLN(8));
```

```
    Z80(count)=abs(ZLO(8));
end;
figure
subplot(811), plot(Xp,Z1N,Xp,Z1P,Xp,Z10)
legend('DC NPS','DC PPS','DC ZPS')
grid
title('Harmonic sequence components (Ipcc)');

subplot(812), plot(Xp,Z2P,Xp,Z2N,Xp,Z20)
legend('1st PPS','1st NPS','1st ZPS')
grid

subplot(813), plot(Xp,Z3P,Xp,Z3N,Xp,Z30)
legend('2nd PPS','2nd NPS','2nd ZPS')
grid

subplot(814), plot(Xp,Z4P,Xp,Z4N,Xp,Z40)
legend('3rd PPS','3rd NPS','3rd ZPS')
grid

subplot(815), plot(Xp,Z5P,Xp,Z5N,Xp,Z50)
legend('4th PPS','4th NPS','4th ZPS')
grid
subplot(816), plot(Xp,Z6P,Xp,Z6N,Xp,Z60)
legend('5th PPS','5th NPS','5th ZPS')
grid
subplot(817), plot(Xp,Z7P,Xp,Z7N,Xp,Z70)
legend('6th PPS','6th NPS','6th ZPS')
grid

subplot(818), plot(Xp,Z7P,Xp,Z7N,Xp,Z70)
legend('7th PPS','7th NPS','7th ZPS')
grid
```

Appendix B – Case study event list

Date	Time	Station	Group	Event	Status
20101005	23:16:54.000	GERUS CVR	CONDITION RFE	AC Voltage Healthy	Alarm
20101006	23:16:54.176	ZBEZI 220	ALARMS	50V Charger Charge Unh	Alarm
20101005	23:16:54.542	ZBEZI CVR	P1 TRF 330 ANALOG	BB2 kV	Low Alarm
20101005	23:16:54.924	ZBEZI CVR	ALARMS	Fast Stop Activated	Alarm
20101005	23:16:55.000	ZBEZI CVR	CNTRL MDE	Passive/Normal Network Indic	Passive
20101005	23:16:55.000	GERUS CVR	CONDITION RFO	TapChanger RFO	Normal
20101005	23:16:55.000	GERUS CVR	CONDITION RFE	AC Voltage Healthy	Normal
20101005	23:16:55.339	ZBEZI CVR	ALARMS	AC Hall Cooling Alarm	Alarm
20101005	23:16:55.362	ZBEZI CVR	ALARMS	Valve Cooling Faulty Sensor	Alarm
20101005	23:16:55.379	ZBEZI CVR	ALARMS	Reactor Hall Cooling Failure	Alarm
20101006	23:16:56.911	SESHEKE	220 ZAMB BREAKER	Breaker position indication	Open
20101006	23:16:58.357	ZBEZI 220	ALARMS	50V Charger Charge Unh	Normal
20101005	23:16:56.714	ZBEZI CVR	P1 TRF 330 ANALOG	BB2 kV	Normal
20101005	23:16:58.000	GERUS CVR	CONDITION RFO	TapChanger RFO	Alarm
20101005	23:16:58.554	ZBEZI CVR	ALARMS	Valve Cooling Faulty Sensor	Normal
20101005	23:17:01.683	GERUS 220	220 OMBUR ANALOGS	MVAr	Normal
20101005	23:17:02.171	ZBEZI CVR	ALARMS	Valve Cooling Urg	Alarm
20101005	23:17:06.587	ZBEZI CVR	ALARMS	Valve Cooling Urg	Normal
20101005	23:19:44.433	ZBEZI 220	220 SESHE ANALOGS	kV	Low Alarm
20101005	23:19:44.433	ZBEZI 220	220 SESHE ANALOGS	MVAr	High Alarm
20101005	23:19:44.433	ZBEZI 220	66 BB1 ANALOGS	kV	Low Alarm
20101005	23:19:44.433	ZBEZI 220	220 SESHE ANALOGS	kV	Normal
20101005	23:20:04.558	ZBEZI 220	66 BB1 ANALOGS	kV	Normal
20101005	23:20:04.558	ZBEZI 220	220 SESHE ANALOGS	MVAr	Normal
20101005	23:20:04.558	SESHEKE	66 KATIMA ANALOGS	kV	Low Alarm
20101005	23:21:07.292	SESHEKE	66kV BBV ANALOGS	kV	Low Alarm
20101005	23:21:07.292	SESHEKE	220 VICFAL ANALOGS	kV	Low Alarm
20101005	23:21:55.339	ZBEZI CVR	ALARMS	AC Hall Cooling Failure	Alarm
20101005	23:27:24.656	SESHEKE	220 ZAMB BREAKER	Breaker position indication	Closed
20101005	23:27:24.909	ZBEZI CVR	ALARMS	AC Bus Prot Unh	Alarm
20101005	23:27:24.946	ZBEZI CVR	ALARMS	AC Yard W2.W1.Q1 BKR Unh	Alarm
20101005	23:27:24.948	ZBEZI CVR	ALARMS	AC Yard Brkr Unsynchr Oper	Alarm
20101005	23:27:24.948	ZBEZI CVR	ALARMS	DC Yard P1.WP.Q3 Fail	Alarm
20101005	23:27:24.950	ZBEZI CVR	ALARMS	DC Yard P1.WP.Q2 Fail	Alarm
20101005	23:27:24.952	ZBEZI CVR	ALARMS	DC Yard P1.WP.Q4 Fail	Alarm
20101005	23:27:24.952	ZBEZI CVR	ALARMS	AC Bus Prot Unh	Normal
20101006	23:27:24.956	ZBEZI 220	ALARMS	50V Charger Charge Unh	Alarm
20101005	23:27:24.964	ZBEZI CVR	P1 TRF 330kV BKR	Breaker position indication	Open
20101005	23:27:24.965	ZBEZI CVR	ALARMS	AC Yard W2.W3.Q1 BKR Unh	Alarm
20101005	23:27:24.967	ZBEZI CVR	ALARMS	AC Yard W2.W2.Q1 BKR Unh	Alarm

20101005	23:27:24.967	ZBEZI CVR	ALARMS	DC Yard P1.WP.Q1.Q1 Fail	Alarm
20101005	23:27:24.971	ZBEZI CVR	P1_H60FIL BREAKER	Breaker position indication	Open
20101005	23:27:24.976	ZBEZI CVR	ALARMS	AC Yard P1.Z2.Q1 BKR Unh	Alarm
20101005	23:27:24.977	ZBEZI CVR	ALARMS	AC Yard W2.W3.Q2 BKR Unh	Alarm
20101005	23:27:24.991	ZBEZI CVR	FLTR 3P1 330kV BKR	Breaker position indication	Open
20101005	23:27:24.994	ZBEZI CVR	ALARMS	Aux Power LV Sw/gear Unh	Alarm
20101005	23:27:24.995	ZBEZI CVR	FLTR 32P1 330kV BKR	Breaker position indication	Open
20101005	23:27:25.000	ZBEZI CVR	SEQUENCE	P1 Conv Blocked Status	Blocked
20101005	23:27:25.000	GERUS CVR	CONDITION RFE	AC Voltage Healthy	Alarm
20101005	23:27:25.000	ZBEZI CVR	SEQUENCE	P1 Conv TRF Breakers Status	Open
20101005	23:27:25.000	GERUS CVR	CONDITION RFE	AC Voltage Healthy	Normal
20101005	23:27:25.017	ZBEZI CVR	ALARMS	AC Yard Brkr Unsynchr Oper	Normal
20101005	23:27:25.620	ZBEZI CVR	P1 TRF 330 ANALOG	BB2 kV	Low Alarm
20101005	23:27:25.690	ZBEZI CVR	ALARMS	Cnvter TRF Transform Dryer	Alarm
20101005	23:27:26.012	ZBEZI CVR	ALARMS	Valve Cooling Faulty Sensor	Alarm
20101005	23:27:26.040	ZBEZI CVR	P1 TRF 330RES BKR	Breaker position indication	Open
20101005	23:27:26.634	ZBEZI CVR	ALARMS	Valve Cooling Power Faulty	Alarm
20101005	23:27:27.954	ZBEZI CVR	ALARMS	Cnvter TRF Aux Supply Unh	Alarm
20101005	23:27:36.691	ZBEZI CVR	ALARMS	Valve Cooling Urg	Alarm
20101005	23:27:41.855	ZBEZI CVR	ALARMS	AC Yard P1.Z2.Q1 BKR Unh	Normal
20101005	23:27:41.856	ZBEZI CVR	ALARMS	DC Yard P1.WP.Q1.Q1 Fail	Normal
20101005	23:27:41.856	ZBEZI CVR	ALARMS	DC Yard P1.WP.Q2 Fail	Normal
20101005	23:27:41.856	ZBEZI CVR	ALARMS	AC Yard W2.W2.Q1 BKR Unh	Normal
20101005	23:27:41.856	ZBEZI CVR	ALARMS	AC Yard W2.W3.Q1 BKR Unh	Normal
20101005	23:27:41.857	ZBEZI CVR	ALARMS	DC Yard P1.WP.Q3 Fail	Normal
20101005	23:27:41.857	ZBEZI CVR	ALARMS	DC Yard P1.WP.Q4 Fail	Normal
20101005	23:27:41.857	ZBEZI CVR	ALARMS	AC Yard W2.W3.Q2 BKR Unh	Normal
20101005	23:27:41.858	ZBEZI CVR	ALARMS	AC Yard W2.W1.Q1 BKR Unh	Normal
20101005	23:27:41.874	ZBEZI CVR	ALARMS	Valve Cooling Power Faulty	Normal
20101005	23:27:42.402	ZBEZI CVR	ALARMS	Cnvter TRF Aux Supply Unh	Normal
20101005	23:27:43.024	ZBEZI CVR	ALARMS	Cnvter TRF Transform Dryer	Normal
20101005	23:27:43.667	ZBEZI CVR	ALARMS	Aux Power LV Sw/gear Unh	Normal
20101005	23:27:49.636	ZBEZI CVR	P1 TRF TC POS IND	Tap position	22
20101005	23:27:56.589	ZBEZI CVR	P1 TRF TC POS IND	Tap position	23
20101005	23:28:02.347	ZBEZI CVR	ALARMS	Valve Cooling Faulty Sensor	Normal
20101005	23:28:03.136	ZBEZI CVR	P1 TRF TC POS IND	Tap position	24
20101005	23:28:09.667	ZBEZI CVR	P1 TRF TC POS IND	Tap position	25
20101005	23:30:02.526	ZBEZI 220	66 BB1 ANALOGS	kV	Low Alarm
20101005	23:30:02.526	ZBEZI 220	220 BB2 ANALOGS	kV	Low Alarm
20101005	23:30:02.526	ZBEZI 220	220 SESHE ANALOGS	kV	Low Alarm
20101005	23:30:32.050	ZBEZI CVR	ALARMS	Valve Cooling Urg	Normal
20101005	23:36:01.495	ZBEZI CVR	CNTRL MDE	Reduced UDC Cmd	Selected
20101005	23:36:02.495	ZBEZI CVR	CNTRL MDE	Reduced UDC Cmd	Activate
20101005	23:38:52.507	ZBEZI CVR	ALARMS	AC Hall Cooling Failure	Normal

20101005	23:42:30.261	ZBEZI CVR	CNTRL MDE	Reduced UDC Cmd	Selected
20101005	23:42:31.261	ZBEZI CVR	CNTRL MDE	Reduced UDC Cmd	Activate
20101005	23:50:22.792	GERUS CVR	CNTRL MDE	Reduced UDC Cmd	Selected
20101005	23:50:23.792	GERUS CVR	CNTRL MDE	Reduced UDC Cmd	Activate
20101005	23:56:14.026	NatC	Monitor 28	User: NDAPONA	Logout
20101005	23:56:22.635	NatC	Monitor 28	User: NDAPONA	Login
20101005	23:56:36.698	ZBEZI CVR	CNTRL MDE	Passive / Normal Cmd	Selected
20101005	23:56:37.698	ZBEZI CVR	CNTRL MDE	Passive / Normal Cmd	Normal
20101005	23:56:38.000	ZBEZI CVR	CNTRL MDE	Passive/Normal Network Indic	Normal
20101005	23:56:38.482	ZBEZI CVR	ALARMS	Fast Stop Activated	Normal
20101005	23:56:39.000	ZBEZI CVR	SEQUENCE	P1 Pole Connection Status	Disconnected
20101005	23:56:39.000	ZBEZI CVR	CNTRL MDE	P / UDC Setting Indic	P_Cntl
20101005	23:56:39.033	ZBEZI CVR	P1 PBUS DC PBKR	Breaker position indication	Open
20101005	23:56:39.103	ZBEZI CVR	P1 PBUS DC HSSW2	Switch position indication	Open
20101005	23:56:39.118	ZBEZI CVR	P1 PBUS DC HSSW3	Switch position indication	Open
20101005	23:56:39.188	ZBEZI CVR	P1 PBUS DC HSSW4	Switch position indication	Open
20101005	23:56:39.376	ZBEZI CVR	P1 PBUS DC PBKR	Breaker position indication	Closed
20101005	23:56:42.776	ZBEZI CVR	CNTRL MDE	Passive / Normal Cmd	Selected
20101005	23:56:43.776	ZBEZI CVR	CNTRL MDE	Passive / Normal Cmd	Passive
20101005	23:56:44.000	ZBEZI CVR	CNTRL MDE	P / UDC Setting Indic	UDCCntl
20101005	23:56:44.000	ZBEZI CVR	CNTRL MDE	Passive/Normal Network Indic	Passive

Appendix C – Complex vector, Clarke's ($\alpha\beta$) components and d-q components

C.1) Complex vector

Let $\boldsymbol{y}(\boldsymbol{t}) = Ye^{j(\omega t+\delta)}$ (C1)

The purpose of the complex vector notation as defined by (C1) is to be able to represent a three-phase system comprising of three sinusoidal quantities as a single rotating vector. The complex vector, also known as the space vector, is chosen such that the three-phase instantaneous quantities are projected to three orthogonal axes $e^{j0}, e^{-j\frac{2\pi}{3}}$ and $e^{j\frac{2\pi}{3}}$. [**10**], [**22**].

$$x_a(t) = Re(\boldsymbol{x}(t).e^{j0}) = \frac{1}{2}\left(\boldsymbol{x}(t).e^{j0} + \boldsymbol{x}(t)^*.(e^{j0})^*\right) \quad \text{(C2)}$$

$$x_b(t) = Re(\boldsymbol{x}(t).e^{-j\frac{2\pi}{3}}) = \frac{1}{2}\left(\boldsymbol{x}(t).e^{-j\frac{2\pi}{3}} + \boldsymbol{x}(t)^*.(e^{-j\frac{2\pi}{3}})^*\right) \quad \text{(C3)}$$

and

$$x_c(t) = Re(\boldsymbol{x}(t).e^{j\frac{2\pi}{3}}) = \frac{1}{2}\left(\boldsymbol{x}(t).e^{j\frac{2\pi}{3}} + \boldsymbol{x}(t)^*.(e^{j\frac{2\pi}{3}})^*\right) . \quad \text{(C4)}$$

Projecting all three phases on the reference phase "a" gives the following results:

$$x_a(t) + x_b(t).e^{j\frac{2\pi}{3}} + x_c(t).e^{-j\frac{2\pi}{3}}$$

$$= \frac{1}{2}\left((\boldsymbol{x}(t) + \boldsymbol{x}(t)^*) + \left(\boldsymbol{x}(t) + \boldsymbol{x}(t)^*e^{j\frac{4\pi}{3}}\right) + \left(\boldsymbol{x}(t) + \boldsymbol{x}(t)^*e^{-j\frac{4\pi}{3}}\right)\right)$$

$$= \frac{3}{2}\boldsymbol{x}(t) \quad \text{(C5)}$$

Let $\boldsymbol{T} = \frac{2}{3}\begin{bmatrix}1 & e^{j\frac{2\pi}{3}} & e^{-j\frac{2\pi}{3}}\end{bmatrix}$, (C6)

then $\boldsymbol{x}(t) = \boldsymbol{T}\begin{bmatrix}x_a(t)\\ x_b(t)\\ x_c(t)\end{bmatrix}$. (C7)

C.2) $\alpha\beta$-components

The α and β components are defined as the real and imaginary components of the complex vector [**10**] as given by the relationship

$$\boldsymbol{x_{\alpha\beta}}(t) \stackrel{\text{def}}{=} \boldsymbol{x}(t) \; = \; x_{\alpha}(\mathrm{t}) + \; \mathrm{j}\, x_{\beta}(\mathrm{t})\,, \tag{C8}$$

where

$$x_{\alpha}(\mathrm{t}) = \frac{2}{3}x_a(t) - \frac{1}{3}x_b(t) - \frac{1}{3}x_c(t) \tag{C9}$$

and

$$x_{\beta}(\mathrm{t}) = \frac{1}{\sqrt{3}}x_b(t) - \frac{1}{\sqrt{3}}x_c(t)\,. \tag{C10}$$

C.3) d-q components

In order to achieve a static reference frame from a rotating reference frame, the d-q components can be used [**10**] by using the relationship

$$\boldsymbol{x_{dq}}(t) \stackrel{\text{def}}{=} \; x_{\mathrm{d}}(\mathrm{t}) + \; \mathrm{j}\, x_q(\mathrm{t}) = \; \boldsymbol{x_{\alpha\beta}}(t).\, e^{-j\omega t}, \tag{C11}$$

where

$$x_{\mathrm{d}}(\mathrm{t}) = x_{\alpha}(\mathrm{t}).\cos(\omega t) + \; x_{\beta}(\mathrm{t}).\sin(\omega t) \tag{C12}$$

and

$$x_{\mathrm{q}}(\mathrm{t}) = -x_{\alpha}(\mathrm{t}).\sin(\omega t) + \; x_{\beta}(\mathrm{t}).\cos(\omega t). \tag{C13}$$